NUMERICAL ANALYSIS OF AIR INJECTION INTO AN AQUIFER

by

John C. Halepaska

Submitted to the faculty of the

NEW MEXICO INSTITUTE OF MINING AND TECHNOLOGY

in partial fulfillment
of the requirements for the degree of
Doctor of Philosophy in Geoscience

September 1970

Table of Contents

Abstract

Using a saturation form of the differential equations, two-phase flow with one of the phases compressible was simulated numerically. The process investigated is adiabatic air injection into a confined aquifer, because it is believed that air injection can be used to slow down or arrest encroachment of salt water.

The gaseous phase is treated as compressible. An incompressible description of the gas leads to large errors.

A constant mass rate of gas injection results in very high pressures near the well after a short time. Maintaining a constant gas pressure at the well face results in a much slower rate of head increase in the aquifer. Higher permeabilities slow down the head buildup.

Acknowledgements

The writer is grateful to the late Prof. C. E. Jacob who suggested the problem upon which this work is based. Thanks are also extended to Mr. Merle Hanson who acted as advisor through the major portion of the work, to Dr. Gerardo Wolfgang Gross who made many valuable suggestions, to Dr. Rafi Al-Hussainy, Don Beaver, Chester McKee, and Dr. Albert Petschek who offered much help, encouragement, and constructive criticism; to Tom Schellhase and Gary Mosely who programmed the plot routines and did much of the machine plotting; to Dr. Dennis E. Williams who drafted the graphs; to my wife who typed the rough drafts, and to Suzi Nevergold who toiled over the final manuscript.

Figures

INTRODUCTION

General

A study of the hydrology of the Pecos Valley in eastern New Mexico was undertaken by the New Mexico Institute of Mining and Technology in 1967.

One of the initial purposes of this study was to investigate salt water encroachment near the city of Roswell. Salt water encroachment is a common occurrence along coastlines or along inland areas where salt water is overlain by fresh water. Areas of encroachment normally occur near large pumping centers.

A number of techniques are available to control salt water encroachment. One technique is to slow down pumping; another is to inject fluids into the reservoir being pumped to keep the head in the system from declining.

Fresh water or air are suitable for injection into reservoirs. Re-injection of fresh water into the reservoir is not desirable from an economic standpoint. Air, however, would be economical and is believed not to impair the reservoir in most cases.

The injection of air into a water reservoir creates a complicated two-phase flow system. Under these conditions each phase encounters a relative permeability that varies as a function of saturation. Capillary effects also exist in the two-phase zone as a function of saturation. To analyze the problem properly the gas must be treated as a compressible phase.

Previous Work

Darcy's law and the continuity equation constitute the basic differential equations governing single-phase flow. Darcy's law is:

$$v = Q/A = - K \text{ grad } P$$

where:

v = Darcy velocity

Q = fluid discharge

A = area

K = hydraulic conductivity

$P = P/\gamma + z$

The continuity equation for an inelastic system,

$$\frac{\partial(\rho v_x)}{\partial x} + \frac{\partial(\rho v_y)}{\partial y} + \frac{\partial(\rho v_z)}{\partial z} = \frac{\partial \rho}{\partial t}$$

where:

ρ = fluid density

t = time

v_x = velocity in x direction

v_y = velocity in y direction

v_z = velocity in z direction

The question of two-phase flow and the interdependence of the two phases was largely answered in a paper by Wyckoff and Botset (1936). The work prior to this time involved experiments and theories on the microscopic aspects of two-phase flow.

Wyckoff and Botset essentially ignored all phenomena taking place in simultaneous flow on a microscopic scale. Instead, a macroscopic view was adopted and empirical relations were obtained relating capillary pressure to saturation, and the relative permeabilities to the saturation. Determination of critical aspects of two-phase flow was thus reduced to a relatively simple experiment without determining the physics on a microscopic scale.

Muskat and Meres (1936) postulated the differential equations that govern simultaneous flow of fluids. Muskat and Meres pointed out that the principal obstacle to the formulation of the differential equations is the variability of volume composition of the fluids as they move through the porous medium. With the description from the work of Wyckoff and Botset, Muskat and Meres were able to formulate the necessary equations.

Buckley and Leverett (1942) solved a one-dimensional version of two-phase flow. The equations were solved neglecting the effects of capillary pressure by the technique of characteristics. According to Buckley and Leverett, an indiscriminate application of the method of characteristics yields multiple values of saturation at the same point.

The solution of the equations governing two-phase flow had to wait for the development of large digital computers and adequate numerical techniques.

Considerable effort was expended in solving systems of equations for two-phase flow where the phases are completely separated except at a front. Solutions of this type were generally associated with a simple geologic structure such as a dome.

The renewed emphasis on understanding two-phase flow was largely stimulated by secondary and tertiary recovery operations in oil fields. Also of great importance was the secondary injection of gas for storage purposes.

Douglas, Peaceman and Rachford (1959) published a numerical technique for the solution of two-phase, two-dimensional flow. The model included relative permeabilities, fluid viscosities, densities, gravity, and capillary pressure. Several cases were treated, and the results compared favorably with model studies.

Higgins and Leighton (1962) published a technique to calculate two-phase flow in irregularly bounded porous media. A potentiometric model gives streamlines and equipotentials which are used in a computer program that solves a form of the Buckley-Leverett equation. While the model is much simpler than the Douglas, Peaceman and Rachford model, the results compare well.

Woods and Comer (1962) presented a study on secondary gas storage. In general, the model compared favorably with the field history of a gas storage reservoir. Relative permeabilities and capillary pressures were ignored, resulting in poor prediction of gas bubble size. Woods and Comer suggested that inclusion of relative permeabilities and capillary pressure along with the choice of a simpler geologic shape would enhance the ability of the model to predict gas bubble shape.

Peaceman (1967) comprehensively investigated two-phase flow. and summed up the state of the art. Several techniques were discussed for coupling the differential equations. Problems involved in

calculating relative permeability were discussed and various techniques were presented to minimize numerical oscillation. Peaceman concluded that it was very difficult to match solutions by the method of finite differences without very small grid size. This problem is directly related to the particular solution algorithm that was applied. Severe restrictions are placed upon the grid type and the time step.

McFarlane, Mueller and Miller (1967) analyzed two-phase oil reservoirs undergoing gas injection. Their model is primarily concerned with unsteady-state fluid composition distributions. Capillary pressure and gravitational effects are ignored.

Coats and Richardson (1967) formulated a numerical model of water displacement by gas in reservoir storage. Their model describes a cross section of an 80 percent water-saturated reservoir under gas injection. It assumes that one cell of the grid is receiving injected fluid. It is further assumed that both phases are incompressible. Their model also includes the use of both positive and negative values of capillary pressure to determine values of saturation. The model is compared to the Buckley-Leverett theory and it is found that displacement efficiencies are predicted better by the numerical model.

Knapp, Henderson, Dempsey and Coats (1967) investigated gas recovery upon depletion of reservoir storage. This work solved the differential equations:

$$\nabla \cdot \frac{kk_{rw}}{\mu_w} \rho_w{}^2 \nabla \Phi_w + q_w = \phi \frac{\partial}{\partial t} (S_w \rho_w)$$

$$\nabla \cdot \frac{kk_{rn}}{\mu_n} \rho_n{}^2 \nabla \Phi_n + q_n = \phi \frac{\partial}{\partial t} (S_n \rho_n)$$

where:

$$\nabla . e = \left(\frac{\partial}{\partial x} e_x + \frac{\partial}{\partial y} e_y + \frac{\partial}{\partial z} e_z\right) .$$

k = Specific permeability of the medium

k_{rw} = Ratio of k_r/k

k_r = Relative permeability

k_{rn} = Relative permeability of the non-wetting phase

ρ_w = Density of the wetting phase

ρ_n = Density of the non-wetting phase

$$\Phi_w = \int_p^{p_0} \frac{dp_w^*}{\rho_w} - \frac{ga}{144gc} h_r$$

$$\Phi_n = \int_p^{p_0} \frac{dp_n^*}{\rho_n} - \frac{ga}{144gc} h_r$$

p^*= Pressure

g_a = Acceleration of gravity

g_c = Gravitational constant

e_i = Cartesian basis vectors

h_r = Vertical dimension measured from aquifer top

q = Injection rate

ϕ = Porosity

t = Time

S_w = Saturation of the wetting phase

S_n = Saturation of the non-wetting phase

μ_w = Viscosity of the wetting phase

μ_n = Viscosity of non-wetting phase

These two differential equations are for multi-dimensional, two-phase, compressible fluid flow. This work represents the first effort to solve differential equations governing two-phase compressible flow. The previous work did not take into account the compressibility of the gas phase.

Purpose

The purpose of this study is to solve a set of differential equations governing the flow of air in a completely water-saturated porous medium taking into account the compressibility of the gas phase. It is assumed that the well totally penetrates a homogeneous and isotropic aquifer, that the well is axisymmetric and that the aquifer characteristics remain constant in space and time. It is also assumed that the aquifer area is infinite and that the initial head distribution in the system is constant.

Basic Differential Equations

The differential equations for two-phase compressible flow are:

$$\nabla \cdot \left[\frac{k k_{rw}}{\mu_w} \nabla P_w \right] = \phi \frac{\partial S}{\partial t}$$

$$\nabla \cdot \left[\frac{k k_{rn}}{\mu_n} \nabla P_n^{m+1} \right] = (m+1)\, \phi \frac{\partial [p^m (1-S)]}{\partial t}$$

subject to the auxiliary conditions:

$$\left. \frac{r \partial P_n}{\partial r} \right|_{r=r_w} = \frac{Q}{2\pi T} \qquad \left. \frac{\partial P_w}{\partial r} \right|_{r=r_w} = 0$$

$$P_w(r,z,0) = 0 \qquad \frac{\partial P_w}{\partial z}(r,b,t) = 0$$

$$P_w(\infty,z,t) = 0 \qquad \frac{\partial P_w}{\partial z}(r,0,t) = 0$$

$$P_n(r,z,0) = 0 \qquad \frac{\partial P_n}{\partial z}(r,b,t) = 0$$

$$P_n(\infty,z,t) = 0 \qquad \frac{\partial P_n}{\partial z}(r,0,t) = 0$$

where:

μ_w = Viscosity of the wetting phase

μ_n = Viscosity of the non-wetting phase

m = Generalized exponent characterizing state of the system

m = C_v/C_p for adiabatic ($\simeq$ 0.7 for air)

m = 0 for incompressible

m = 1 for isothermal

C_v = Specific heat at constant volume

C_p = Specific heat at constant pressure

r = Radial coordinate

z = Vertical coordinate

$P_w = (p_w^*/\gamma_w) + z$

$P_n = (p_n^*/\gamma_w) + z$

p_w^* = Pressure of the wetting phase

p_n^* = Pressure of the non-wetting phase

T = Transmissivity

and other terms are as previously defined.

For complete derivation of the above differential equation, see Appendix A.

GENERAL THEORY

Mathematical Formulation

The solution of nonlinear multi-dimensional differential equations that are analytically intractable depends upon many basic numerical techniques. Fundamental in this development is the derivation of numerical analogs for the various parts of the differential equation. Expanding $u(x + \Delta x, y)$ about any point (x,y) in a Taylor series:

$$u(x+\Delta x,y) = u(x,y) + \Delta x \frac{\partial u}{\partial x}(x,y) + \frac{(\Delta x)^2}{2!}\frac{\partial^2 u}{\partial x^2}(x,y) \tag{1}$$

$$+ \frac{(\Delta x)^3}{3!}\frac{\partial^3 u}{\partial x^3}(x,y) + 0\ [(\Delta x)^4]$$

where:

u = a continuous function of x and has finite single-valued derivatives

Δx = increment between points

(x,y) = coordinates of any point

$0[(\Delta x)^4]$ = error associated with truncating the series after three terms.

Expanding $u(x - \Delta x, y)$ about (x,y):

$$u(x-\Delta x,y) = u(x,y) - \Delta x \frac{\partial u}{\partial x}(x,y) + \frac{(\Delta x)^2}{2!}\frac{\partial^2 u}{\partial x^2}(x,y)$$

$$- \frac{(\Delta x)^3}{3!}\frac{\partial^3 u}{\partial x^3}(x,y) + 0[(\Delta x)^4] \tag{2}$$

Simple addition of Eqs. (1) and (2) gives:

$$\frac{\partial^2 u}{\partial x^2} = \frac{u_{i+1,j} - 2u_{i,j} + u_{i-1,j}}{(\Delta x)^2} + O[(\Delta x)^2] \tag{3}$$

Using Crank-Nicholson differencing, Eq. (3) can be written in the following form:

$$\left(\frac{\partial^2 u}{\partial x^2}\right)_{i,j}^{n+1/2} = 1/2\left[\frac{u_{i+1,j}^{n+1} - 2u_{i,j}^{n+1} + u_{i-1,j}^{n+1}}{(\Delta x)^2}\right] + 1/2\left[\frac{u_{i+1,j}^{n} - 2u_{i,j}^{n} + u_{i-1,j}^{n}}{(\Delta x)^2}\right] \tag{4}$$

Eq. (4) is second-order correct in space.

A similar development is also desirable for the time variable in the differential equation. Expanding a Taylor series in time about the point $(x_i, t^{n+1/2})$

$$\left(\frac{\partial u}{\partial t}\right)_{i,j}^{n+1/2} = \frac{u_{i,j}^{n+1} - u_{i,j}^{n}}{\Delta t} - \left(\frac{\partial^3 u}{\partial t^3}\right)_{i,j}^{n+1/2} \frac{(\Delta t)^2}{24} \tag{5}$$

Eq. (5) in more usable form:

$$\left(\frac{\partial u}{\partial t}\right)_{i,j}^{n+1/2} = \frac{u_{i,j}^{n+1} - u_{i,j}^{n}}{\Delta t} \tag{6}$$

The preceding development allows the differential equation to be broken down into finite difference form. The development is second-order correct in both time and space.

Once the differential equation is broken down into numerical form a solution technique is chosen, depending upon the type of equation. The

Thomas algorithm was used to solve the differential equations for two-phase flow. The equations are first arranged in the form:

$$a_i\, u_{i-1} + b_i\, u_i + C_i\, u_{i+1} = d_i \tag{7}$$

where a_i, b_i, c_i, and d_i are coefficients of the dependent variable. The algorithm can then be stated as follows:

$$x_i = b_i - \frac{a_i\, C_{i-1}}{x_{i-1}} \quad \text{with} \quad u_1 = b_1 \tag{8}$$

$$v_i = \frac{d_i - d_i\, v_{i-1}}{x_i} \quad \text{with } v_1 = \frac{d_1}{b_1} \tag{9}$$

Values of the dependent variable are then computed from:

$$u_i = v_i - \frac{C_i\, u_{i+1}}{x_i} \tag{10}$$

The Thomas algorithm is powerful in that it solves a series of equations, such as Eq. (7), explicitly for the dependent variables. Inversion of a matrix equation is thus avoided. In addition, starting values for Eqs. (8) and (9) allow for efficient handling of boundary conditions. For a full development of the use of the Thomas algorithm see Appendix A.

In an effort to develop more efficient computational routines, values of the dependent variable are often extrapolated. The extrapolation routine used in this development is:

$$p_{i,j}^{n+2} = p_{i,j}^{n+1} + \frac{\Delta t^{n+1/2}}{\Delta t^{n-1/2}} \left(p_{i,j}^{n+1} - p_{i,j}^{n}\right) + 0.01\, \frac{\Delta t^{n+1/2}}{\Delta t^{n-1/2}} \left(p_{i,j}^{n+1} - p_{i,j}^{n}\right) \tag{11}$$

where the last term in Eq. (11) alternates in sign from computing cycle to computing cycle and where:

$P_{i,j}^{n+2}$ = Dependent variable at time step n + 2

$P_{i,j}^{n+1}$ = Dependent variable at time step n + 1

$\Delta t^{n+1/2}$ = Present time step

$\Delta t^{n-1/2}$ = Last time step

It was found that, by alternately over-extrapolating and under-extrapolating, the addition of the last term of Eq. (11), drift could be eliminated from numerical truncation.

Computational Techniques

The internal mechanics of a computer program are variable in the technique applied, which reflects the person's programming methods. The general technique outlined below is not highly sophisticated but is adequate. A general flow chart is given in Appendix C.

Initially the system is completely at rest. A given pressure is applied in the form of injected fluids, and heads are extrapolated by means of Eq. (11).

Using extrapolated values of head, capillary pressure is calculated from the relation:

$$Pc_{i,j}^{n+1} = p_w^{n+1} - p_{ni,j}^{n+1} - \rho_w gh \tag{12}$$

where:

$Pc_{i,j}^{n+1}$ = Capillary head at time n+1.

Other terms are as previously defined.

Values of saturation, relative permeability and slope are then calculated from the following expressions:

$$S_{i,j}^{n+1} = 1.21 - \sqrt{1.47 - 0.327(4.36 - Pc_{i,j})} \tag{13}$$

$$\frac{dS^{n+1}}{dPc} = \frac{1.0}{(6.12)S_{i,j}^{n+1} - 7.42} \tag{14}$$

$$(k_{rw})_{i,j}^{n+1} = S_{i,j}^{n+1} \tag{15}$$

$$(k_{rn})_{i,j}^{n+1} = 1.0 - S_{i,j}^{n+1} \tag{16}$$

where:

$\frac{dS^{n+1}}{d\,Pc}$ = slope at time (n + 1)

$S_{i,j}^{n+1}$ = water saturation at time (n + 1)

Eq. (13) is a parabola fitted through the points (0.2, 3), (1.0, 0.0), (1.05, 0.05) (see Fig. 1). This expression for saturation vs. capillary pressure was used because it generally fit data found in the literature and allowed direct calculation of saturation. This expression was found to be faster and numerically much smoother than using a function created by using straight line segments to input data points defining the function. Eq. (13) also avoided the necessity for extrapolating between data points.

Eq. (14) is simply the derivative of Eq. (13) (see Appendix A, eqs. (9) and (22)).

Eqs. (15) and (16) are equations of straight lines used for calculating relative permeabilities from values of saturation. (See Fig. 2.)

While the values of relative permeability vs. saturation are never straight lines, they can be approximated very closely by straight lines.

All four of the preceding expressions were modified in the following way:

$$S_{i,j} = 0.5\ (1.21 - \sqrt{1.47 - 0.33(4.36 - Pc_{i,j})}\ ) + 0.5\ S_{i,j}^{\alpha} \tag{17}$$

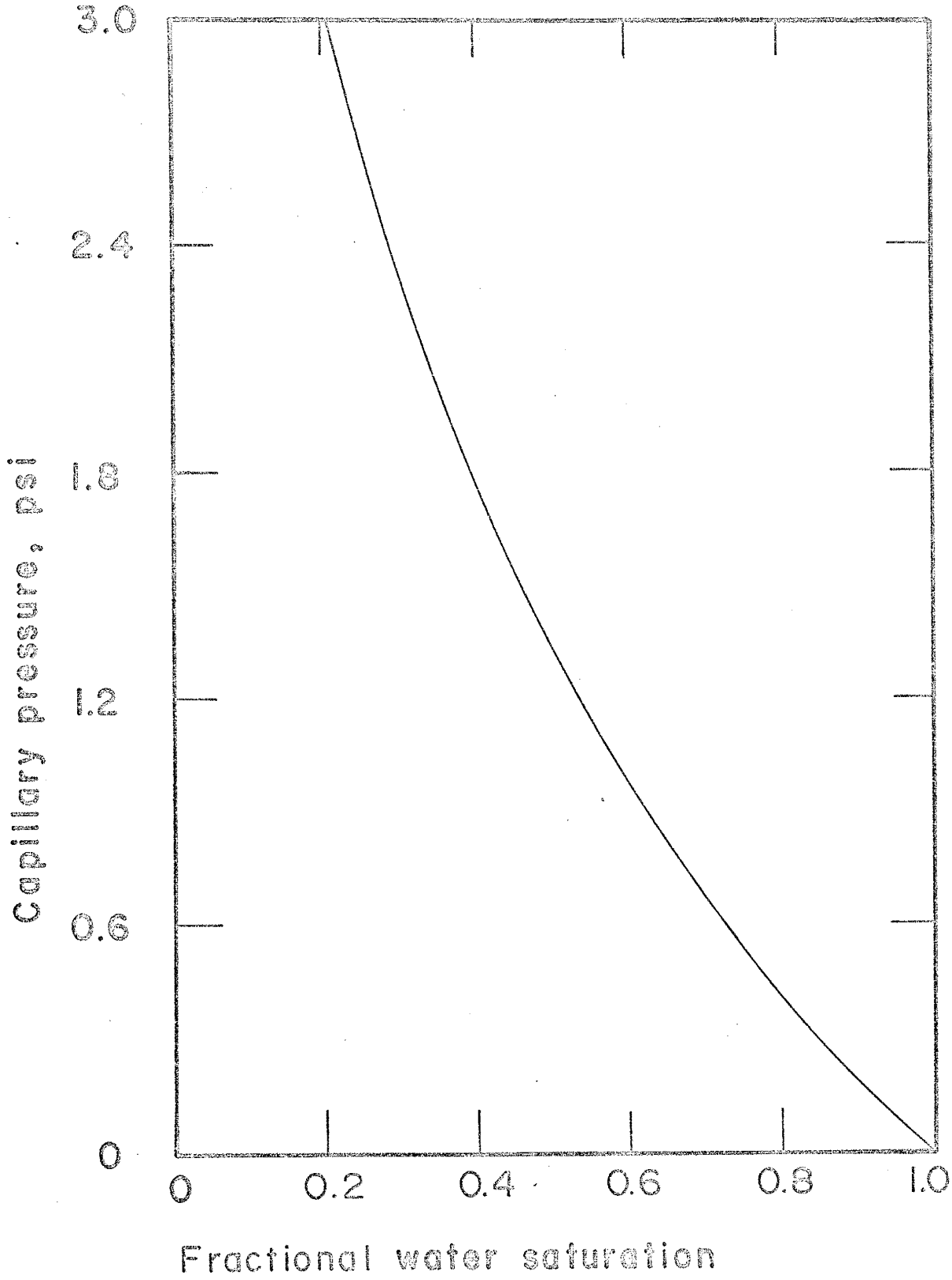

FIG. 1

CAPILLARY PRESSURE CURVE

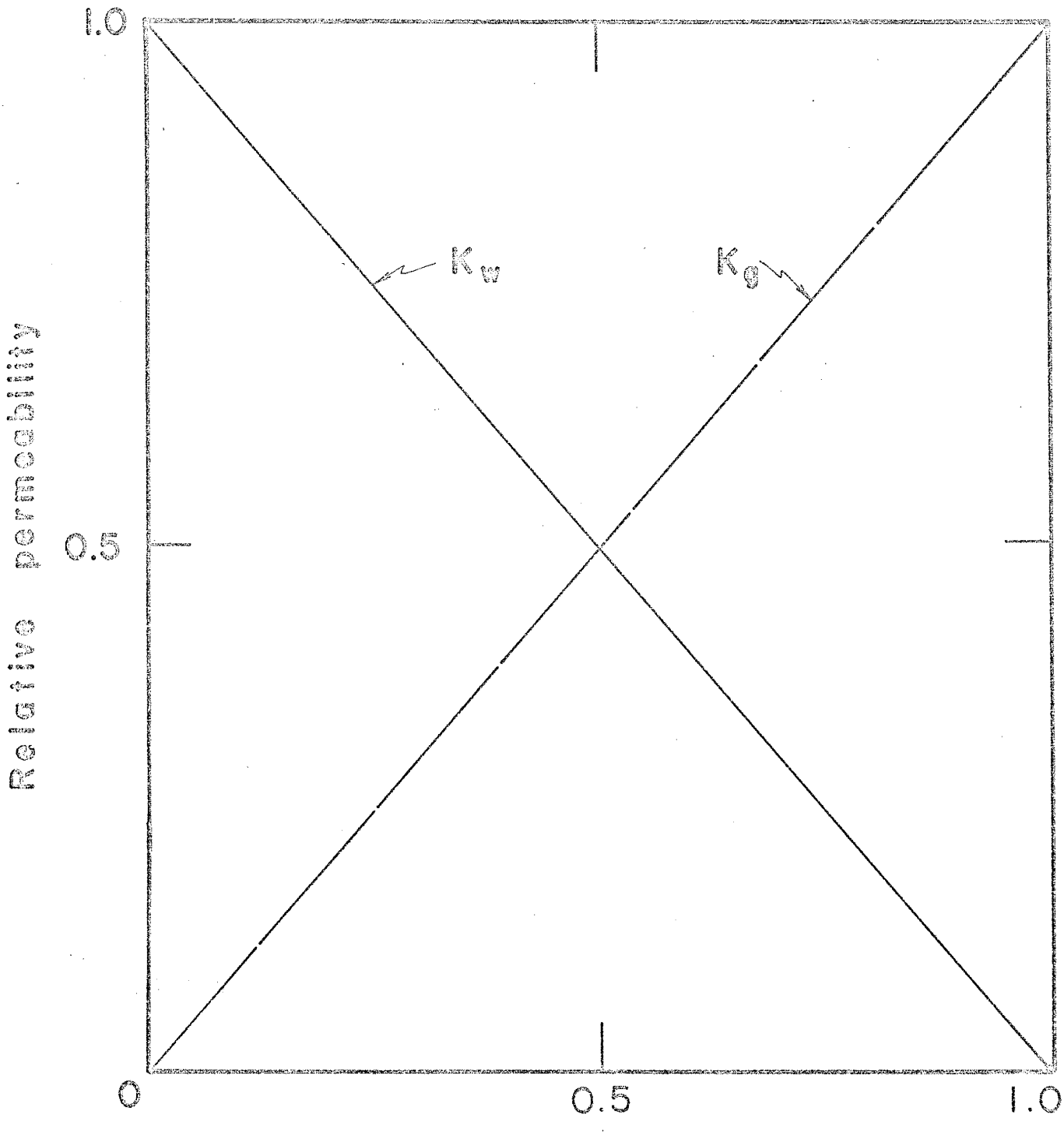
1.0
0.5
0
0.5
1.0
K_w
K_g
Relative permeability
Fractional water saturation

FIG. 2

$$\left(\frac{dS}{dPc}\right)^{n+1}_{i,j} = 0.5\left[\frac{1.0}{(6.12)S_{i,j}-7.42}\right] + 0.5\left(\frac{dS}{dPc}\right)^{\alpha}_{i,j} \tag{18}$$

$$(k_{rw})^{n+1}_{i,j} = 0.5\,(S^{n+1}_{i,j} + S_{i,j}) \tag{19}$$

$$(k_{rn})^{n+1}_{i,j} = 0.5\,(1.0 - S^{n+1}_{i,j}) + 0.5\,(k_{rn})^{\alpha}_{i,j} \tag{20}$$

where:

$S_{i,j}$ = last value of saturation calculated for any point i,j

$\left(\frac{dS}{dPc}\right)^{\alpha}_{i,j}$ = last value of slope calculated for any point i,j

$(k_{rn})^{\alpha}_{i,j}$ = last value of relative permeability calculated for any point i,j

The routine used to calculate values of saturation, slope $\frac{dS}{dPc}$, and relative permeability was a procedure developed from trial and error. It was found that by weighting the calculations for saturation, slope, and relative permeability with the values at the previous time step or last iterate, the calculations were more stable than by an unweighted calculation at the present time step. The use of this routine eased the values of these various parameters up to the values desired at the present time step. This eliminated any sharp change in the values of these coefficients. The use of this particular scheme enhanced computational stability of the routine.

The various coefficients necessary to solve the differential equations are calculated next. The Thomas algorithm is then used to calculate the dependent variable.

Fig. 3 shows the calculation molecule used to determine values of the dependent variable. The routine starts at the lower left and moves to the lower right calculating values of $P_{i,j}$. The molecule then moves up a row and again calculates from left to right. $PK_{i,j+1}$ is an extrapolated value during the first iterate and the latest calculated value for subsequent iterates.

After all values of the dependent variable are calculated, a check is made for convergence. Convergence is considered achieved if all values of the last iterate of the dependent variable are within 1.0×10^{-3} of the previously calculated or extrapolated values of head.

Should the convergence criterion not be satisfied, new values of saturation, relative permeability and slope must be calculated from the latest values of the dependent variables. This iteration cycle continues until the convergence criterion is satisfied.

Once the convergence criterion is satisfied, time is incremented, new values of the dependent variable are extrapolated, and the routine as outlined above begins again.

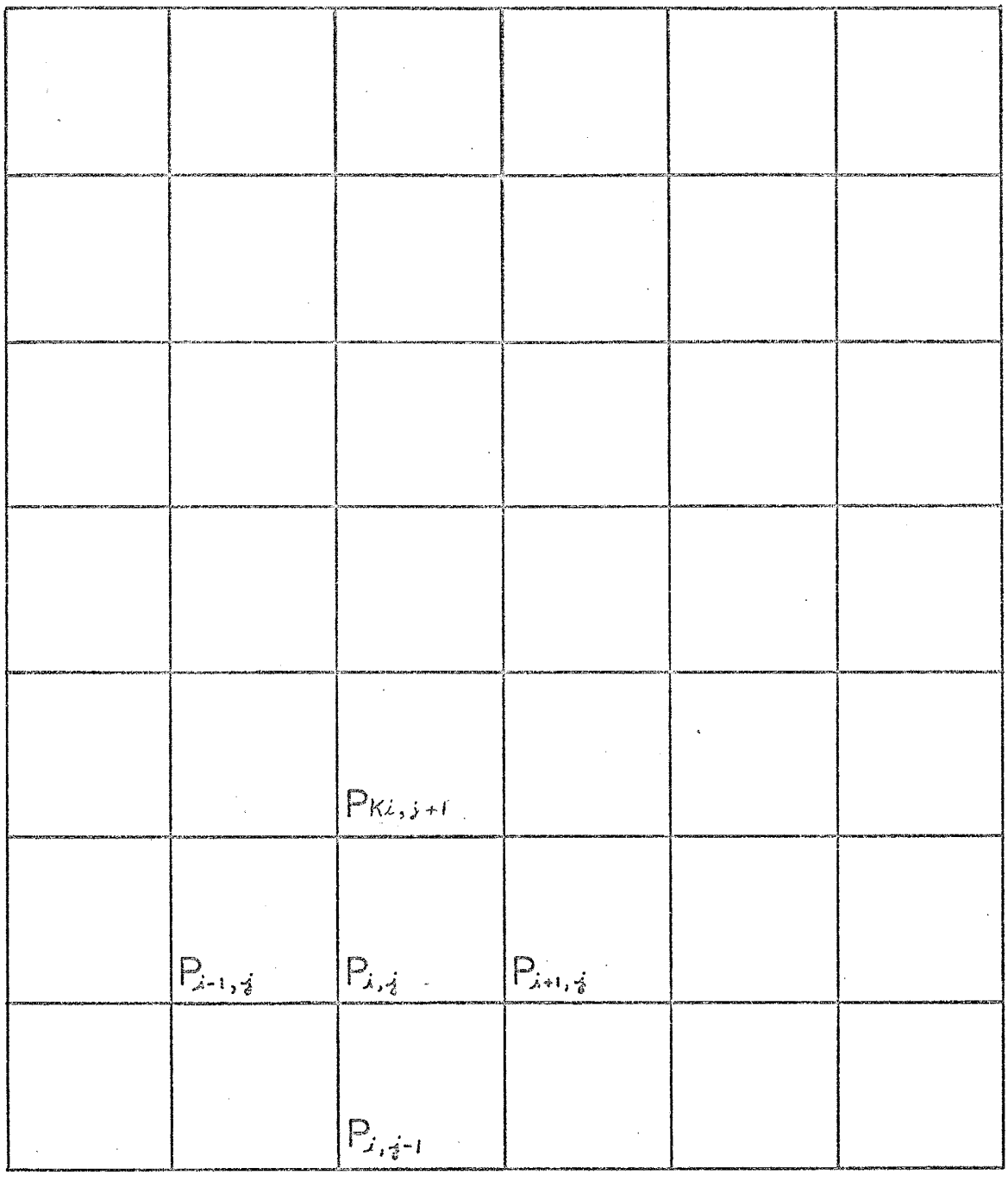

FIG. 3

Calculation molecule

Physics of the Problem

The system analyzed is that of an axisymmetric well fully penetrating a homogeneous and isotropic confined aquifer. The aquifer is infinite in areal extent and the initial head distribution is constant. The aquifer skeleton is sand with a porosity of 30 percent. The system is initially 100 percent saturated with water. The formation thickness is 30 feet and the well diameter one foot. The initial head in the aquifer is 100 feet.

The density of water is one gram per cubic centimeter, and air 1.226×10^{-3} grams per cubic centimeter. The viscosity of water is 1.124 centipoises and air 0.017 centipoises.

Muskat (1946) derived the equation for compressible gas flow. The power of the dependent variable is derived in terms of a polytropic relation (see Appendix A, Eqs. (3) and (4)). Raising the dependent variable to the $1+m$ power, where $m=0$, corresponds to treating gas as an incompressible fluid. For isothermal expansion $m=1$, and for adiabatic flow, m is the ratio of specific heat at constant volume to specific heat at constant pressure ($m=C_v/C_p$). A value of $m=0.7$ approximately corresponds to the ratio of specific heats for air. A value of $m=0.6$ or 0.8 is used for gases, or mixtures of gases, that may be available for injection. The isothermal case is not treated because a complete thermodynamic description was not included in the formulation of the differential equations and was therefore beyond the scope of this work. The viscosity of both phases is constant.

The physical constants for the various parameters are consistent with values found in a handbook of physical constants. The parameters of the aquifer itself, porosity, saturated thickness and well diameter, are similar to those found in many groundwater basins. The model did not treat the compressibility of the aquifer skeleton, or the compressibility of water. The average compressibility factor used in a confined aquifer for the expansion or contraction of the aquifer skeleton and the expansion or contraction of water is in the range of 10^{-3} to 10^{-5}, which is insignificant.

Air is injected into the reservoir, and the head and saturation distribution are calculated as a function of space and time. Two techniques may be used to inject air into the aquifer. One technique is to inject air at a constant mass rate per time, which results in pressure at the well face constantly increasing with time. Another technique is to hold a constant pressure on the well face. A constant well face pressure results in a diminishing mass rate per time as the pressure in the aquifer builds up.

To hold a constant pressure at the well face is consistent with using centrifugal compressor equipment that is designed to deliver a specific volume of air at a constant pressure. A constant mass rate of injection is consistent with using positive displacement equipment designed to deliver air at a constant mass rate and a variable pressure. The two techniques are then consistent with using equipment presently available in industry. The range of parameters for the various cases covered in the study was chosen to take into account real aquifer situations. Thus the results obtained should apply to a typical well subject to injection.

Results

Three physical parameters were varied over a practical range in the study. In addition, the grid parameter, $u = \log r$, was varied to show the effect of grid size on the numerical forms. Zone sizes corresponding to Δu of 0.3 and 0.4 were used in the r direction. Specific permeabilities of 1, 2.5, and 4 darcys were chosen. The values of the variable m, which is the inverse of the polytropic gas constant for the compressible phase, were 0.0, 0.6, 0.7, and 0.8. Two techniques of injection were studied, constant pressure injection, and a constant mass rate of injection. The constant pressure injection studies included constant well face pressures of 220 and 300 lb/in.^{2}, while the constant mass rate injection was 0.1 lb/sec. Since it is not feasible to show the results of all these calculations, seven representative cases (see Table 1) were chosen to show the effect of the parameters changed. The calculation showing the gas as an incompressible phase is shown as one of the seven. With constant pressure injection, changes in specific permeability within the range taken did not show differences plottable on the scales used.

In Figures 4 through 29, the graphs are vertical cross sections with the zero ordinate being the well. All values of saturation represent percent water saturation. Figures 4 through 7 show saturation distributions for various intervals of time. Figures 8, 9, and 10 display values of head for specified intervals of time.

It is easily noted in the saturation profiles that, as the radial velocity of the injected gas decreases, buoyancy becomes predominant, resulting in a curved air-water interface.

Table 1

Coefficients of Cases Considered

Case	C_v/C_p	u(spacing)	k	Injection rate	Injection pressure	Comment
1	0.7	0.3	4 darcy	0.1 lb/sec		
2	0.0	0.3	4 darcy	0.1 lb/sec		
	0.7	0.3	4 darcy	0.1 lb/sec		
3	0.7	0.3	1 darcy		220 PSI	
3a	0.7	0.3	2.5 darcy		220 PSI	Differences between cases 3 and 3a not plottable on scale used.
4	0.7	0.3	2.5 darcy		300 PSI	
5	0.7	0.3	4 darcy		300 PSI	
6	0.6	0.4	4 darcy		300 PSI	
6a	0.6	0.3	4 darcy		300 PSI	Differences between cases 5 and 6a not plottable on scale used.
7	0.8	0.4	4 darcy		300 PSI	
7a	0.8	0.3	4 darcy		300 PSI	Differences between cases 5 and 7a not plottable on scale used.

CASE 1. The formation has an absolute permeability of 4.0 darcys. Gas is being injected at the well face at a constant rate of 0.1 pound of mass per second.

In this solution for the differential equations, the dependent variable in the gas equation is raised to the power $1+m$, where m is 0.7. Raising the power of the dependent variable to 1.7 is considered to be a sufficiently accurate solution for adiabatic expansion of air being injected into water.

Case I

m = 0.7 k = 4 darcys Injection rate = 0.1 lb/sec

t = 444 sec

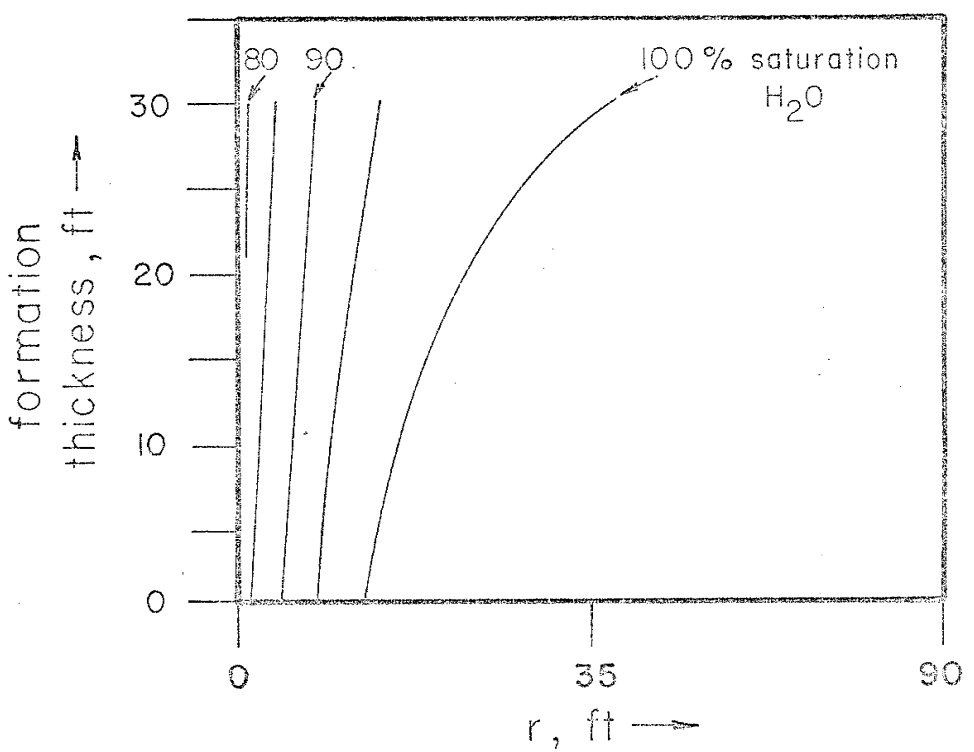

FIG. 4

Case 1

m = 0.7 k = 4 darcys Injection rate = 0.1 lb/sec

t = 1625 sec

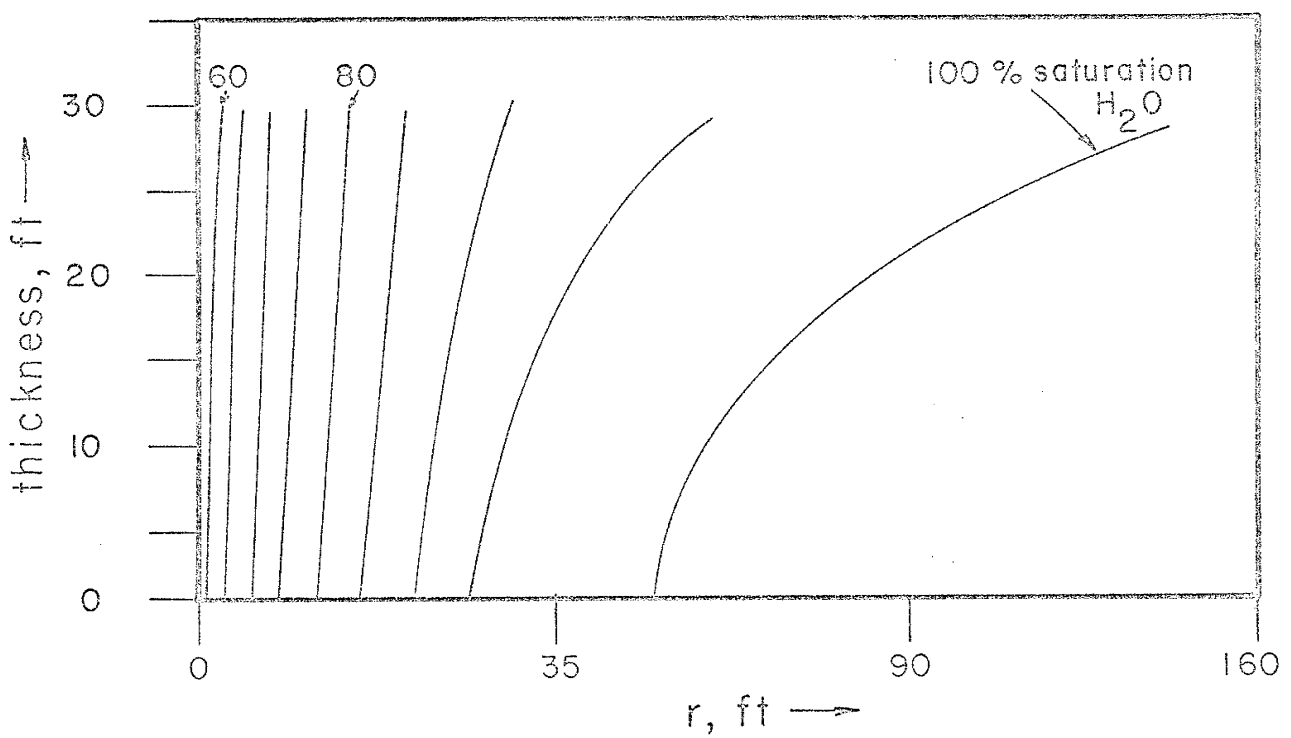

FIG. 5

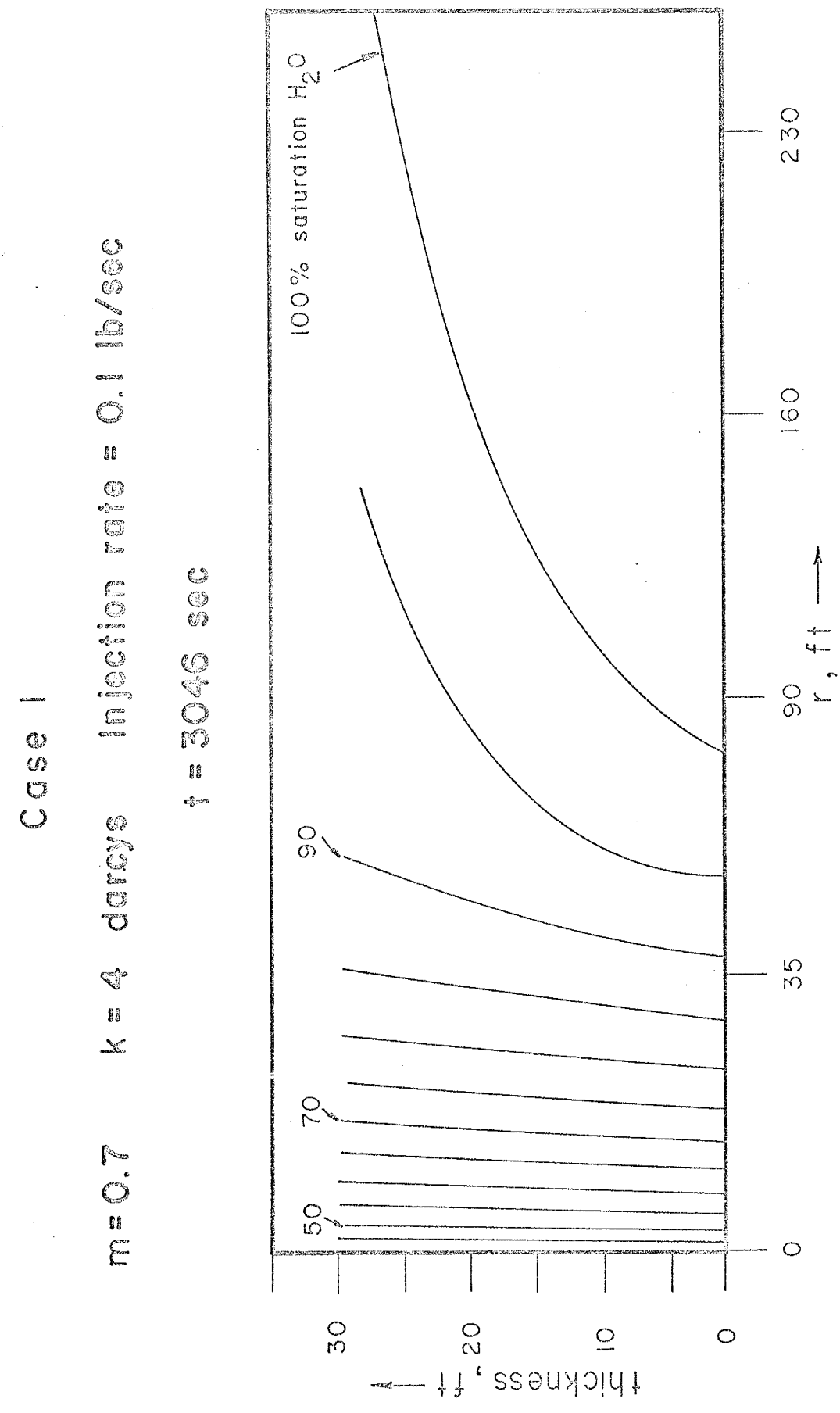
Case I
m=0.7 k=4 darcys Injection rate = 0.1 lb/sec
t = 3046 sec
100% saturation H_2O
90
70
50
thickness, ft
30
20
10
0
0
35
90
160
230
r, ft

FIG. 6

Case 1

m = 0.7 k = 4 darcys Injection rate = 0.1 lb/sec

t = 7284 sec

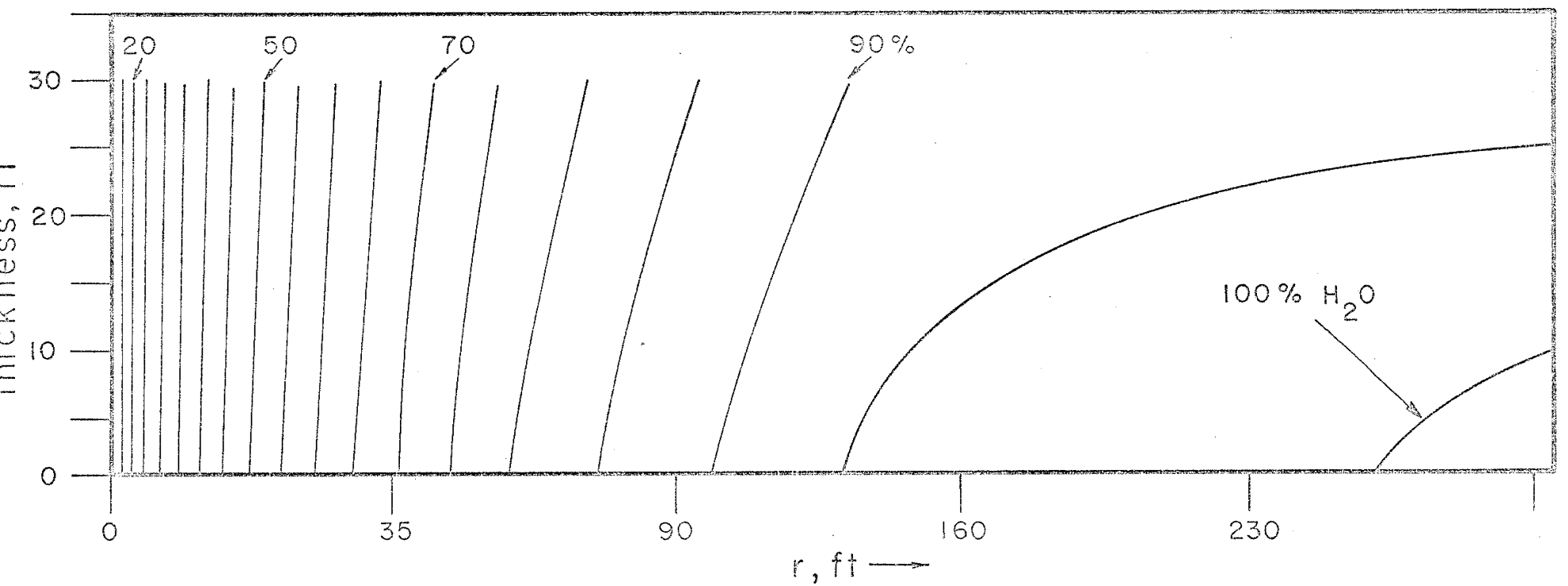

FIG. 7

Case 1

m = 0.7 k = 4 darcys Injection rate = 0.1 lb/sec

t = 444 sec

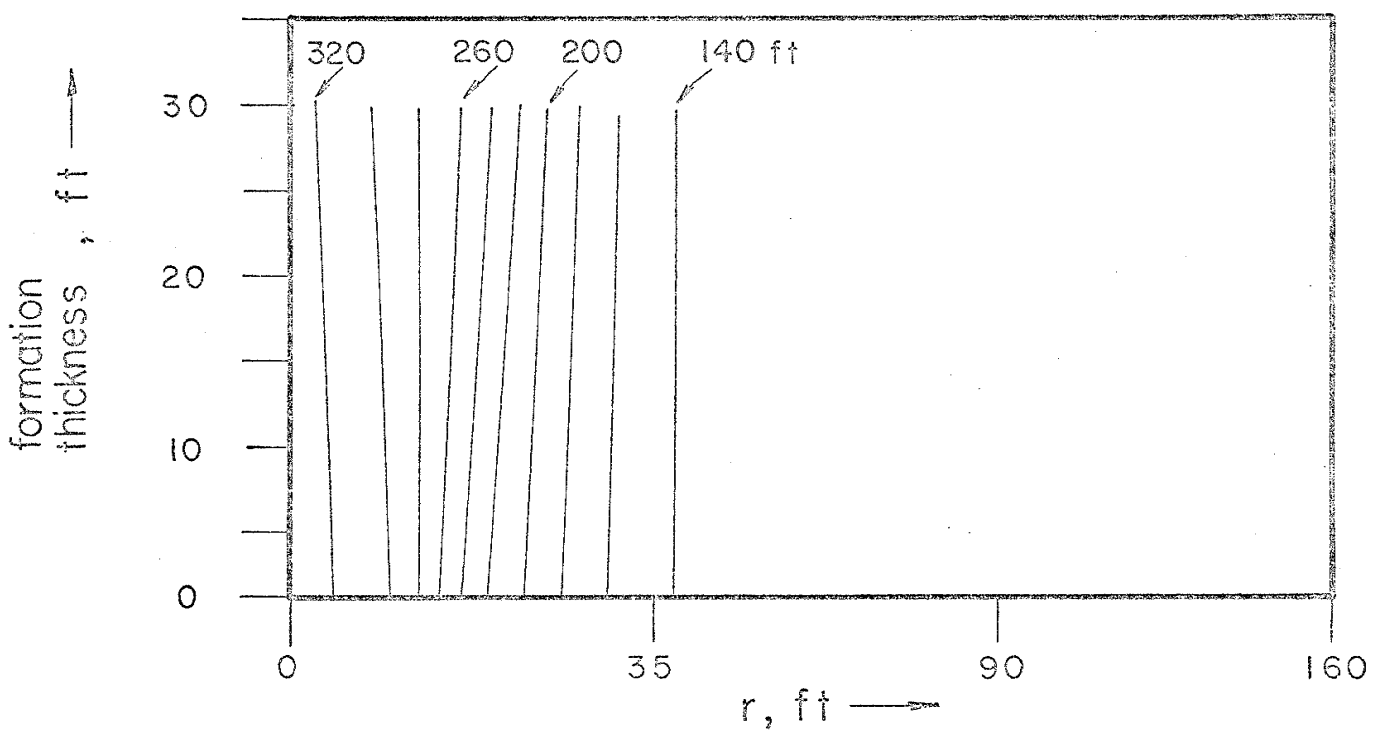

FIG. 8

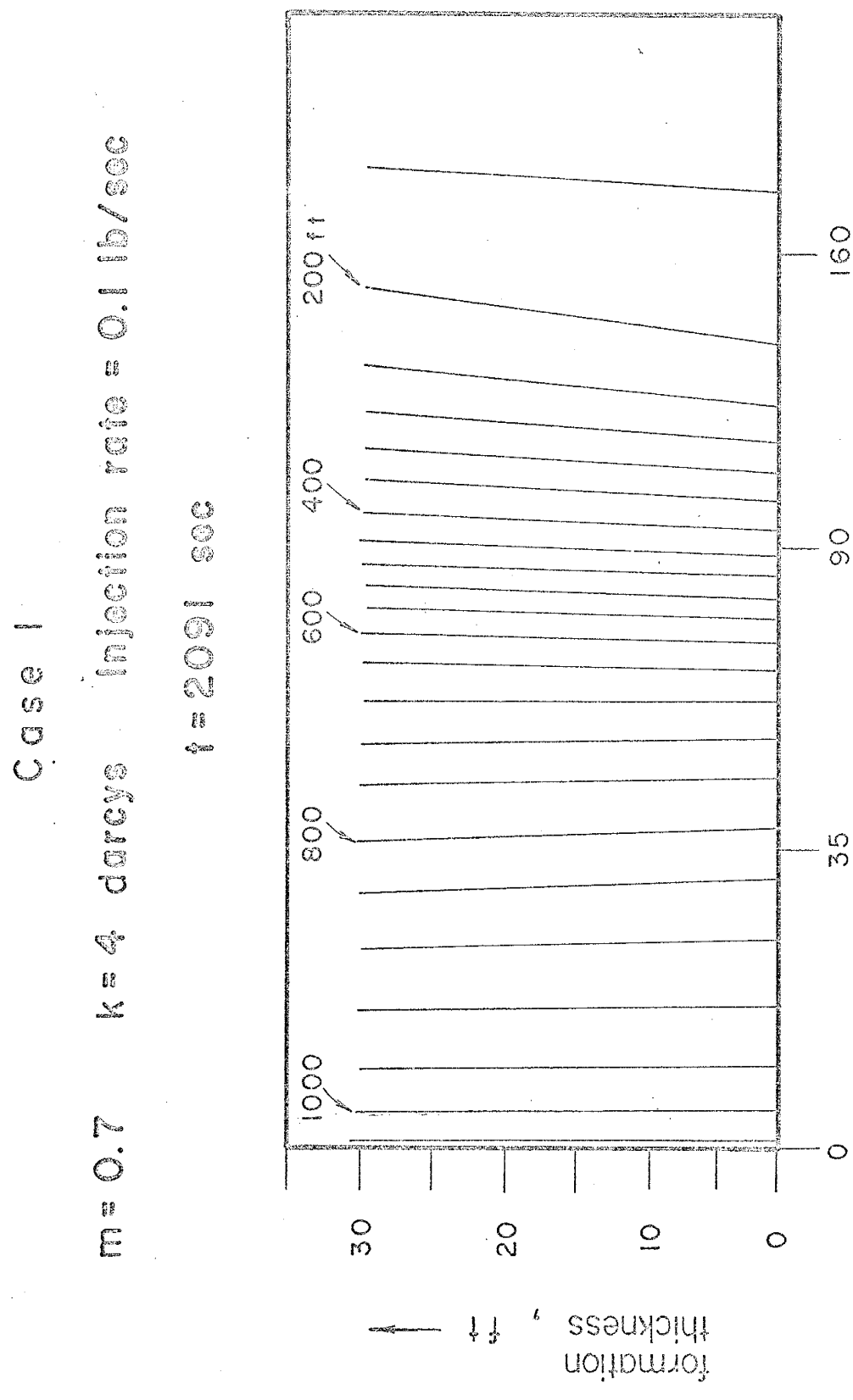
Case I
m = 0.7 k = 4 darcys injection rate = 0.1 lb/sec
t = 2091 sec
formation thickness, ft
30
20
10
0
1000
800
600
400
200 ft
0
35
90
160
r, ft

FIG. 9

Case 1

m = 0.7 k = 4 darcys Injection rate = 0.1 lb/sec

t = 3452 sec

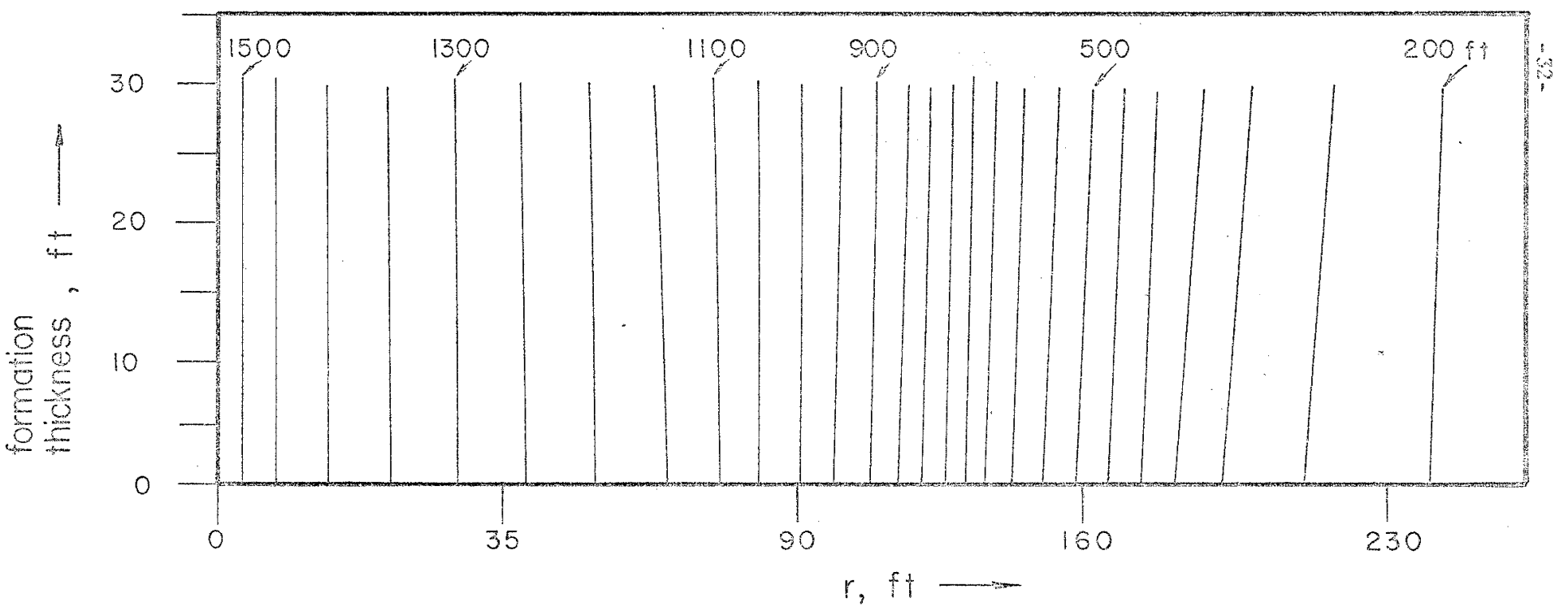

FIG. 10

CASE 2. The formation has an absolute permeability of 4.0 darcys. Gas is being injected at the well face at a constant rate of 0.1 pounds per second.

This case is a direct comparison between gas being compressible ($m = 0.7$) and incompressible ($m = 0.0$). Comparing equal saturation profiles for the same time, it is noted that a significant difference exists in radial growth. This difference is due to the consideration of compressibility in the gas phase.

Figures 11 through 14 compare saturation profiles for compressible and incompressible gas. All physical constants are the same in the comparisons.

Case 2

Injection rate = 0.1 lb/sec

k = 4 darcys

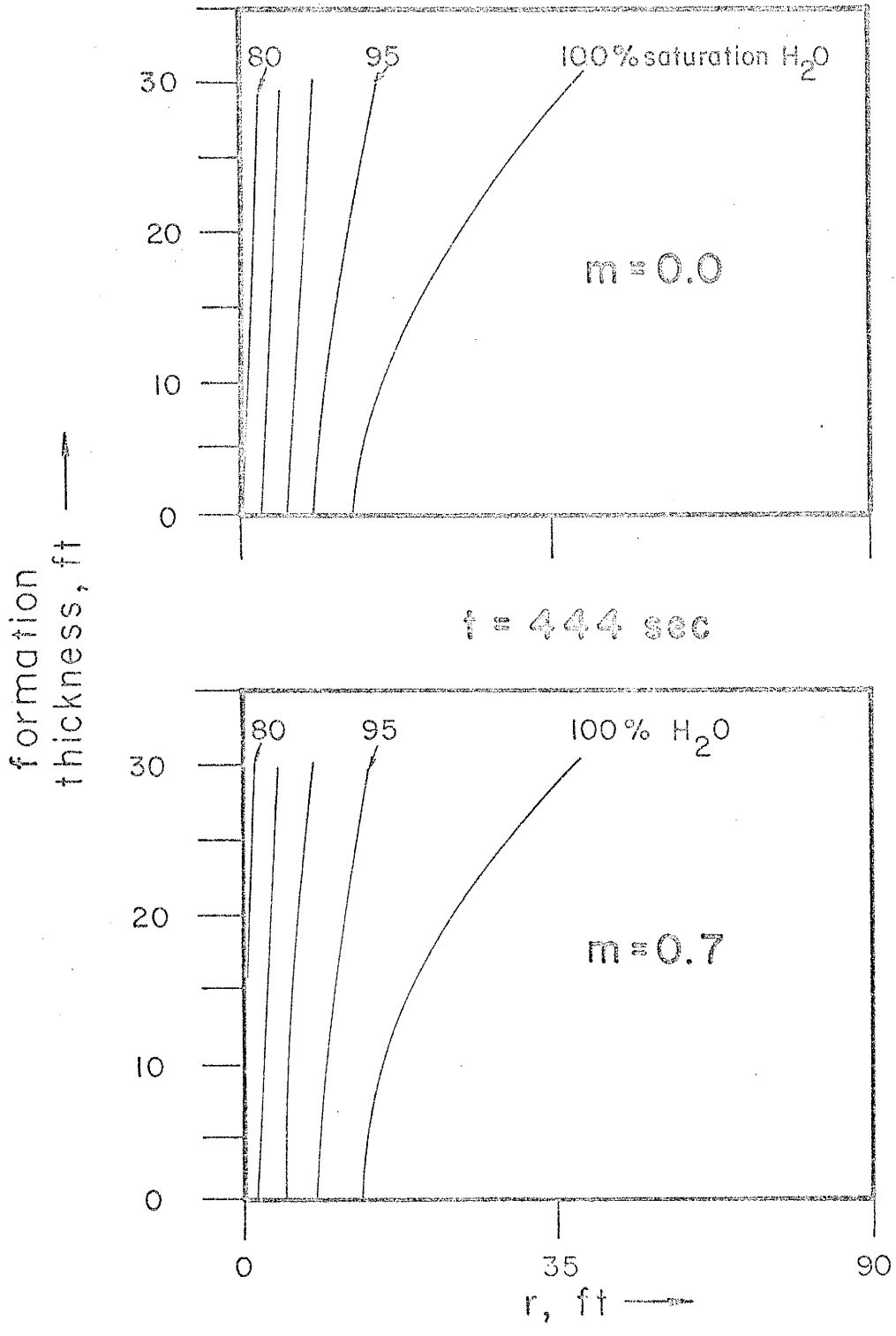

FIG. 11

Case 2

Injection rate = 0.1 lb/sec

k = 4 darcys

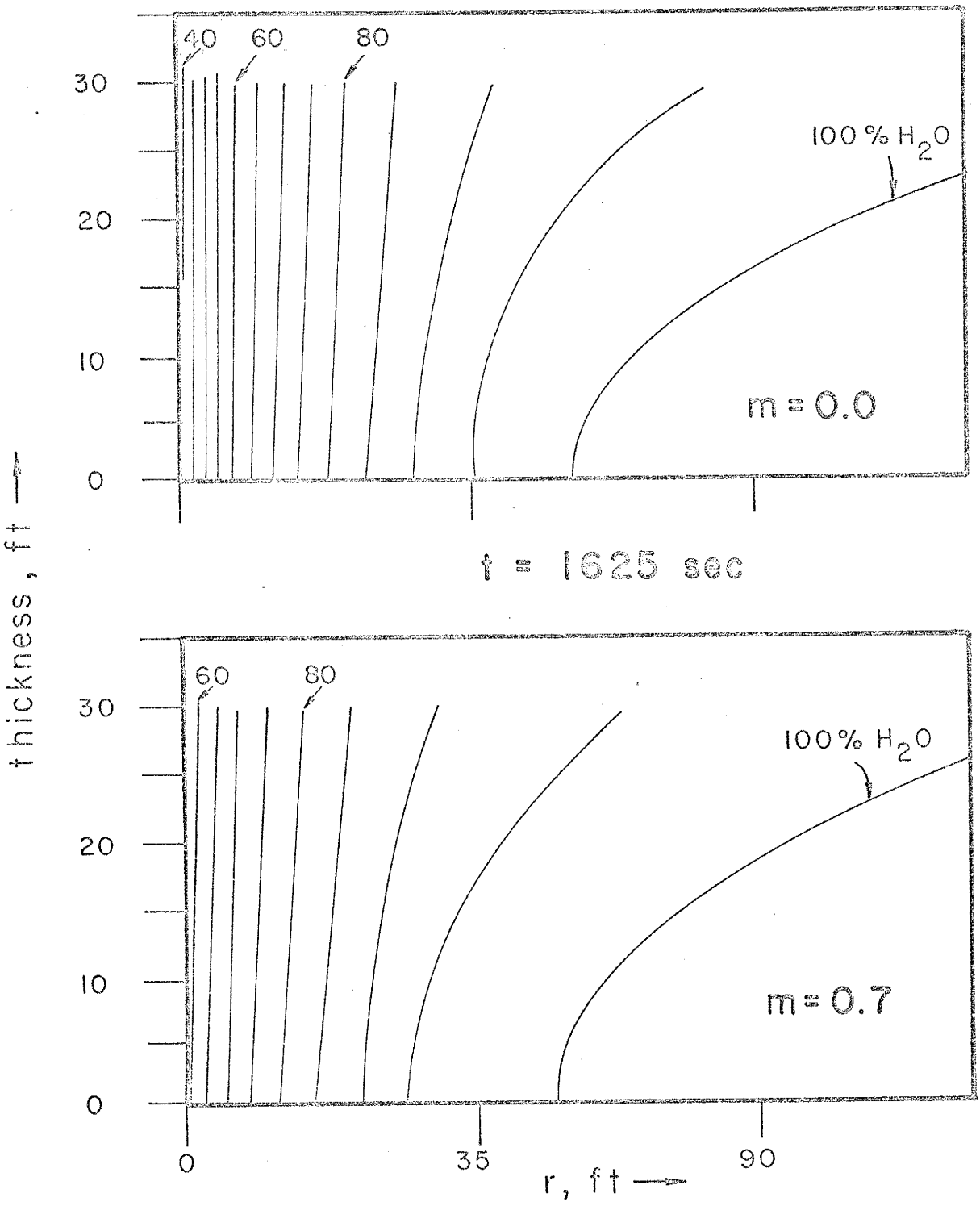

FIG. 12

Case 2

Injection rate = 0.1 lb/sec

k = 4 darcys

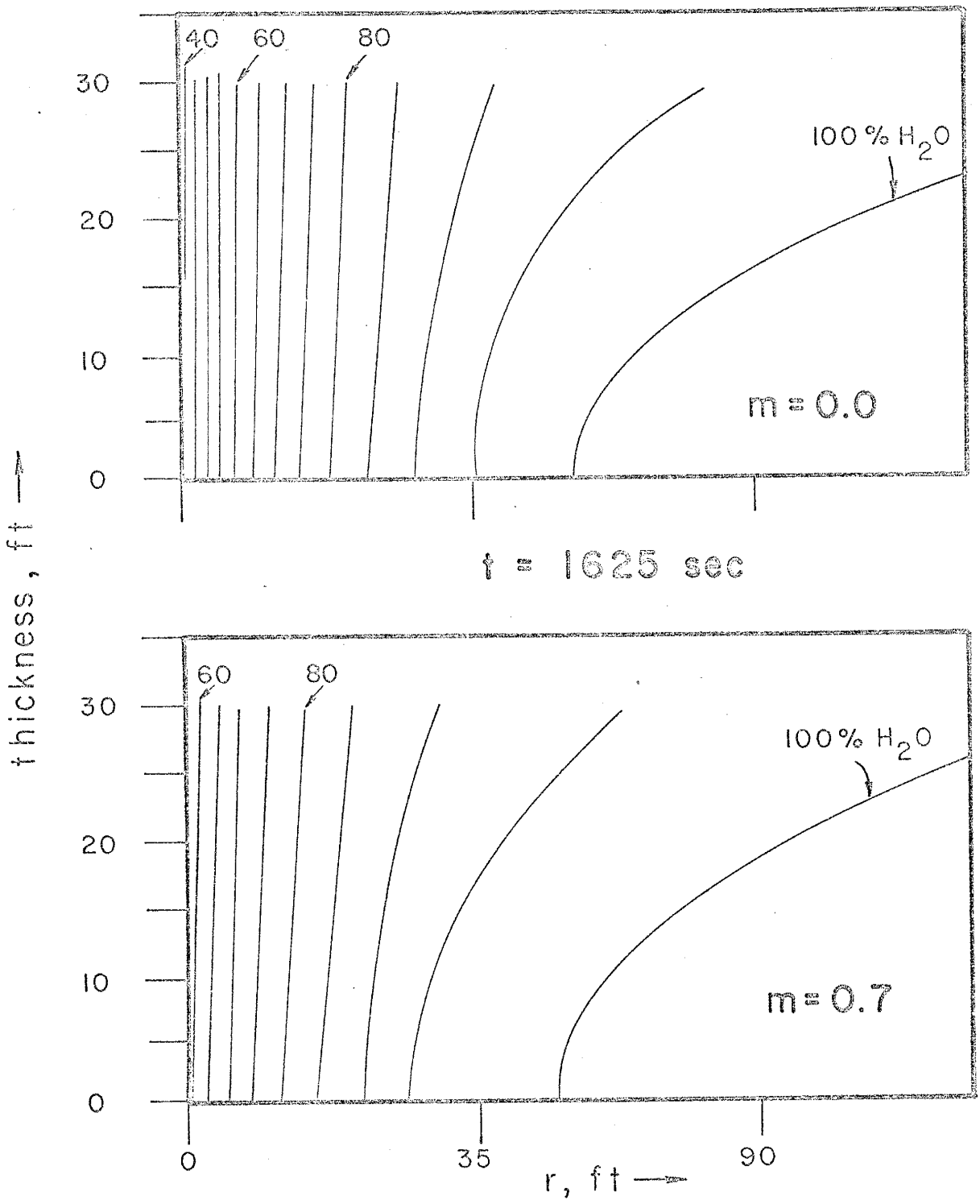

FIG. 12

Case 2

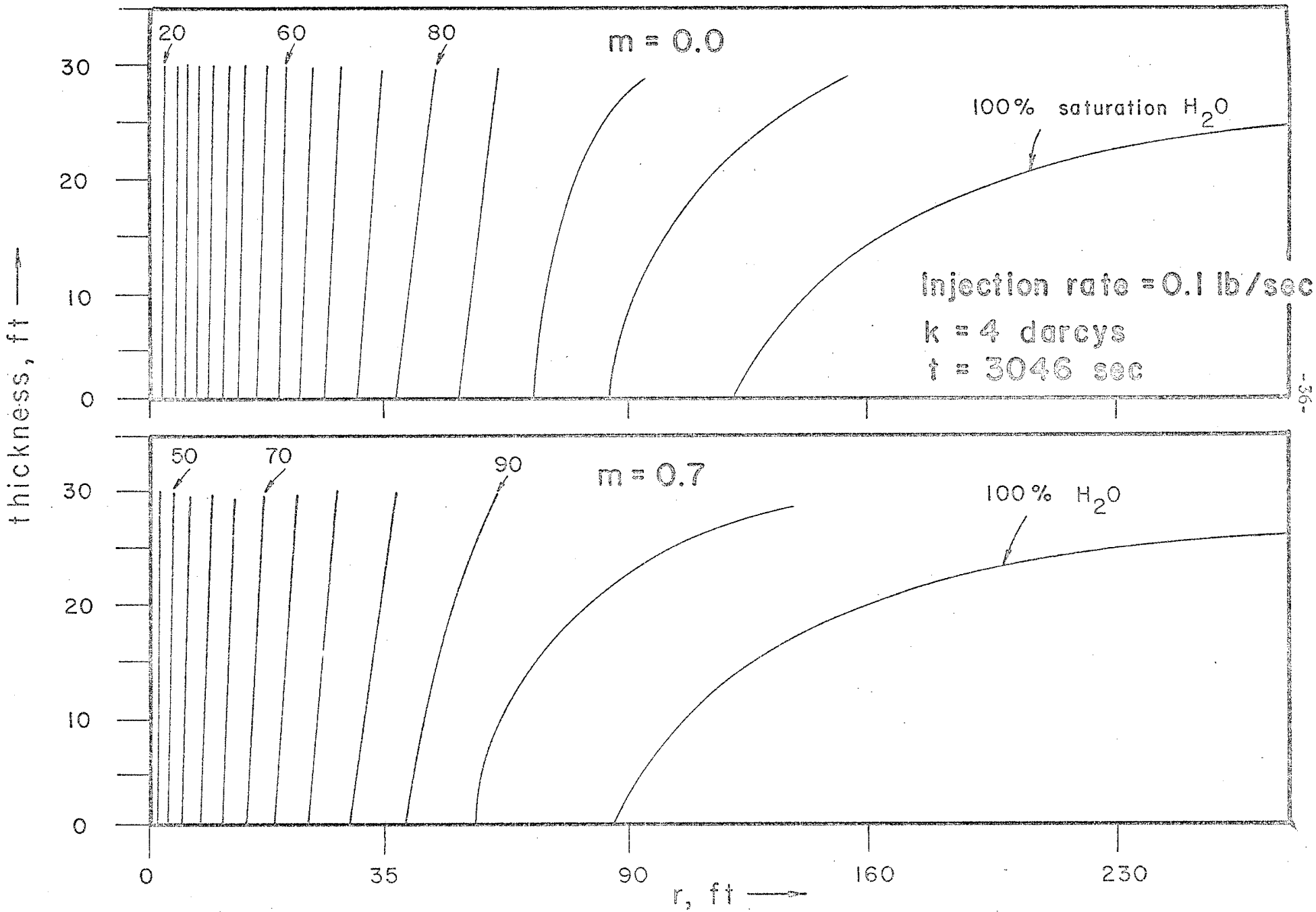
20
60
80
m = 0.0
100% saturation H_2O
Injection rate = 0.1 lb/sec
k = 4 darcys
t = 3046 sec
50
70
90
m = 0.7
100% H_2O
thickness, ft
30
20
10
0
0
35
90
160
230
r, ft

FIG. 13

Case 2

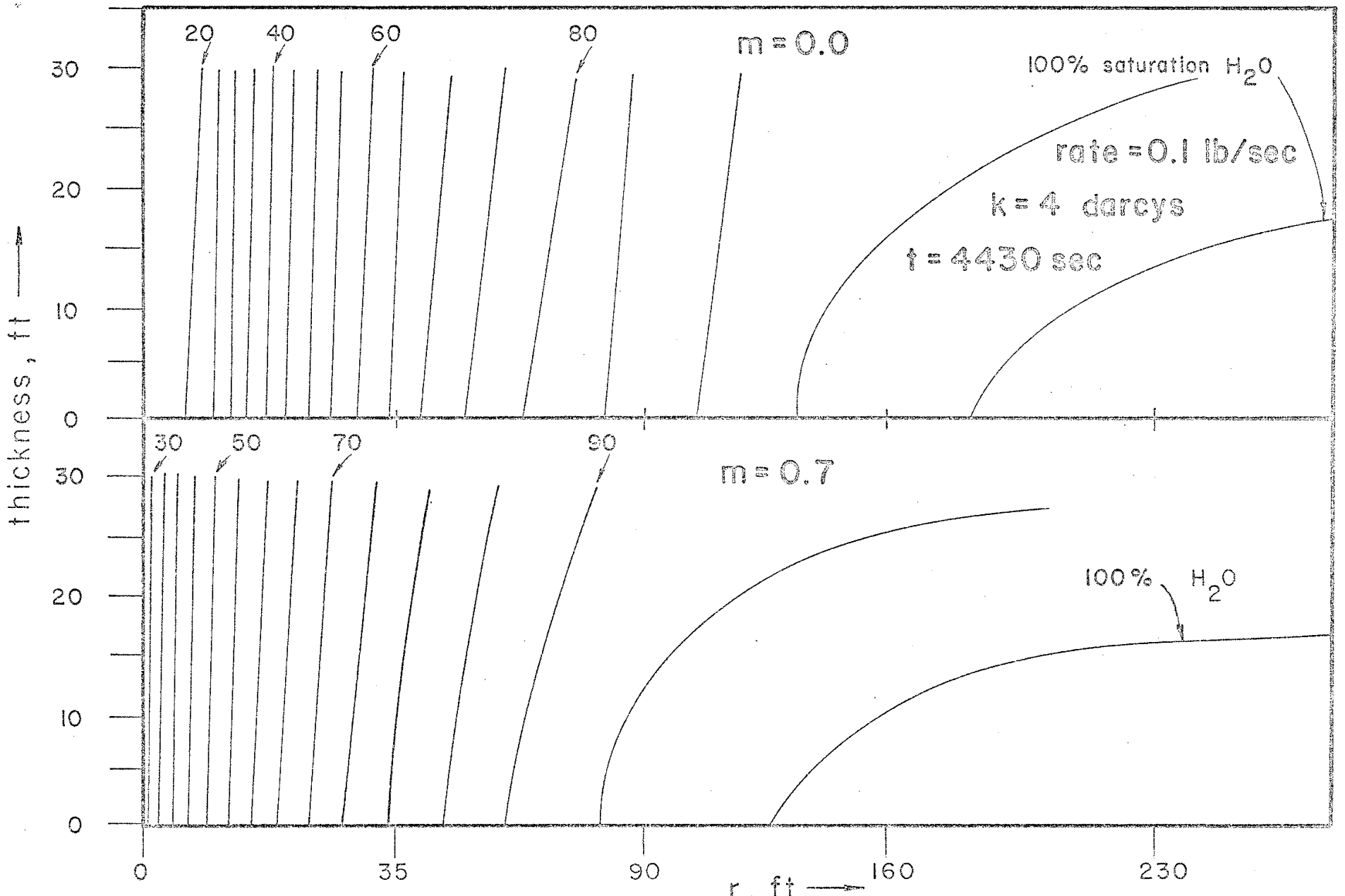
20
40
60
80
m = 0.0
100% saturation H_2O
rate = 0.1 lb/sec
k = 4 darcys
t = 4430 sec
30
50
70
90
m = 0.7
100% H_2O
thickness, ft
r, ft
0
10
20
30
35
90
160
230

FIG. 14

CASE 3. The formation has an absolute permeability of 1.0 darcy. The injection pressure is held at a constant 220 pounds per square inch. The dependent variable in the gas equation is raised to $m + 1 = 1.7$.

In Cases 3 through 7 the pressure at the interior boundary or well face is brought up by the relation:

$$p_f = p_o + p_x \left[1.0 - \exp\left(\frac{t_o}{c}\right)\right]$$

where:

p_f = pressure at the well face

p_o = initial pressure

p_x = ultimate well face pressure

t_o = time from start of injection

c = some constant with units of time

Use of the above expression allowed the well face pressure to be brought up in a physically reasonable period of time. In Case 3 the value of c was 50 seconds.

It should be noted that a constant well face pressure means a variable mass injection rate.

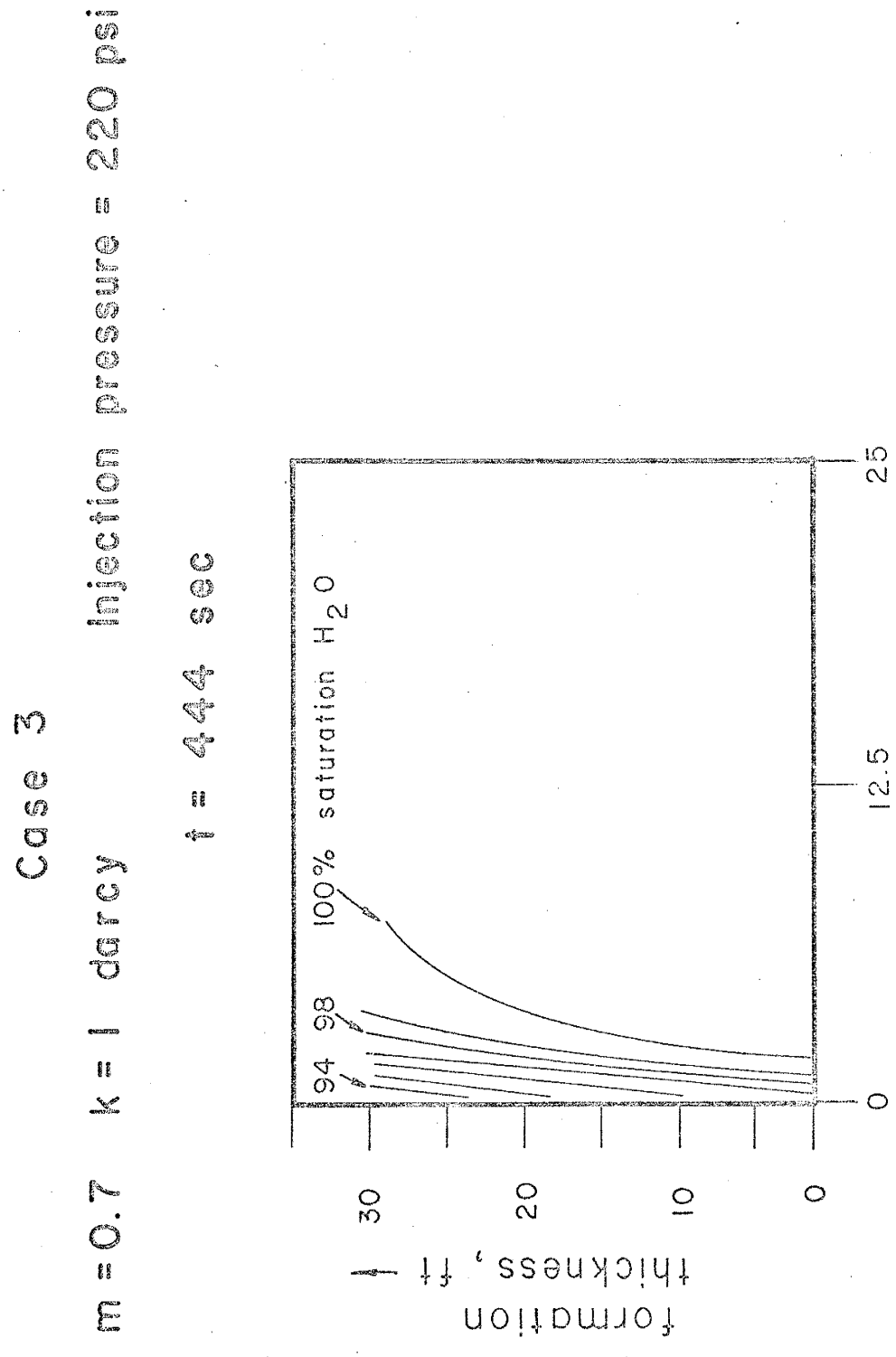
Case 3
m = 0.7 k = 1 darcy
injection pressure = 220 psi
t = 444 sec
100% saturation H_2O
98
94
formation thickness, ft
30
20
10
0
0
12.5
25
r

FIG. 15

Case 3

m = 0.7 k = 1 darcy Injection pressure = 220 psi

t = 1260 sec

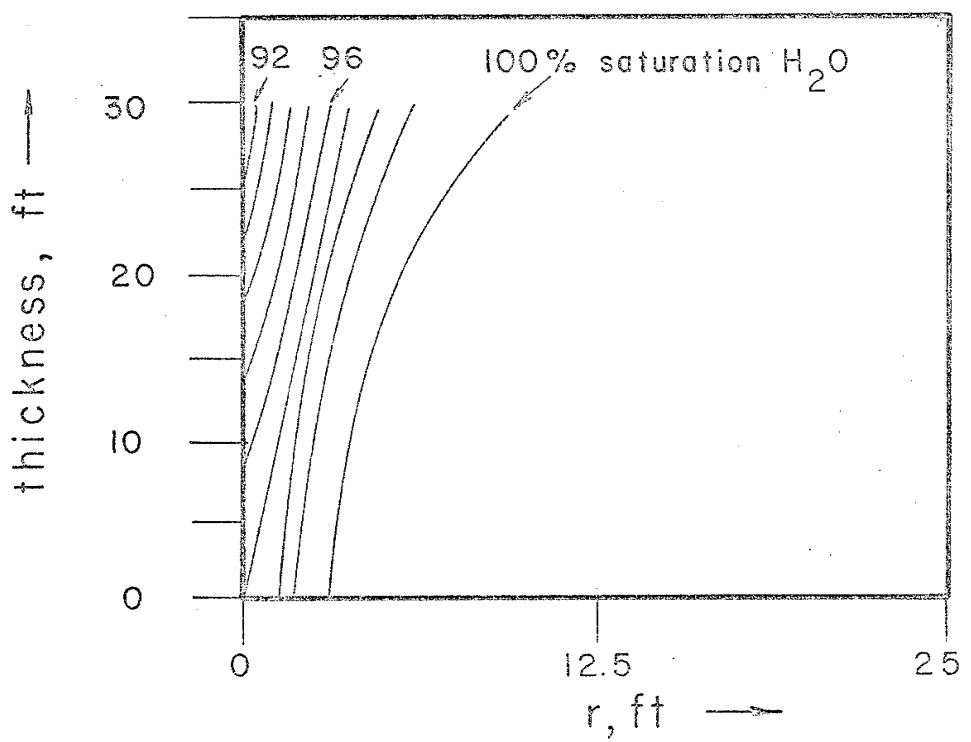

FIG. 16

Case 3

m = 0.7 k = 1 darcy Injection pressure = 220 psi

t = 2090 sec

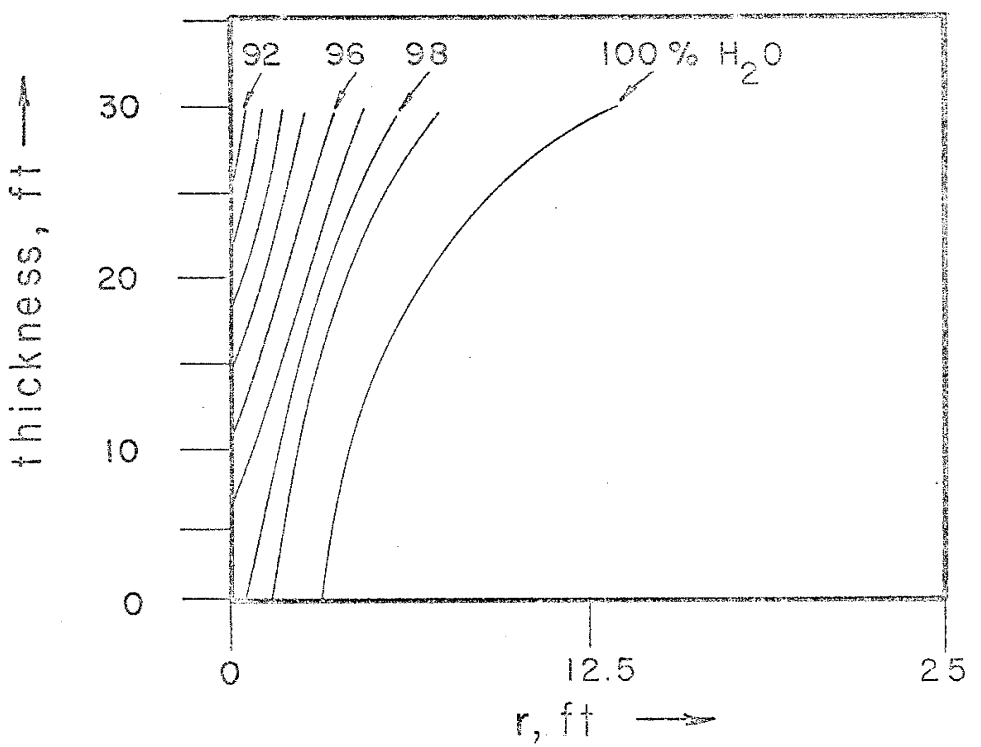

FIG. 17

CASE 4. The formation has an absolute permeability of 2.5 darcys. The injection pressure is held at a constant 300 pounds per square inch. The dependent variable in the gas equation is raised to $\underline{m + 1} = 1.7$.

Comparison between Cases 3 and 4 shows much faster radial advance of the air-water interface in Case 4. This is primarily due to the increase in well-face pressure from 220 to 300 pounds per square inch.

Case 4

m = 0.7 k = 2.5 darcys Injection pressure = 300 psi

t = 444 sec

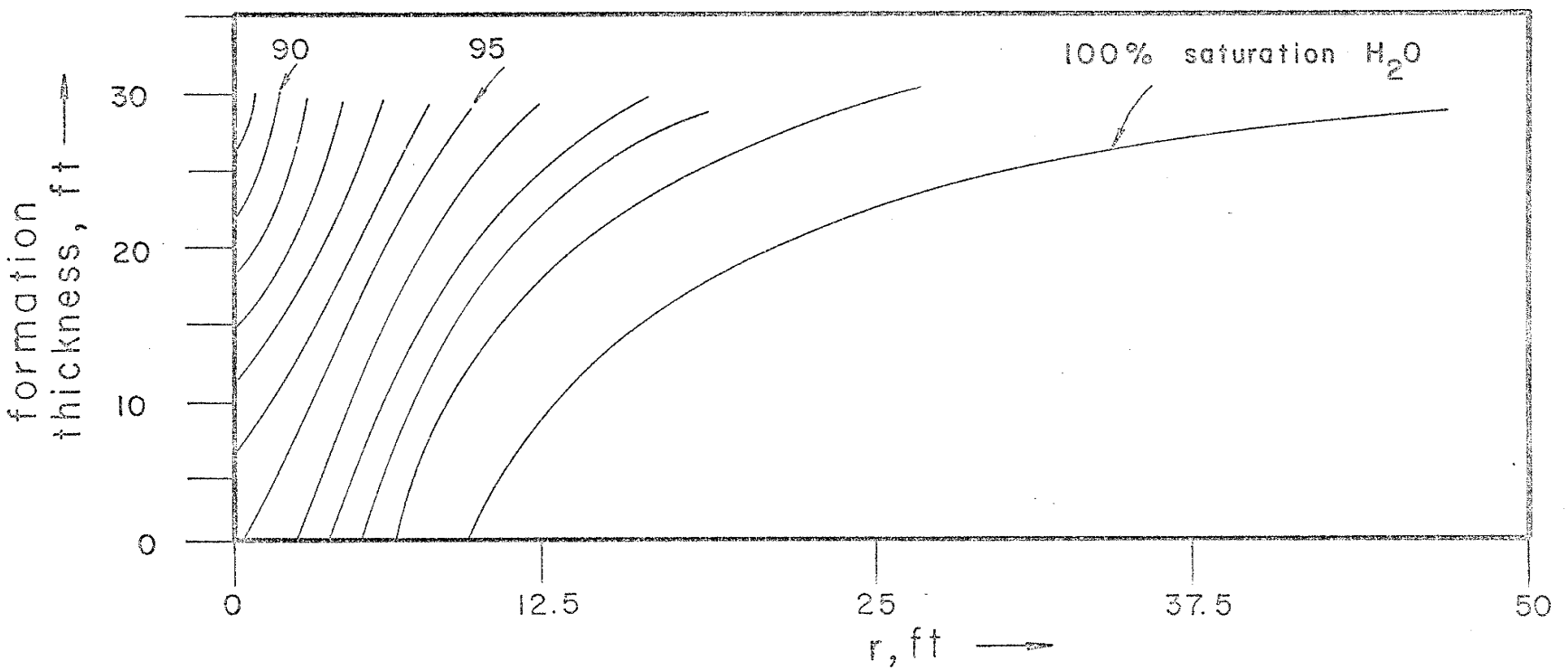

FIG. 18

Case 4

n = 0.7 k = 2.5 darcys injection pressure = 300 psi

t = 1260 sec

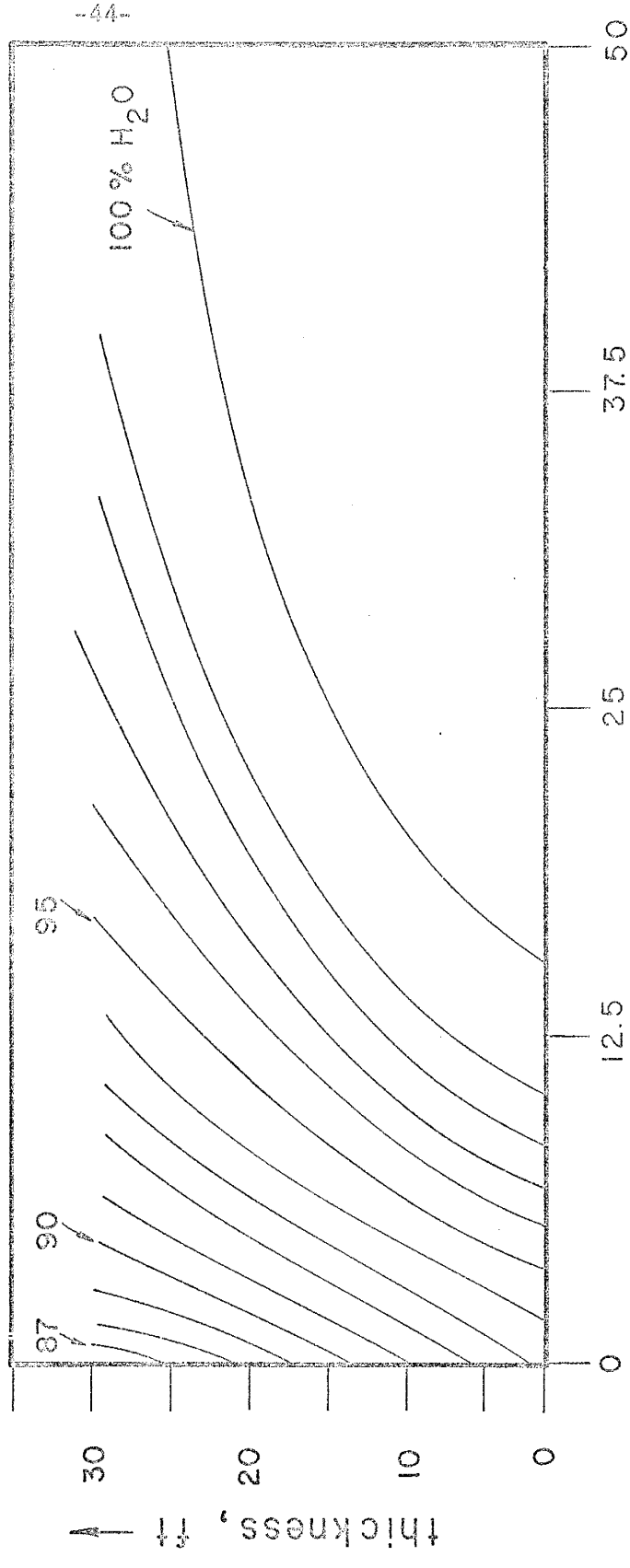

FIG. 19

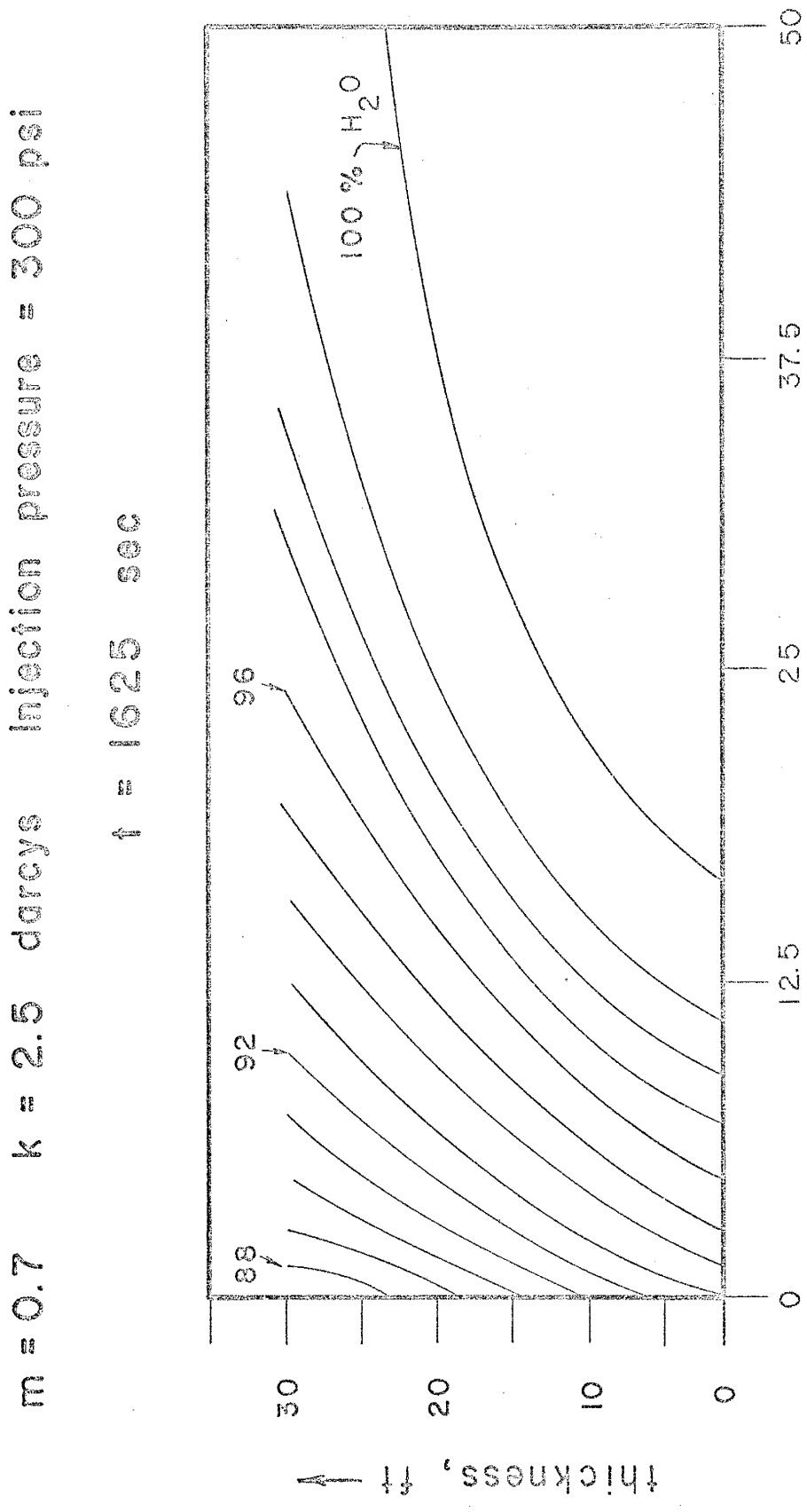
Case 4
m = 0.7 k = 2.5 darcys injection pressure = 300 psi
t = 1625 sec
100 % H_2O
96
92
88
thickness, ft
30
20
10
0
0
12.5
25
37.5
50
r, ft

FIG. 20

CASE 5. The formation has an absolute permeability of 4.0 darcys. The injection pressure is held at a constant 300 pounds per square inch. The dependent variable in the gas equation is raised to $\frac{m+1}{} = 1.7$.

Comparison between Cases 4 and 5 again shows an even greater rate of radial advance of the air-water interface in Case 5. This is due to a marked decrease in formation resistance as indicated by the increase in permeability.

Case 5

m = 0.7 k = 4 darcys Injection pressure = 300 psi

t = 444 sec

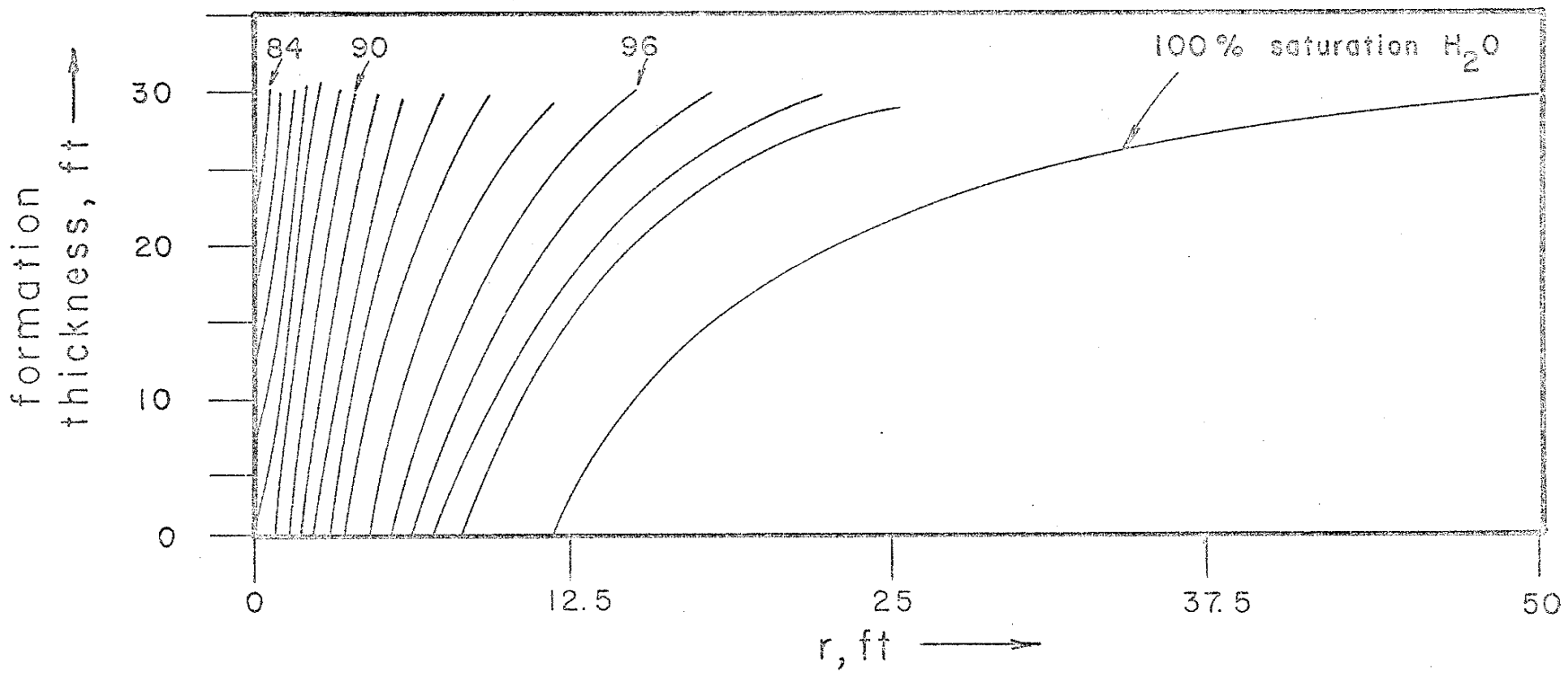

FIG. 21

Case 5

m = 0.7 k = 4 darcys Injection pressure = 300 psi

t = 1260 sec

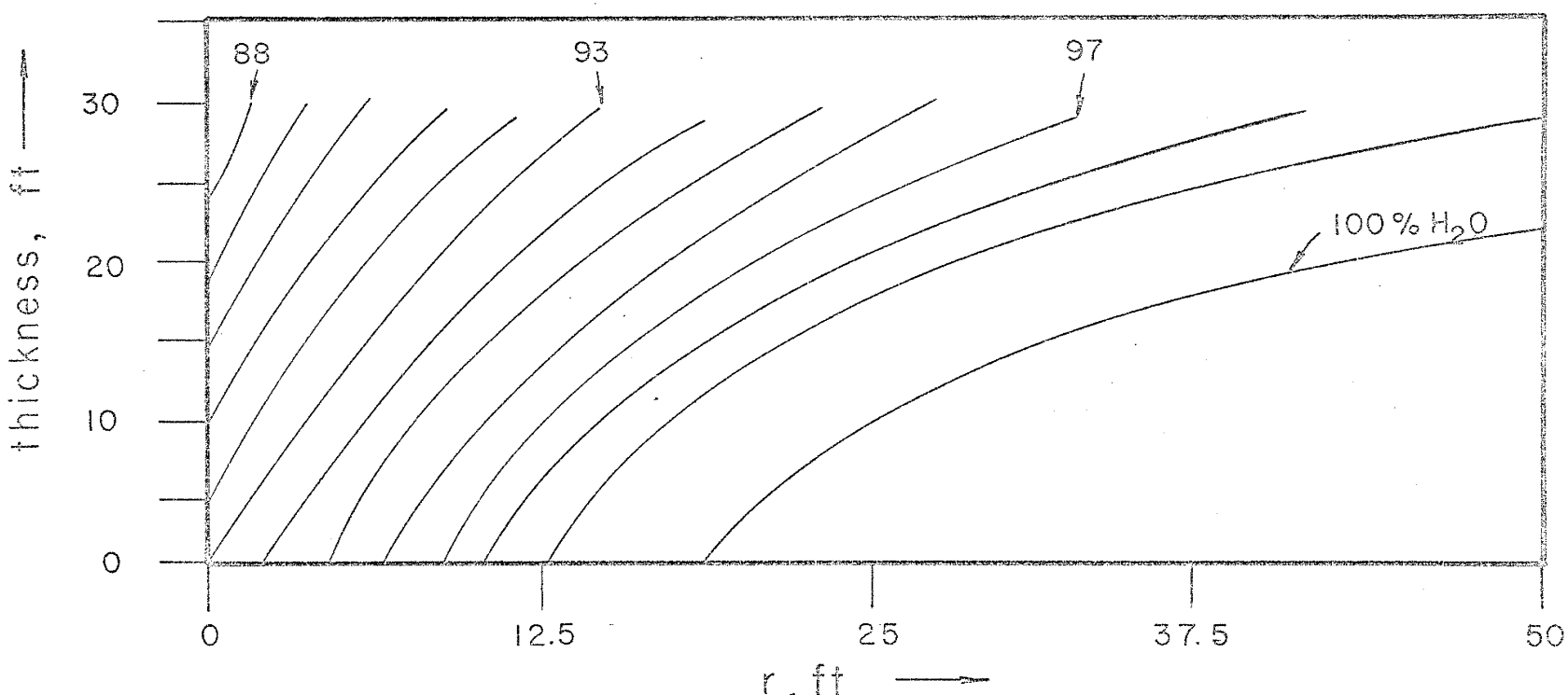

FIG. 22

Case 5

m = 0.7 k = 4 darcys Injection pressure = 300 psi

t = 2092 sec

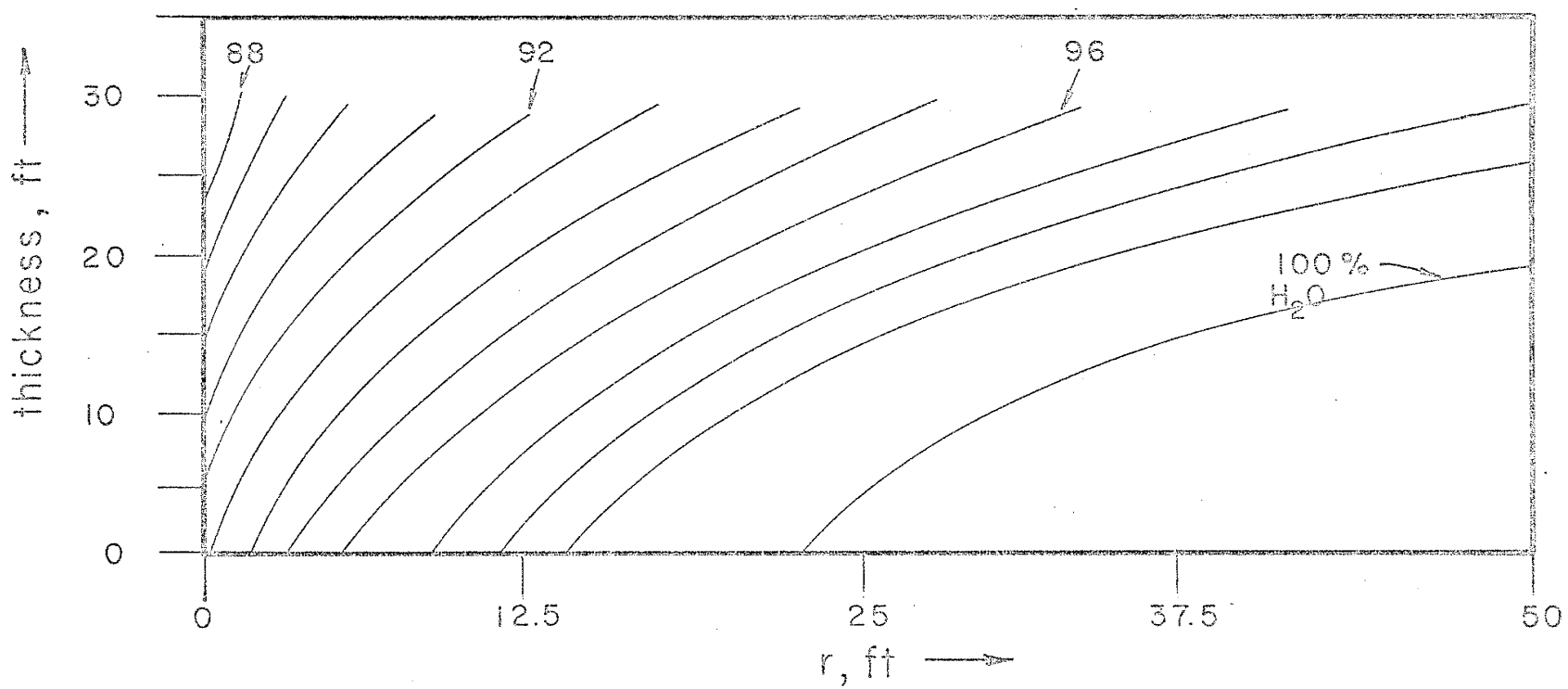

FIG. 23

CASE 6. The formation has an absolute permeability of 4.0 darcys. The injection pressure at the well face is held at a constant 300 pounds per square inch. The dependent variable in the gas equation is raised to $\underline{m} + 1 = 1.6$.

In comparing this case to Case 5, it is immediately apparent that a marked dissimilarity exists. This is due to the marked increase in mesh spacing. The radial coordinate is transformed according to the relation $u = \ln r/rw$. In Cases 3 through 5 the value of $\underline{u}$ is 0.3. In Cases 6 and 7 the value of $\underline{u}$ is 0.4.

Cases 6 and 7, included here for completeness, show that by increasing grid spacing the results become increasingly poor in comparison. The solution appears to approach a steady state very rapidly and a "bubble" shape begins to appear.

Case 6

m = 0.6 k = 4 darcys Injection pressure = 300 psi

t = 444 sec

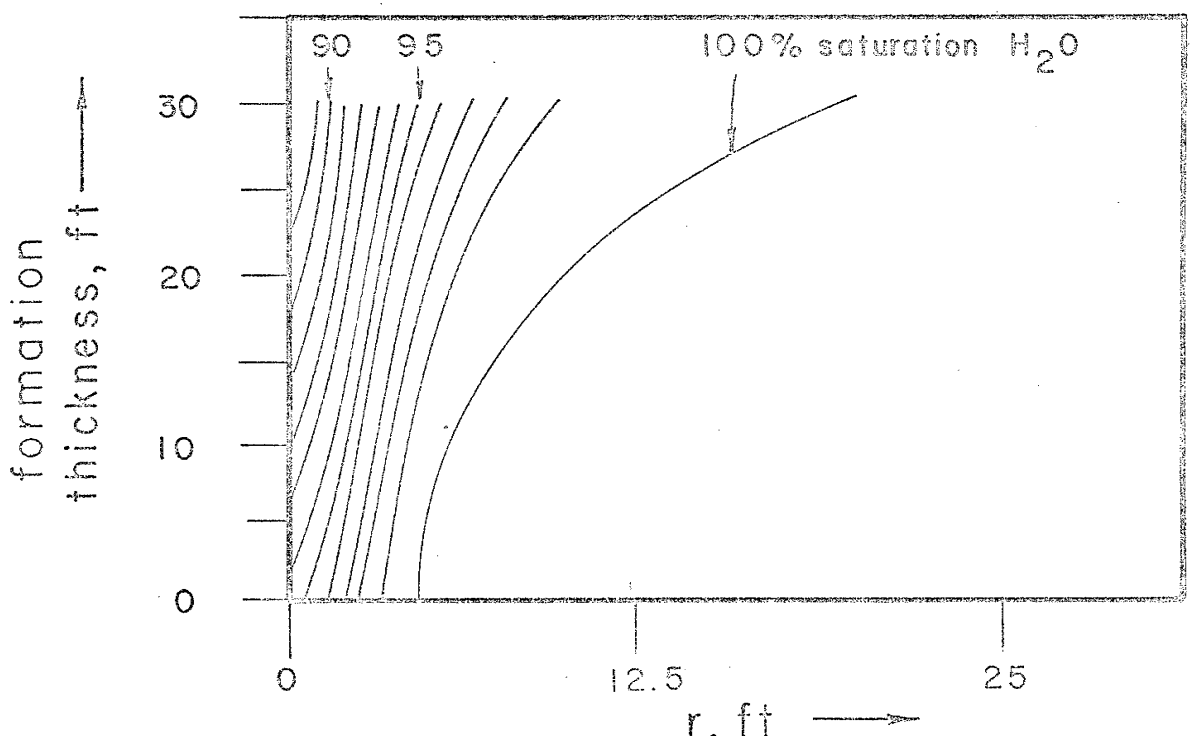

FIG. 24

Case 6

m = 0.6 k = 4 darcys Injection pressure = 300 psi

t = 1260 sec

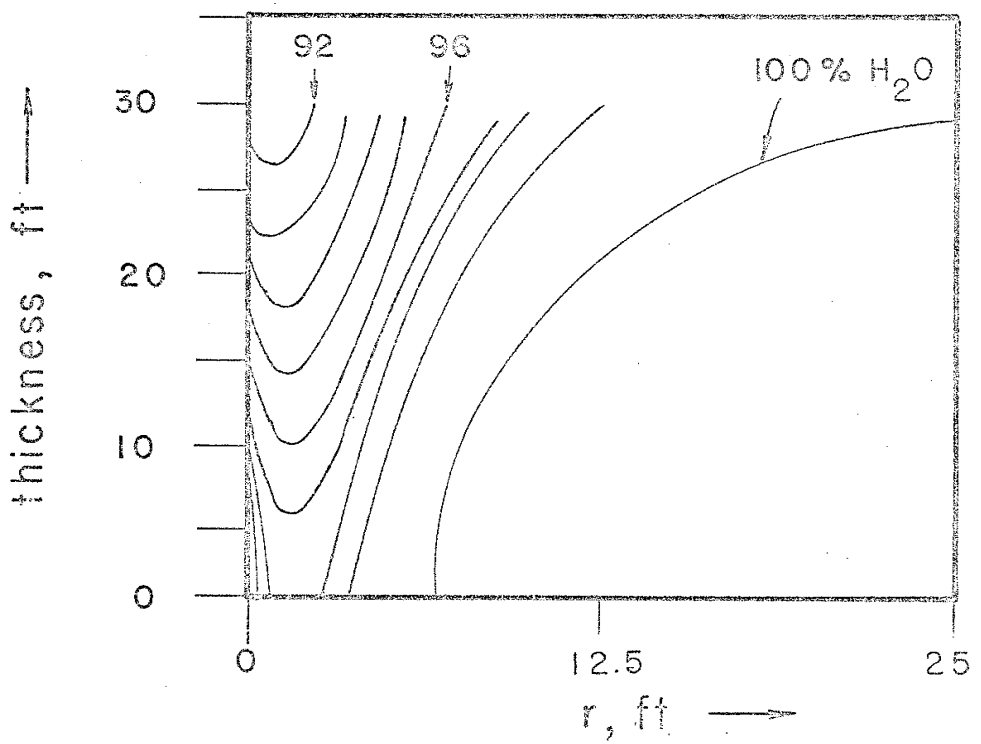

FIG. 25

Case 6

m = 0.6 k = 4 darcys Injection pressure = 300 psi

t = 2091 sec

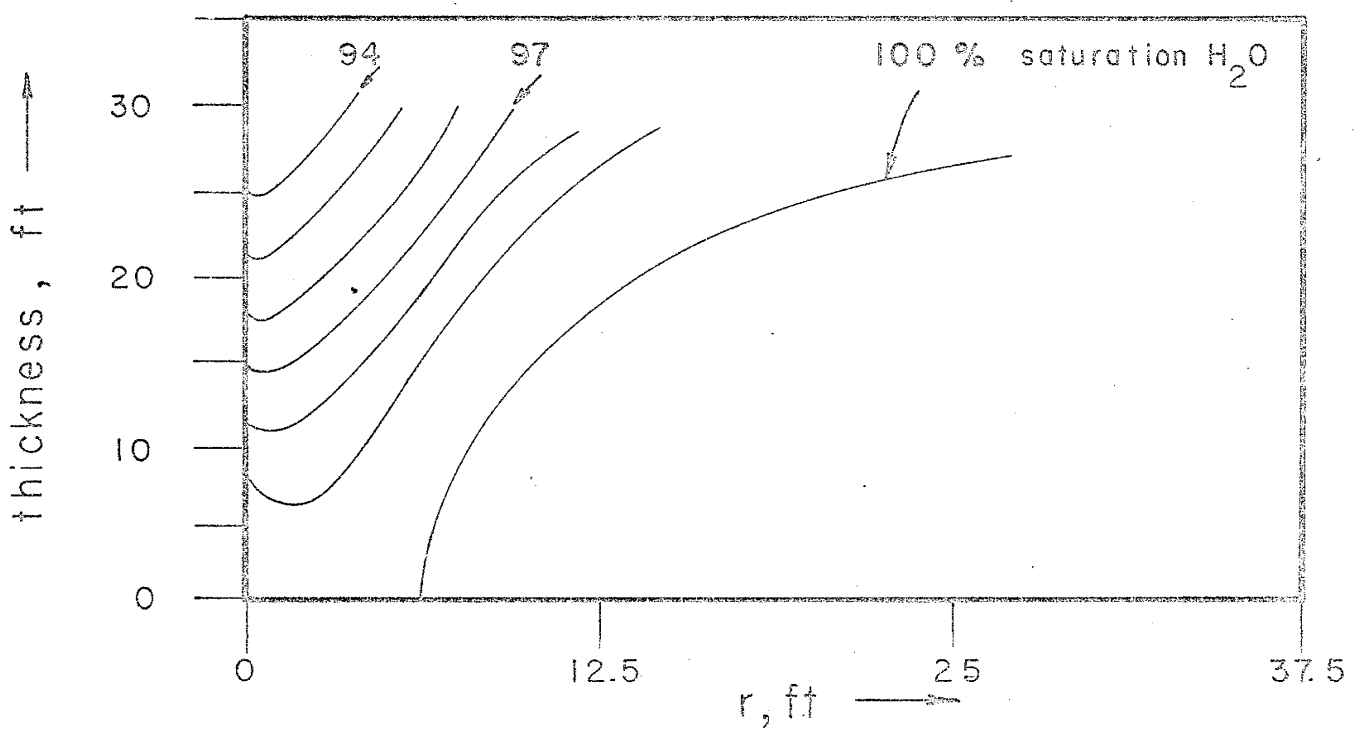

FIG. 26

CASE 7. The formation has an absolute permeability of 4.0 darcys. The injection pressure at the well face is held at a constant 300 pounds per square inch. The dependent variable in the gas equation is raised to $m + 1 = 1.8$.

Case 7, as Case 6, is included here for completeness. The discussion for Case 6 is also applicable to Case 7.

Case 7

m = 0.8 k = 4 darcys Injection pressure = 300 psi

t = 444 sec

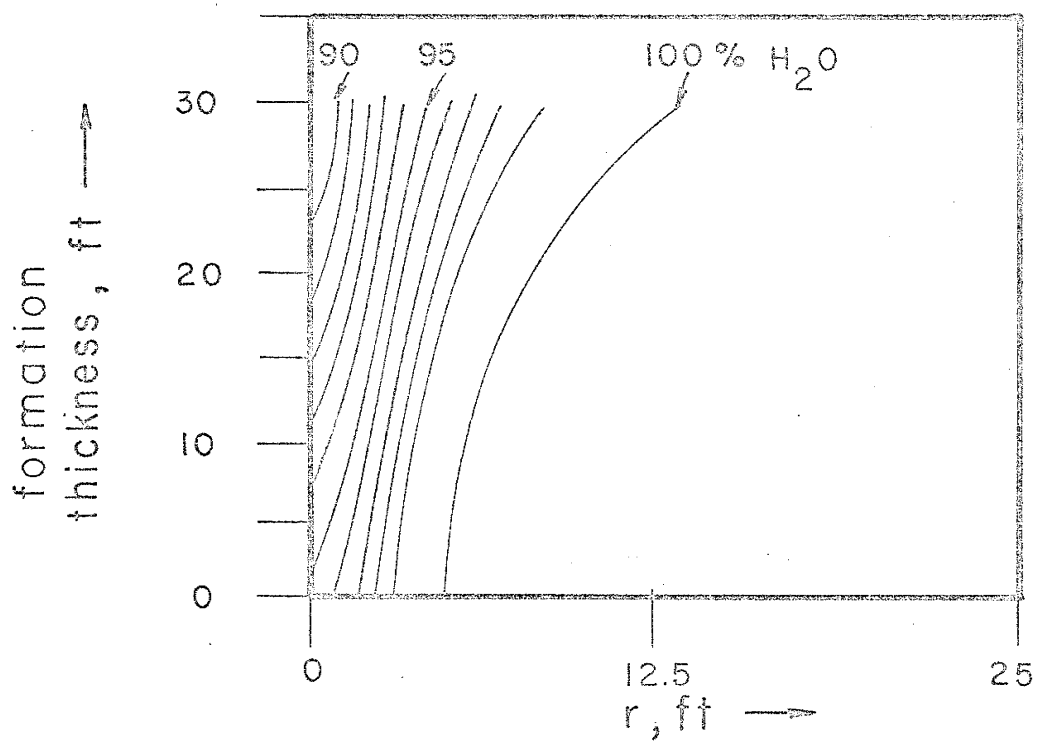

FIG. 27

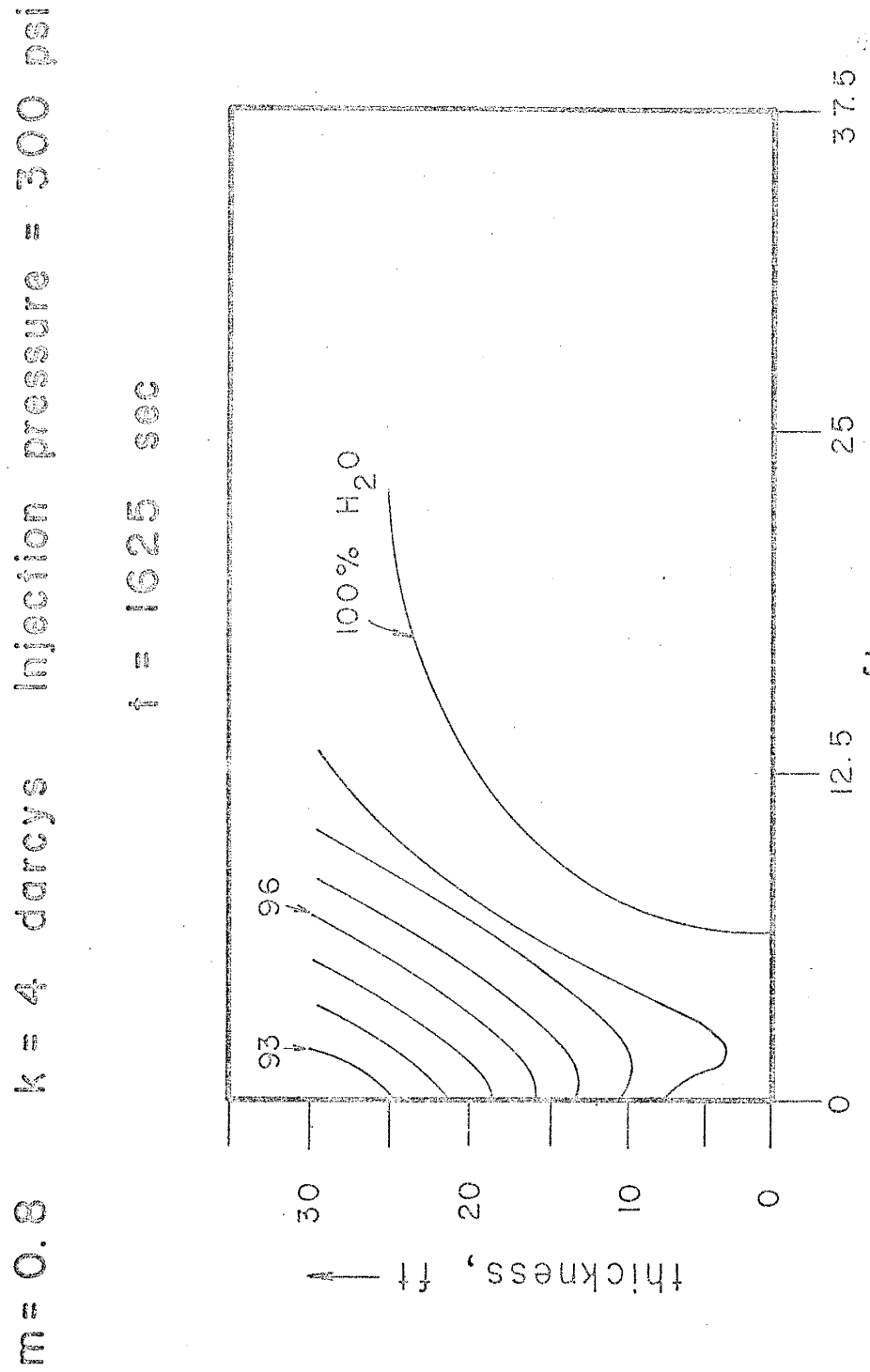
Case 7
m = 0.8 k = 4 darcys Injection pressure = 300 psi
t = 1625 sec
100% H_2O
96
93
thickness, ft
30
20
10
0
0
12.5
25
37.5
r, ft

FIG. 28

Case 7

m = 0.8 k = 4 darcys Injection pressure = 300 psi

t = 4430 sec

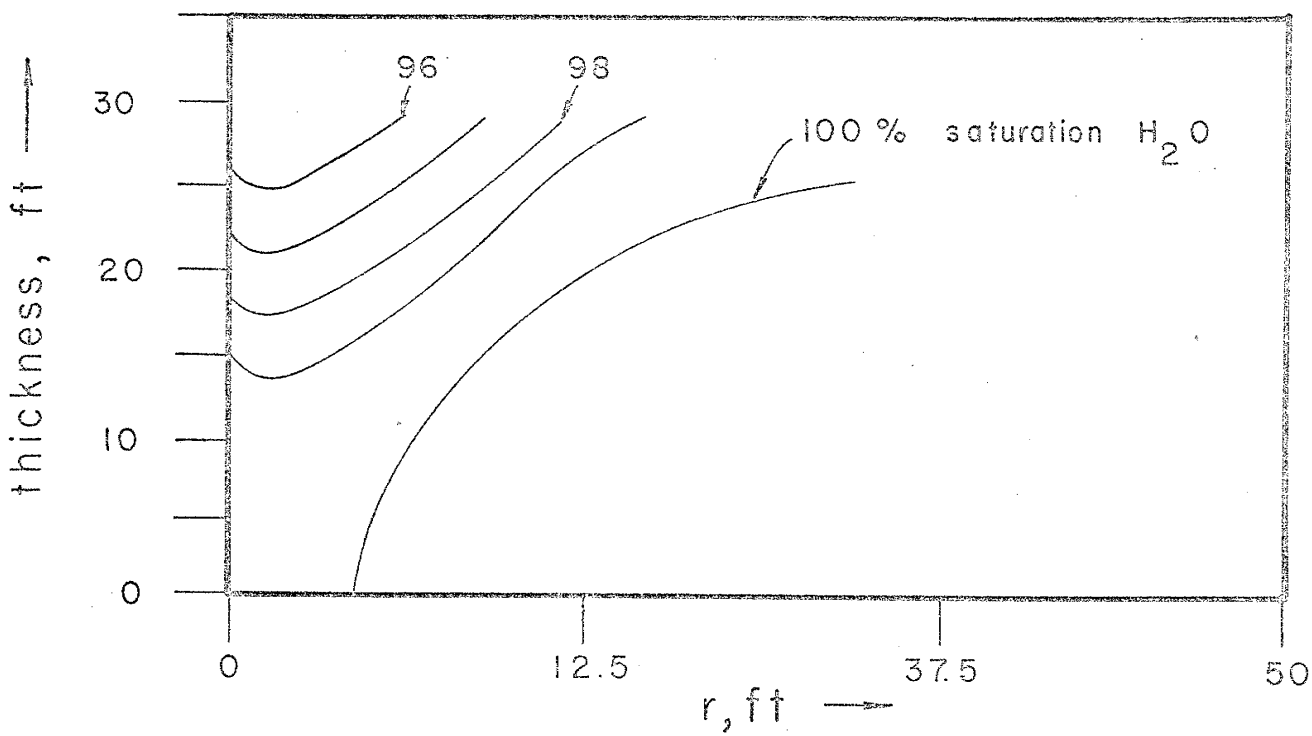

FIG. 29

Discussion

In the introduction to this study, it was mentioned that air injected into a reservoir could possibly be a means of arresting or slowing down salt water encroachment. This study did not include economics or chemistry. The economics of injecting air into the ground would be based upon many factors, not the least of which are geographical and geological.

As with the case of economics, whether or not air would harm a reservoir is a function of the geology, the chemistry of the water, and the composition of the rock matrix.

Discussion of the Technique

In the section on previous work, the discussion included Coats and Richardson's (1967) model of water displacement by gas in reservoir storage. Their model uses both positive and negative values of capillary pressure vs. saturation. The physical meaning of using both positive and negative capillary pressures is not clear. In personal communication with Dr. Rafi Al-Hussainy of Mobil Research Labs, it was learned that the use of a graph of this nature helped in stabilizing the particular type of model treated in that paper. The present author did not find the use of both positive and negative capillary pressures vs. saturation necessary for stability in the calculations.

In the mathematical formulation, numerical analogs are derived for the various parts of the differential equation using Crank-Nicholson differencing. This particular scheme was chosen because the derived

analogs are second-order correct in both space and time. Other schemes which are faster are available for the solution of the differential equation but are not second-order correct.

Numerous trials were made in an effort to find the optimum time step change. It was found that stability was affected if the time step exceeded two percent of the previous time step. The fact that a time step change was no more than two percent made the computational routine slow. The average computer time requirement was approximately 85 minutes for a simulation of 10^6 seconds problem time.

The extrapolation routine used in this development is based upon the use of prior values of the dependent variable for the last two time steps to extrapolate values of the dependent variable for the present time step. It was found necessary to modify this routine slightly in an effort to overcome a tendency for the numerical routine to drift under zero injection conditions. This procedure alternately over-extrapolates for one time step and under-extrapolates for the next time step. It was found that over- and under-extrapolating by one percent was adequate to eliminate numerical drift resulting from round off and truncation.

In the section on computational techniques, Eq. (12) for the calculation of capillary pressure is an approximation in that the static head for the gas portion of the two phases is ignored. This approximation is adequate since the density of gas is approximately 830 times smaller than the density of water. The scheme used in the calculational molecule is a simple, commonly used routine for calculations of this nature.

Convergence in the routine was considered achieved if the last iterates of the last calculated value of the dependent variable were within 1×10^{-3} of the previously calculated or extrapolated value of the dependent variable. This level of convergence is compared to the spectral radius of the difference forms rather than the value of the dependent variable (Smith, 1965). This criterion was found to be adequate for suitable convergence and stability of the problem. The use of the extrapolation routine, which alternately under- and over-extrapolated, improved the convergence rate in the model.

Discussion of the Results

In Figures 4 through 29, the results of this study are displayed. Seven cases are used to investigate a variation in aquifer permeability, injection pressure, injection rate, and power of the dependent variable polytropic exponent for the non-wetting phase.

Four primary parameters control the shape of the saturation profile. They are the radial velocity, capillary pressure vs. saturation curve, the density contrast between the two phases, and the injection rate. Near the well, the radial velocity of the injected gas is a controlling factor. Nearly vertical saturation profiles are indicative of high radial velocities. At the 100% saturation contour, the density contrast is a controlling parameter. The curve of the air-water interface is primarily controlled by the density contrast. The saturation profile between the well and the air-water interface is a function of the radial velocity, the density contrast, and the shape of the capillary pressure vs. saturation curve.

Figures 4 through 10 are for Case 1. The permeability of the system is 4 darcys and gas is being injected at a constant rate of 0.1 pound mass of air per second.

Figures 4 through 7 show the saturation distribution for various specified times. The nearly vertical saturation lines close to the well bore indicate high radial velocities. The curved interface is indicative of the density contrast between air and water. Air, being approximately 830 times lighter than water, is concentrating at the impermeable top surface of the aquifer. The characteristics displayed in the figures are consistent with the dynamics of a real physical situation.

Figure 4, for 444 seconds of injection time, shows a relatively immature saturation distribution. This is because the radial velocity is high in most of the region of multi-phase flow and insufficient time has elapsed for gravity segregation to take place.

Figure 5, for 1625 seconds, shows gravity segregation becoming an increasingly important factor in the shape of the air-water interface. Note that the air-water interface assumes a characteristic shape relatively early in time. The intersection of the base of the air-water interface curve with the bottom of the aquifer is a function of the radial velocity at or near the base of the aquifer. The intersection of the air-water interface curve with the top of the aquifer shows the effect of density segregation and expansion of the gas. The time rate of change in the uppermost part of the interface is therefore much higher than in the bottom part. The overall effect is an elongation of the interface.

Figure 6, for 3046 seconds of injection, displays the saturation profiles in nearly mature form. The general shape of the curves tends to remain relatively constant except for a shift in the radial direction.

Figure 7 is for 7284 seconds of injection time. Again the general shape of the profiles has not changed significantly, but has moved outward.

In comparing Figures 4 through 7, note that the saturation profiles mature to a characteristic shape in a relatively short time.

Figure 8 is for the head distribution after 444 seconds of injection. All the lines shown in Figure 8 would be vertical if water were being injected; mixed phases, however, tend to skew the straight lines. Note that the outermost zones of the flow region, where two-phase flow does not exist, are characterized by head contours.

Figure 9 is for the head distribution at an injection time of 2091 seconds. The diffusion wave has swept far out into the aquifer under a relatively high driving head. The steep potential gradient at about 90 feet in the figure is characteristic of a capillary pressure transition zone. The high potential gradient in this zone results from the two-phase flow resistance. To the right side of this zone, where the pore fluid is primarily water, the head is undisturbed. To the left of the zone, where the phases are mixed more evenly, the head distribution is normal because the relative permeabilities of the two phases are approximately equal.

Figure 10 displays the head distribution at 3452 seconds. In comparing Figs. 9 and 10, note that the steep potential gradient has moved radially outward, to between 90 and 160 feet, from its former position

at about 90 feet. The advance of this transition zone is consistent with the advance of the saturation profiles.

Figures 11 through 14 are for Case 2. This case directly contrasts the compressible and incompressible cases. The permeabilities of both systems are 4 darcys and gas is being injected at a constant mass rate of 0.1 pound per second.

Figure 11 displays saturation profiles for a time of 444 seconds. The figure shows that gas compressibility has little or no effect on the saturation distributions for early times.

Figure 12 shows the saturation profiles at 1625 seconds. The effects of gas compressibility begin to show. Noted in the lower half of Fig. 12 is a definite tendency of the gas to pile up, or show compression, especially near the well bore. This feature is a consistent characteristic with two-phase compressible flow.

Figure 13 displays saturation profiles at 3046 seconds. Tracing of equal saturation lines between the two displays shows the effects of gas compressibility.

Figure 14 contrasts saturation profiles for a time of 4430 seconds. Again the effects of gas compressibility are apparent. Note in the upper graph, at the abscissa, that the saturation does not go below 20 percent water. This value is a minimal value and was chosen because the residual water saturation for most formations is approximately 20 percent.

Figures 15 through 17 are for Case 3. The permeability of the system is one darcy and gas is being injected at a constant well face pressure of 220 pounds per square inch.

Figure 15 shows the saturation distribution for a time of 444 seconds. It is noted from the immaturity of the saturation profiles that a very low mass rate of flow is taking place. This results from the high formation resistance and the small head differential. (For the purpose of more adequately displaying saturation distributions, note the change of horizontal scale between Cases 2 and 3.)

Figure 16 shows the saturation distribution at 1260 seconds. In comparing Figs. 16 and 17, note that little or no change is apparent in the saturation profiles except at the well face. This is primarily because of the low radial velocity and is an indication that water is sweeping in at the bottom, causing most of the air to rise to the top of the formation.

Figure 17 displays the saturation distribution at 2090 seconds. In comparing Fig. 17 with Fig. 16, the only apparent change is a small radial advance of the air-water interface. Hence the head differential in this case is near the minimum necessary to drive the two-phase system.

Figures 18 through 20 are for Case 4. The permeability of the system is 2.5 darcys and gas is being injected at a constant well face pressure of 300 pounds per square inch.

Figure 18 shows the saturation distribution at 444 seconds. Comparison of Fig. 18 to Fig. 17 shows that the saturation profiles displayed on Figure 18 arrive at a mature shape rapidly. This is primarily because of an increase in the head applied at the well face.

Figure 19 shows the saturation distribution for a time of 1260 seconds. Comparison of Fig. 18 to Fig. 19 exhibits little change in the characteristic shape of the saturation profiles. The profiles have simply shifted outward radially.

Figure 20 shows the saturation distribution for a time of 1625 seconds. In comparing Fig. 20 with Figs. 19 and 18, little or no change other than a radial shift is observed in the characteristic saturation profiles.

In comparing Case 4 with the previous three cases, several differences are observed. Cases 1 and 2 are for a specific mass rate of injection and exhibit a steady increase in pressure at the well face. Cases 3 and 4 are for a specific pressure and reflect a steadily decreasing injection mass rate. Case 4 shows the highest mass rate for early times and displays mature saturation profiles early. In comparing Cases 1 and 4, it is observed that the head at the well face in Case 1 starts below that of Case 4 but soon exceeds the head of Case 4. Hence, the characteristic shapes are markedly different.

In Case 4, mass is injected at a high rate for a short time and steadily declines. As the well face head approaches that of the formation, the formation fluids sweep back, or rebound, along the bottom of the formation, resulting in a characteristically skewed saturation profile.

Figs. 21 through 24 are for Case 5. The permeability of the system is 4 darcys and gas is being injected at a constant well face pressure of 300 pounds per square inch.

Figure 21 shows the saturation distribution at 444 seconds. In comparing Fig. 21 with Fig. 18, little or no variation is observed in the saturation profiles. A decrease in formation resistance, for the constant well face pressure applied, does not appreciably change the saturation profiles.

Figure 22 shows the saturation distribution for 1260 seconds. Figs. 21 and 22 show that the saturation profiles become skewed for later times, indicating a return flow of the incompressible fluid at or near the bottom of the aquifer.

Figure 23 shows the saturation distribution for 2092 seconds. The skewed character of Fig. 22 is also present in Fig. 23. The primary difference between the two figures is an expected radial shift in the saturation profiles.

When comparing Case 5 with the previous cases, observe that the jump in well face head between Cases 3 and 4 is more important than the decrease in formation resistance shown in Cases 4 and 5. This can be observed for the range of head differentials and aquifer resistances treated.

Figures 24 through 26 are for Case 6. The permeability of the system is 4 darcys and gas is being injected at a constant well face pressure of 300 pounds per square inch. The power of the dependent variable (m+1) is 1.6 for this case, as compared to 1.7 for the compressible phase discussed previously.

Figure 24 shows the saturation distribution for a time of 444 seconds. In comparing Fig. 24 with Figs. 21 and 18, it is apparent that a large difference in the saturation distribution exists for the same time intervals. This discrepancy is due to a change in horizontal mesh size. The larger mesh size used in this case cannot adequately describe the phenomenon taking place. Hence, there must be an optimum mesh size for this problem which is a function of the parameters of the

problem and probably of the pressure gradient. It was beyond the scope of this study to attempt to find if such a relationship exists and is definable.

Figure 25 shows the saturation distribution at 1260 seconds. Note that the saturation distribution contours appear to form a bubble near the well face. This is due to mesh spacing and generally the inability of the numerical analogs to describe the process properly when mesh spacing is large.

Figure 26 shows the saturation distribution for 2091 seconds. Figs. 25 and 26 show the formation of a bubble near the well face. Again this shape is due to mesh spacing.

Case 6 is included for completeness and cannot be compared quantitatively or qualitatively with any of the previous cases. It shows the importance of mesh spacing.

Figure 27 shows the saturation distribution for 444 seconds. From Figs. 24 and 27, little or no variation is noted in the saturation distribution.

Case 7, as Case 6, is included for completeness, as the mesh spacing is again quite large. Assuming that mesh spacing has the same effect on both cases, comparison of Fig. 27 with Fig. 24 indicates that varying the power of the dependent variable has little or no effect for early times.

Figure 28 shows the saturation distribution for a time of 1625 seconds. Comparison of Figs. 28 and 26 again shows approximately the same saturation profile characteristics.

Figure 29 shows the saturation distribution for 4430 seconds. No similar figure is available for the previous case, therefore no

FIG. 30

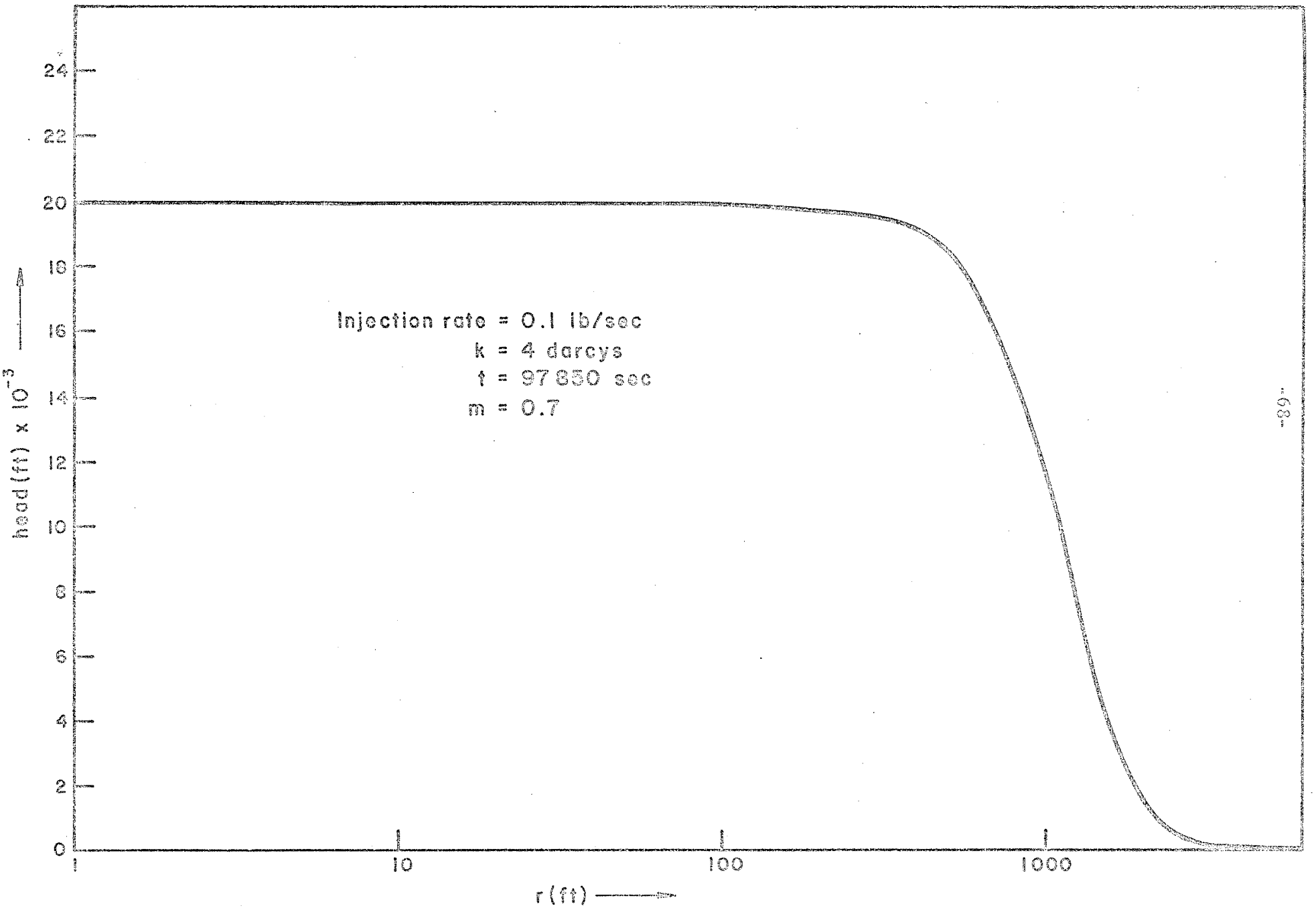
Injection rate = 0.1 lb/sec
k = 4 darcys
t = 97850 sec
m = 0.7
head (ft) x 10^{-3}
r (ft)
0
2
4
6
8
10
12
14
16
18
20
22
24
10
100
1000

comparison can be made. It can be observed, however, that extending the time period substantially does not appreciably change the characteristic saturation profile.

Figure 30 shows the head distribution for $\underline{m} = 0.7$, $\underline{k} = 4$ darcys, an air injection rate of 0.1 pound per second, and a time of 97,850 seconds.

The saturation profile cannot be shown due to the coarseness of the mesh for large $\underline{r}$. This is due to the use of the transformation $u = \ln \frac{r}{r_w}$ necessary for handling large radial distances with a minimum of mesh points. In addition, the transformation permits showing more detail from the calculation near the well bore.

The head displayed in Fig. 30 is much higher than would be encountered in a typical situation. Thus, a constant injection rate of 0.1 pound per second is physically realistic only for short periods of time.

Discussion of Practical Physical Systems

The practical use of an air injection system for slowing down or stopping salt water encroachment would require considerable physical information. The geology should be known in detail. Air should be compatible with the chemistry of the water and skeleton of the aquifer. Such information can only be gained through a detailed geochemical study.

An ideal aquifer should be confined and non-leaky. The geological structure should be such that air could be trapped within the aquifer for long periods. In view of the higher injection pressures shown by this study to be necessary, the aquifer should have no unplugged or partially plugged holes. The injection system should be remote from

pumping wells to exclude the possibility of air-locked wells. The aquifer should be remote from any hydrocarbon production and hydrocarbons must not be present in the system. The system should have an array of monitor wells to determine the advance of the injected air. The injection hole should be cased and cemented from top to bottom to exclude the possibility of air entering any formation other than the intended.

An air injection system could be useful in many types of regional hydrology. In a system with a steadily declining head, it might be desirable to inject air at all times in the system, thereby keeping the head high and allowing the water to be mined for immediate consumption. Such a system would undoubtedly be a stop-gap means in an effort to buy time until other supplies can be obtained.

An air injection system could also be valuable in a regional scheme where, for example, the primary production is during an irrigation season. Air is injected during the overdraft period in an effort to maintain a high head in most of the system. During the winter months when the system is under recovery, the air could then be carefully vented to the atmosphere, allowing recharge to enter the system by replacing the air. In this way air could be used to retard salt water encroachment or upward leakage of salt water during periods of large consumption and vented slowly to allow recharge while maintaining a high head. Should a cyclic scheme of this nature be adopted, the present model would have to be modified to include hysteresis.

An air injection system could probably be used in coastal regions where salt water encroachment is a problem. A line of injection wells could be placed paralleling the coast to inject and maintain a curtain of air.

Recommendations

General

It is recommended that a field pilot project be set up to test the results of the theory. A study of this nature could be undertaken using a relatively shallow aquifer and low injection pressures.

Also needed is a study to determine the economics of an air injection system within certain reasonable limits.

A study to determine the effects of air on the chemistry of a ground water system would also be necessary. For further study of the techniques it might be desirable to determine an optimum grid spacing as a function of the parameters of the system.

Roswell Basin

Prior to the start of this analytic work, a study was made of the Roswell Basin, resulting in the following conclusions.

A system of air injection is not recommended for the area around the city of Roswell. The geology is not known in sufficient detail to determine if the system has a structure adequate to entrap air. The area is filled with unplugged and partially plugged holes which would give rise to air leakage. Since the aquifer system is quite deep, the expense of plugging all holes would be prohibitive. Furthermore, it would be difficult to find an injection site remote enough from all pumping wells to exclude the possibility of air venting through the holes. Also, the area is adjacent to a small oil field producing oil from the same system at approximately the same depths. Such a system could be extremely

hazardous under these conditions. A geologic study would involve drilling deep wells (≈600 ft.). Detailed logging by geological, geophysical, and geochemical methods to determine aquifer characteristics would also be desirable.

Conclusions

Under constraints, dictated by detailed economic, geochemical, geologic and geophysical studies, air could be used to control salt water encroachment.

The numerical analogs used to approximate the differential equations are stable and a high degree of convergence is obtained.

The shape of the saturation distribution curves is determined by the radial velocity, the capillary pressure vs. saturation curve, the density contrast, and the injection rate.

Injecting air at constant pressure produces characteristic saturation curves that are fundamentally different from those produced by a constant mass rate of injection. A constant mass rate of injection would be more desirable if the gas were to be vented after a short time because the two-phase zone would remain relatively localized.

High constant injection rates for relatively shallow wells (<600 ft.) are not realistic because of the high head differentials at the well. Low constant well face injection pressures (<300 psi) are impractical over the range of physical parameters used because gas is injected at very low rates. A variation in the injection rate consistent with available equipment is practical for an injection system.

The high hydraulic gradient associated with the air-water interface could be used to determine physically the spread of the two-phase system. This could be accomplished by a line of observation holes extending radially from the injection well.

In two-phase flow, the compressibility of the gas phase decreases the size of the two-phase part of the system relative to a system in which gas is treated as incompressible. Treating gas as incompressible leads to errors, the magnitude of which increases with time.

For low rates of flow, large changes in permeability do not substantially alter the saturation variation profiles. As flow rates increase, the variation in saturation distribution becomes increasingly dependent upon the resistance of the reservoir.

Small changes in the power of the dependent variable for the gas phase appear to have little or no effect on the saturation distribution. However, this study is considered inconclusive with regard to small changes in the power of the dependent variable.

Symbols Used in This Development

A = Area in ft

C_p = Specific heat at constant pressure BTU/lb mass °R

C_v = Specific heat at constant volume BTU/lb mass °R

$\left(\frac{dS}{dPc}\right)^{\alpha}_{i,j}$ = Last value of slope calculated for any point i,j, units ft^{-1}

$\frac{dS}{dPc}^{n+1}$ = Slope at time (n+1), ft^{-1}

$\hat{e}_i$ = Cartesian basis vectors

h = Thickness, ft

h_r = Elevation, ft

k = Specific permeability, ft^2

k_{rn} = Relative permeability of the non-wetting phase

$(k_{rn})^{\alpha}_{i,j}$ = Last value of relative permeability calculated for any point i,j

k_{rw} = Relative permeability of the wetting phase

K = Hydraulic conductivity, ft/sec.

$m = C_v/C_p$

p = Pressure, $lbs/in.^2$

p_f = Pressure at the well face, lbs/in^2

$p^n_{i,j}$ = Water head at time step n, ft

$p^{n+1}_{i,j}$ = Dependent variable at time step n+1, ft

$p^{n+2}_{i,j}$ = Dependent variable at time step n+2, ft

p^*_n = Pressure of the non-wetting phase, lb/in^2

$p_n = p^*_n/\gamma + z$, ft

p_0 = Initial pressure, lbs/in^2

p_w^* = Pressure of the wetting phase, lbs/in^2

$P_w = p_w/\gamma + z$, ft

P_x = Ultimate constant well face pressure, lbs/in^2

$PA_{i,j}^{n+1}$ = Water head at time step n+1, ft

$Pc_{i,j}^{n+1}$ = Capillary head at time n+1, ft

$PG_{i,j}^{n}$ = Gas head at time step n, ft

$PGA_{i,j}^{n+1}$ = Gas head at time step n+1, ft

q = Injection rate, lb/sec

Q = Fluid discharge, ft^3/sec

r = Radial coordinate, ft

S = Water saturation

$S_{i,j}^{\alpha}$ = Last value of saturation calculated for any point i,j

$S_{i,j}^{n+1}$ = Water saturation at n+1

S_n = Saturation of the non-wetting phase

S_w = Saturation of the wetting phase

t = Time, sec

t_0 = Time from start of injection, sec

u = A continuous function of x and has finite single-valued derivatives

v = Darcy velocity, ft/sec

v_x = Velocity in x direction, ft/sec

v_y = Velocity in y direction, ft/sec

v_z = Velocity in z direction, ft/sec

(x,y) = Coordinates of any point, ft

z = Vertical coordinate, ft

Δt^{n+1} = Old time step, t

$\Delta t^{n+1/2}$ = New time step, t

Δx = Increment between points, ft

μ_n = Viscosity of the non-wetting phase, lb sec/ft^2

μ_w = Viscosity of the wetting phase, lb sec/ft^2

ρ = Fluid density, mass/unit volume

ρ_n = Density of the non-wetting phase, mass/unit volume

ρ_w = Density of the wetting phase, mass/unit volume

ϕ = Porosity

γ = Specific weight, lbs/ft^3

APPENDIX A

THEORY

The differential equations governing the flow of two fluids through a porous medium are as follows (Peaceman, 1967):

$$\nabla \cdot \left[\frac{\rho_n \, k \, k_{rn}}{\mu_n} \nabla P_n \right] = \phi \frac{\partial}{\partial t} \left[\rho_n (1-S) \right] \qquad [1]$$

$$\nabla \cdot \left[\frac{\rho_w \, k \, k_{rw}}{\mu_w} \nabla P_w \right] = \phi \frac{\partial}{\partial t} \left[\rho_w S \right] \qquad [2]$$

where $\nabla e = \frac{\partial}{\partial x} \hat{e}_x + \frac{\partial}{\partial y} \hat{e}_y + \frac{\partial}{\partial z} \hat{e}_z$

ρ_n = Density of the non-wetting phase

ρ_w = Density of the wetting phase

k = Specific permeability

k_{rn} = Relative permeability of the non-wetting phase

k_{rw} = Relative permeability of the wetting phase

μ_n = Viscosity of the non-wetting phase

μ_w = Viscosity of the wetting phase

$P_n = p_n^*/\gamma_n + z$

$P_w = p_w^*/\gamma_w + z$

γ = Specific weight

h = Thickness

ϕ = Porosity

S = Water saturation

p_n^* = Pressure of non-wetting phase

p_w^* = Pressure of wetting phase

Derivation of Gas Differential Equation

Operating just on Eq. [1], discounting the gas gravity term as it is approximately 1×10^{-3} times the water gravity term, and utilizing the polytropic relation

$$\frac{\rho}{\rho_0} = \left(\frac{P}{P_0}\right)^m,$$

where ρ_0 = initial density of the gas

P_0 = initial pressure of the gas

$m = C_v/C_p$

C_p = specific heat at constant pressure

C_v = specific heat at constant volume

$$\nabla \cdot [k_{rn} P_n \nabla P_n] = \frac{\mu_n}{k} \frac{\partial}{\partial t} [P^m(1-S)] \qquad [3]$$

Eq. [3] reduces to

$$\frac{1}{r} \frac{\partial}{\partial r} \left(r\, k_{rn} P^m \frac{\partial P}{\partial r}\right) + \frac{\partial}{\partial z} \left(k_{rn} P^m \frac{\partial P}{\partial z}\right) = \frac{\phi \mu_n}{k} \frac{\partial}{\partial t} [P^m(1-S)]. \qquad [4]$$

Treating the axisymmetric case, we can write Eq. [4] in the following way:

$$\frac{1}{r} \frac{\partial}{\partial r} \left(r k_{rn} \frac{\partial P^{m+1}}{\partial r}\right) + \frac{\partial}{\partial z} \left(k_{rn} \frac{\partial P^{m+1}}{\partial z}\right) = \frac{\phi \mu_n (m+1)}{k} \frac{\partial}{\partial t} [P^m(1-S)]. \qquad [5]$$

Making the transformations $R = \frac{r}{r_w}$, $\bar{z} = \frac{z}{r_w}$, $\bar{P}^{m+1} = \left(\frac{P}{P_0}\right)^{m+1}$,

Eq. [5] can be written in the form

$$\frac{1}{R} \frac{\partial}{\partial R} \left[k_{rw} R \frac{\partial \bar{P}^{m+1}}{\partial R}\right] + \frac{\partial}{\partial \bar{z}} \left[k_{rn} \frac{\partial \bar{P}^{m+1}}{\partial \bar{z}}\right] = \frac{\phi \mu_n (m+1) r_w^2}{k P_0} \frac{\partial}{\partial t} [P^m(1-S)]. \qquad [6]$$

Using the transformation $u = \ln R$, Eq. [6] can be written in the following form:

$$e^{-2u} \frac{\partial}{\partial u} \left[k_{rn} \frac{\partial \bar{P}^{m+1}}{\partial u} \right] + \frac{\partial}{\partial z} \left[k_{rn} \frac{\partial \bar{P}^{m+1}}{\partial z} \right] = \frac{\phi \mu_n (m+1) r_w^2}{k P_0} \frac{\partial}{\partial t} \left[\bar{P}^m (1-S) \right] \qquad [7]$$

Finite Difference Form of Gas Equation

Eq. [7] can be written in finite difference form

$$\frac{e^{-2u}}{\Delta u_i} \left[k^{n+1/2}_{i+1/2} \left(\frac{(P^{m+1})^{n+1/2}_{i+1,j} - (P^{m+1})^{n+1/2}_{i,j}}{\Delta u_{i+1/2}} \right) - k^{n+1/2}_{i-1/2} \left(\frac{(P^{m+1})^{n+1/2}_{i,j} - (P^{m+1})^{n+1/2}_{i-1,j}}{\Delta u_{i-1/2}} \right) \right]$$

$$+ \frac{1}{\Delta z_j} \left[k_{j+1/2} \left(\frac{(P^{m+1})^{n+1/2}_{i,j+1} - (P^{m+1})^{n+1/2}_{i,j}}{\Delta z_{j+1/2}} \right) - k_{j-1/2} \left(\frac{(P^{m+1})^{n+1/2}_{i,j} - (P^{m+1})^{n+1/2}_{i,j-1}}{\Delta z_{i,j-1/2}} \right) \right]$$

$$= \frac{(m+1)\phi \mu_n r_w^2}{k P_0} \frac{1}{\Delta t^{n+1/2}} \left[\bar{P}^m (1-S) \right] \qquad [8]$$

Eq. [8] can be written in the following form:

$$C_i A_{ij} [(P^{m+1})^{n+1/2}_{i+1,j} - (P^{m+1})^{n+1/2}_{i,j}] - CC_i AA_{ij} [(P^{m+1})^{n+1/2}_{i,j} - (P^{m+1})^{n+1/2}_{i-1,j}]$$

$$+ D_j BB_{ij} [(P^{m+1})^{n+1/2}_{i,j+1} - (P^{m+1})^{n+1/2}_{ij}] - BB_{i,j} DD_j [(P^{m+1})^{n+1/2}_{ij} - (P^{m+1})^{n+1/2}_{i,j-1}]$$

$$= (EA)(F)(1-S^n_{i,j})[(P^m)^{n+1}_{i,j} - (P^m)^n_{i,j}] - (EA)(F)(P^m)^n_{i,j}(zA)[PGA_{i,j} - PG_{i,j} - PA_{i,j} + P_{i,j}] \qquad [9]$$

where

$$A_{i,j} = 1/4[(k_{rn})^{n+1}_{i,j} + (k_{rn})^{n}_{i,j} + (k_{rn})^{n+1}_{i+1,j} + (k_{rn})^{n}_{i+1,j}] ,$$

$$AA_{i,j} = 1/4[(k_{rn})^{n+1}_{i,j} + (k_{rn})^{n}_{i,j} + (k_{rn})^{n+1}_{i-1,j} + (k_{rn})^{n}_{i-1,j}] ,$$

$$B_{i,j} = 1/4[(k_{rn})^{n+1}_{i,j} + (k_{rn})^{n}_{i,j} + (k_{rn})^{n+1}_{i,j+1} + (k_{rn})^{n}_{i,j+1}] ,$$

$$BB_{i,j} = 1/4[(k_{rn})^{n+1}_{i,j} + (k_{rn})^{n}_{i,j} + (k_{rn})^{n+1}_{i,j-1} + (k_{rn})^{n}_{i,j-1}] ,$$

$$C_i = e^{-2u}/(\Delta u_i)(\Delta u_{i+1/2}) ,$$

$$CC_i = e^{-2u}/(\Delta u_i)(\Delta u_{i-1/2}) ,$$

$$D_j = 1/(\Delta z_j)(\Delta z_{j+1/2}) ,$$

$$DD_j = 1/(\Delta z_j)(\Delta z_{j-1/2}) ,$$

$$EA = \frac{(n+1)\phi\mu_n r_w^2}{k\ P_0} ,$$

$$F = 1/\Delta t^{n+1/2} ,$$

$$zA = \frac{dS}{dP_c} ,$$

$PGA_{i,j}$ = gas pressure at time step n+1,

$PG_{i,j}$ = gas pressure at time step n,

$PA_{i,j}$ = water pressure at time step n+1, and

$P_{i,j}$ = water pressure at time step n.

Applying Crank-Nicolson differencing to Eq. [9]

$$(P^{m+1})^{n+1/2}_{i,j} = 1/2[(P^{m+1})^{n+1}_{i,j} + (P^{m+1})^{n}_{i,j}] ,$$

Eq. [9] can be written in the following form:

$$C_iA_{i,j}[(PGA^{m+1})_{i+1,j} - (PGA^{m+1})_{i,j}] - CC_iAA_{i,j}[(PGA^{m+1})_{i,j} \qquad [10]$$

$$- (PGA^{m+1})_{i-1,j}] + D_jBB_{i,j}[(PGA^{m+1})_{i,j+1} - (PGA^{m+1})_{i,j}]$$

$$- BB_{i,j}DD_j[(PGA^{m+1})_{i,j} - (PGA^{m+1})_{i,j-1}] = (EA)(F)(1-S_{i,j})[(PGA)_{i,j}-(PG)_{i,j}]$$

$$- (EA)(F)(PG^m)_{i,j}(zA)[PGA_{i,j} - PG_{i,j} - PA_{i,j} - P_{i,j}]$$

$$- C_iA_{i,j}[(PG^{m+1})_{i+1,j} - (PG^{m+1})_{i,j}] + CC_iAA_{i,j}[(PG^{m+1})_{i,j} - (PG^{m+1})_{i-1,j}]$$

$$- D_jBB_{i,j}[(PG^{m+1})_{i,j+1} - (PG^{m+1})_{i,j}] + BB_{i,j}DD_j[(PG^{m+1})_{i,j} - (PG^{m+1})_{i,j-1}].$$

Eq. [10] can be reduced to a form linear in $PGA_{i,j}$ by using the following expression, $PGA^{m+1}_{i,j} \simeq PG^{m+1}_{i,j} + (m+1)PG^{m}_{i,j}[PGA_{i,j} - PG_{i,j}]$; then

$$C_iA_{i,j}[H_{i+1,j}PGA_{i+1,j} - H_{i,j}PGA_{i,j}]$$

$$- CC_iAA_{i,j}[H_{i,j}PGA_{i,j} - H_{i-1,j}PGA_{i-1,j}]$$

$$+ D_jBB_{i,j}[H_{i,j+1}PGA_{i,j+1} - H_{i,j}PGA_{i,j}]$$

$$- BB_{i,j}DD_j[H_{i,j}PGA_{i,j} - H_{i,j-1}PGA_{i,j-1}]$$

$$= (EA)(F)(1-S_{i,j})(mPG^{m-1}_{i,j}PGA_{i,j} + PG^{m}_{i,j}(1-m) - P^{m}_{i,j})$$

$$- (EA)(F)PG^{m}_{i,j}zA(PGA_{i,j} - PG_{i,j} - PA_{i,j} - P_{i,j}) + G_{i,j} \qquad [11]$$

where

$$H_{i,j} = (m+1)PG^{m}_{i,j}$$

$$G_{i,j} = C_iA_{i,j}[(PG^{m+1})_{i+1,j} - PG^{m+1})_{i,j}](m-1)$$

$$+ CC_iAA_{i,j}[PG^{m+1})_{i,j} - (PG^{m+1})_{i-1,j}](1-m)$$

$$+ D_jBB_{i,j}[(PG^{m+1})_{i,j+1} - (PG^{m+1})_{i,j}](m-1)$$

$$+ BB_{i,j}DD_j[(PG^{m+1})_{i,j} - (PG^{m+1})_{i,j-1}](1-m).$$

Rearranging Eq. [11],

$$- PGA_{i,j}[(C_iA_{i,j} + CC_iAA_{i,j} + D_jBB_{i,j} + BB_{i,j}DD_j)H_{i,j}$$

$$+ (EA)(F)\{(1-S_{i,j})MPG^{m-1}_{i,j} - PG^{m}_{i,j}ZA)] + CiA_{i,j}H_{i+1,j}PGA_{i+1,j}$$

$$+ CC_iAA_{i,j}H_{i-1,j}PGA_{i-1,j} = HH_{i,j} \qquad [12]$$

where,

$$HH_{i,j} = G_{i,j} - D_jBB_{i,j}H_{i,j+1}PGA_{i,j+1} - CC_iAA_{i,j}H_{i-1,j}PGA_{i,j-1}$$

$$+ (EA)(F)PG^{m}_{i,j}[-(1-S_{i,j})(m) - ZA(P_{i,j} - PG_{i,j} - PA_{i,j})].$$

Utilizing the Thomas algorithm,

$PGA_{i-1,j} = ux_{i-1}PGA_{i,j} + V_{i-1}$, Eq. [12] reduces to the form

$$- PGA_{i,j}[(C_iA_{i,j} + CC_iAA_{i,j} + D_jBB_{i,j}DD_j)H_{i,j}$$

$$+ (EA)(F)\ (1-S_{i,j})mPG^{m-1}_{i,j} - PG^{m}_{i,j}zA\ - CC_iAA_{i,j}H_{i-1,j}ux_{i-1}]$$

$$= HH_{i,j} - CC_iAA_{i,j}H_{i-1,j}V_{i-1} - C_iA_{i,j}H_{i+1,j}PGA_{i+1,j}. \qquad [13]$$

Eq. [13] reduces to the form

$$PGA_{i,j} = (C_iA_{i,j}H_{i+1,j}PGA_{i+1,j} + CC_iAA_{i,j}H_{i-1,j}V_{i-1} - HH_{i,j})/DELTA,$$

where

$$DELTA = (C_i A_{i,j} + CC_i AA_{i,j} + D_j BB_{i,j} DD_j) H_{i,j}$$

$$+ (EA)(F)[(1-S_{i,j})mPG^{m-1}_{i,j} - PG^{m}_{i,j} zA]. \quad [14]$$

Since

$$PGA_{i,j} = ux_i PGA_{i+1,j} + V_i,$$

$$ux_i = C_i A_{i,j} H_{i+1,j}/DELTA, \quad [15]$$

$$V_i = (CC_i AA_{i,j} H_{i-1,j} V_{i-1} - HH_{i,j})/DELTA. \quad [16]$$

We have thus obtained the matrix coefficients necessary to solve the differential equation governing the flow of gas in a two-phase system.

Derivation of Water Differential Equation

Eq. [2] governing the flow of water,

$$\nabla \cdot \left[\frac{\rho_w kk_{rw}}{\mu_w} (\nabla P_w) \right] = \phi \frac{\partial}{\partial t} [\rho_w S]$$

Treating the axisymmetric case, Eq. [2] reduces to the form

$$\frac{1}{r} \frac{\partial}{\partial r} \left(rk_{rw} \frac{\partial P}{\partial r} \right) + \frac{\partial}{\partial z} \left(k_{rw} \frac{\partial P}{\partial z} \right) = \frac{\phi \mu_w}{k} \frac{\partial S}{\partial t} . \quad [17]$$

Allowing $P = \frac{P}{P_0}$, $R = \frac{r}{r_w}$, $z = \frac{z}{r_w}$, Eq. [17] reduces to the form

$$\frac{1}{R} \frac{\partial}{\partial R} \left(Rk_{rw} \frac{\partial P}{\partial R} \right) + \frac{\partial}{\partial z} \left(k_{rw} \frac{\partial P}{\partial z} \right) = \frac{\phi \mu_w r_w^2}{k P_0} \frac{\partial S}{\partial t} . \quad [18]$$

Using the transformation $u = \ln R$, Eq. [18] further reduces to

$$e^{-2u} \frac{\partial}{\partial u} \left(k_{rw} \frac{\partial P}{\partial u} \right) + \frac{\partial}{\partial z} \left(k_{rw} \frac{\partial P}{\partial z} \right) = \frac{\phi \mu_w r_w^2}{k P_0} \frac{\partial S}{\partial t} . \quad [19]$$

Finite Difference Form of Water Equation

Writing Eq. [19] in finite difference form

$$\frac{e^{-2u}}{\Delta u_i}\left[(k_{rw})^{n+1/2}_{i+1/2,j}\left(\frac{P^{n+1/2}_{i+1,j}-P^{n+1/2}_{i,j}}{\Delta u_{i+1/2}}\right) - (k_{rw})^{n+1/2}_{i-1/2,j}\left(\frac{P^{n+1/2}_{i,j}-P^{n+1/2}_{i-1,j}}{\Delta u_{i-1/2}}\right)\right]$$

$$+ \frac{1}{\Delta z_j}\left[(k_{rw})^{n+1/2}_{i,j+1/2}\left(\frac{P^{n+1/2}_{i,j+1}-P^{n+1/2}_{i,j}}{\Delta z_{j+1/2}}\right) - (k_{rw})^{n+1/2}_{i,j-1/2}\left(\frac{P^{n+1/2}_{i,j}-P^{n+1/2}_{i,j-1}}{\Delta z_{j-1/2}}\right)\right]$$

$$= \frac{\phi\mu_w r_w^2}{k\ P_0}\frac{\partial S}{\partial t} \,. \qquad [20]$$

Eq. [20] can also be written in the following form

$$Ax_{i,j}C_i(P^{n+1/2}_{i+1,j}-P^{n+1/2}_{i,j}) - AAx_{i,j}CC_i(P^{n+1/2}_{i,j}-P^{n+1/2}_{i-1,j}) + Bx_{i,j}D_j(P^{n+1/2}_{i,j+1}-P^{n+1/2}_{i,j})$$

$$- BBx_{i,j}DD_j(P^{n+1/2}_{i,j}-P^{n+1/2}_{i,j-1}) = EE\frac{\partial S}{\partial t} \,, \qquad [21]$$

where,

$$Ax_{i,j} = 1/4[(k_{rw})^{n+1}_{i,j} + (k_{rw})^{n}_{i,j} + (k_{rw})^{n+1}_{i+1,j} + (k_{rw})^{n}_{i+1,j}],$$

$$AAx_{i,j} = 1/4[(k_{rw})^{n+1}_{i,j} + (k_{rw})^{n}_{i,j} + (k_{rw})^{n+1}_{i-1,j} + (k_{rw})^{n}_{i-1,j}],$$

$$Bx_{i,j} = 1/4[(k_{rw})^{n+1}_{i,j} + (k_{rw})^{n}_{i,j} + (k_{rw})^{n+1}_{i,j+1} + (k_{rw})^{n}_{i,j+1}],$$

$$BBx_{i,j} = 1/4[(k_{rw})^{n+1}_{i,j} + (k_{rw})^{n}_{i,j} + (k_{rw})^{n+1}_{i,j-1} + (k_{rw})^{n}_{i,j-1}],$$

$$EE = \frac{\phi\mu_w r_w^2}{k\ P_0} \,.$$

Applying Crank-Nicolson differencing,

$$P_{i,j}^{n+1/2} = 1/2[P_{i,j}^{n+1} + P_{i,j}^{n}]$$

Eq. [21] can be written in the following form

$$C_i Ax_{i,j}(PA_{i+1,j}-PA_{i,j}) - CC_i AAx_{i,j}(PA_{i,j}-PA_{i-1,j})$$

$$+ D_j Bx_{i,j}(PA_{i,j+1}-PA_{i,j}) - BBx_{i,j} DD_j (PA_{i,j}-PA_{i,j-1})$$

$$= 2(EE)(F)(zA)[PGA_{i,j}-PG_{i,j}-PA_{i,j}+P_{i,j}] + GG_{i,j}, \qquad [22]$$

where,

$$zA = \frac{dS}{dP_c},$$

$$GG_{i,j} = -Ax_{i,j} C_i (P_{i+1,j}-P_{i,j}) + AAx_{i,j} CC_i (P_{i,j}-P_{i-1,j})$$

$$- Bx_{i,j} D(P_{i,j+1}-P_{i,j}) + BBx_{i,j} DD_j (P_{i,j}-P_{i,j-1}),$$

Rewriting Eq. [22]

$$- PA_{i,j}[Ax_{i,j}C_i+AAx_{i,j}CC_i+Bx_{i,j}D_j+BBx_{i,j}DD_j-(EE)(zA)(F)]$$

$$+ Ax_{i,j} C_i PA_{i+1,j} + AAx_{i,j} CC_i PA_{i-1,j} = HHH_{i,j}, \qquad [23]$$

where

$$HHH_{i,j} = GG_{i,j}+2(EE)(F)(zA)[PGA_{i,j}-PG_{i,j}+P_{i,j}]$$

$$- Bx_{i,j} D_j PA_{i,j+1} - BBx_{i,j} DD_j PA_{i,j-1},$$

Using the Thomas algorithm,

$$PA_{i-1,j} = u_{i-1} PA_{i,j} + V_{i-1}$$

Eq. [23] reduces to the form

$$PA_{i,j} = \frac{Ax_{i,j} CC_i PA_{i+1,j} + AAx_{i,j} CC_i V_{i-1} - HHH_{i,j}}{DEL} \qquad [24]$$

where

$$DEL = C_i Ax_{i,j} + CC_i AAx_{i,j} + D_j Bx_{i,j} + BBx_{i,j} DD_j - (EE)(F)(zA)2 \cdot - CC_i AAx_{i,j} u_{i-1}$$

Since $PA_{i,j} = u_i PA_{i+1,j} + V_i$

$$u_i = \frac{Ax_{i,j} C_j}{DEL} \qquad [25]$$

$$V_i = \frac{AAx_{i,j} CC_i V_{i-1} - HHH_{i,j}}{DEL} \qquad [26]$$

We have thus obtained the matrix coefficients necessary to solve the differential equation governing the flow of water in a two-phase system.

The boundary conditions are grouped in two classes. Class I boundary conditions are for a constant pressure at the well face. Class II boundary conditions are for a constant flux at the well face.

Boundary Conditions

The preceding differential equations are solved numerically subject to the following boundary conditions:

Class I: Constant Pressure at the Well Face

a) $$k_n \frac{\partial P_n}{\partial z}\Big|_{z=0} = 0 = k_w \frac{\partial P_w}{\partial z}\Big|_{z=0}$$

b) $k_n \left.\frac{\partial P_n}{\partial z}\right|_{z=b} = 0 = k_w \left.\frac{\partial P_w}{\partial z}\right|_{z=b}$

c) $k_n \left.\frac{\partial P_n}{\partial R}\right|_{R=\infty} = 0 = k_w \left.\frac{\partial P_w}{\partial R}\right|_{R=\infty}$

d) $PGA_{i-1,j} = P_0 + P_b(1 - e^{t/c})$

$PA_{i-1,j} = 0$

where P_0 = initial pressure

P_b = pressure at the interior boundary

t = time

c^* = parameter with units of time arbitrarily selected, allowing the pressure at the well face to approach asymptotically a predetermined value within a period of time.

Conditions a and b above are satisfied by setting the permeabilities equal to zero along the upper and lower boundaries.

Condition c is realized simply by setting up the mesh spacing such that no pressure differential exists in the outer zones due to injection in the innermost zones.

Condition d for the gas equation is set by direct substitution into the difference equation. This form of the difference equations holds just for the innermost cells receiving flux. Eq. [11] is,

$$C_i A_{i,j}[H_{i+1,j}PGA_{i+1,j} - H_{i,j}PGA_{i,j}] - CC_i AA_{i,j}[H_{i,j}PGA_{i,j} - H_{i-1,j}PGA_{i-1,j}]$$

$$+ D_j BB_{i,j}[H_{i,j+1}PGA_{i,j+1} - H_{i,j}PGA_{i,j}] - BB_{i,j} DD_j[H_{i,j}PGA_{i,j} - H_{i,j-1}PGA_{i,j-1}]$$

$$= (EA)(F)(1-S_{i,j})(mPG^{m-1}_{i,j}PGA_{i,j} + PG^m_{i,j}(1-m) - PG^m_{i,j})$$

$$- (EA)(F)PG^m_{i,j} zA(PGA_{i,j} - PG_{i,j} - PA_{i,j} - P_{i,j}) + G_{i,j}.$$

Substituting in condition d, Eq. [11] takes the form:

$$C_1A_{1,j}[H_{2,j}PGA_{2,j} - H_{1,j}PGA_{1,j}] - CC_1AA_{1,j}[H_{1,j}PGA_{1,j} - PB^{n+1}]$$

$$+ D_jBB_{1,j}[H_{1,j+1}PGA_{2,j+1} - H_{1,j}PGA_{2,j}]$$

$$= (EA)(F)(1-S_{1,j})(mPG_{1,j}^{m-1}PGA_{1,j} + PG_{1,j}^{m}(1-m) - PG_{1,j}^{m})$$

$$- (EA)(F)PG_{1,j}^{m}zA(PGA_{1,j} - PG_{1,j} - PA_{1,j} - P_{1,j}) + G_{1,j}, \qquad [27]$$

where,

$$G_{1,j} = C_1A_{1,j}[(PG^{m+1})_{2,j} - (PG^{m+1})_{1,j}](m-1)$$

$$+ CC_1AA_{1,j}[(PG^{m+1})_{1,j} - PB\ ](1-m)$$

$$+ D_jBB_{1,j}[(PG^{m+1})_{1,j+1} - (PG^{m+1})_{1,j}](m-1)$$

$$+ BB_{1,j}DD_j[(PG^{m+1})_{1,j} - (PG^{m+1})_{1,j-1}](1-m),$$

PB^{n+1} = boundary pressure at time step (n+1),

PB^{n} = boundary pressure at time step (n).

Rearranging Eq. [27],

$$- PGA_{1,j}\{(C_1A_{1,j} + CC_1AA_{1,j} + D_jB_{1,j} + BB_{1,j}DD_j)H_{1,j}$$

$$+ (EA)(F)[(1-S_{1,j})mPG_{1,j}^{m-1} - PG_{1,j}^{m}zA]\} + C_1A_{1,j}H_{2,j}PGA_{2,j} = HH_{1,j}, \qquad [28]$$

where,

$$HH_{1,j} = - D_jB_{1,j}H_{1,j+1}PGA_{1,j+1} - BB_{1,j}DD_jH_{1,j-1}PGA_{1,j-1}$$

$$- CC_1AA_{1,j}PB^{n+1} + G_{1,j} + (EA)(F)[(S_{1,j}-1)m - PG_{1,j}^{m}zA]PG_{1,j}.$$

Eq. [28] further reduces to the form

$$PGA_{1,j} = \frac{C_1\ \ A_{1,j}H_{2,j}PGA_{2,j} - HH_{1,j}}{DELT}, \qquad [29]$$

where,

$$DELT = (C_1A_{1,j} + CC_1AA_{1,j} + D_jB_{1,j} + BB_{1,j}DD_j)H_{1,j}$$

$$+ (EA)(F)[(1-S_{1,j})mPG_{1,j}^{m-1} - PG_{1,j}^{m}zA].$$

Since $PGA_{1,j} = u_1PGA_{2,j} + V_1$,

$$ux_1 = \frac{C_1A_{1,j}H_{2,j}}{DELT} \qquad [30]$$

$$V_2 = -\frac{HH_{1,j}}{DELT}, \qquad [31]$$

ux_2 and V_1 are the initial coefficients in the matrix solution of the gas equation. Condition d for the water equation is directly substituted into the difference equation. This form of the difference equations holds just for the innermost zones.

Eq. [22] is,

$$C_iAx_{i,j}(PA_{i+1,j} - PA_{i,j}) - CC_iAAx_{i,j}(PA_{i,j} - PA_{i-1,j})$$

$$+ D_jBx_{i,j}(PA_{i,j+1} - PA_{i,j}) - BBx_{i,j}DD_j(PA_{i,j} - PA_{i,j-1})$$

$$= 2(EE)(F)(zA)[PGA_{i,j} - PG_{i,j} - PA_{i,j} + P_{i,j}] + GG_{i,j} \qquad [22]$$

Substituting condition d into Eq. [22] takes the form,

$$C_1Ax_{1,j}(PA_{2,j} - PA_{1,j}) - CC_1AAx_{1,j}PA_{1,j}$$

$$+ D_jBx_{1,j}(PA_{1,j+1} - PA_{1,j}) - BBx_{1,j}DD\ (PA_{1,j} - PA_{1,j-1})$$

$$= 2(EE)(F)(zA)[PGA_{1,j} - PG_{1,j} - PA_{1,j} + P_{1,j}] + GG_{1,j}, \qquad [32]$$

where,

$$GG_{1,j} = C_1 Ax_{1,j}(P_{2,j} - P_{1,j}) - CC_1 AAx_{1,j} P_{1,j}$$

$$+ D_j Bx_{1,j}(P_{1,j+1} - P_{1,j}) - BBx_{1,j} DD_j (P_{1,j} - P_{1,j-1}).$$

Rearranging Eq. [32],

$$- PA_{1,j}[Ax_{1,j} C_1 + Bx_{1,j} D_j + BBx_{1,j} DD_j - (EE)(F)(zA)]$$

$$+ Ax_{1,j} C_1 PA_{2,j} = HHH_{1,j}, \qquad [33]$$

where,

$$HHH_{1,j} = (EE)(F)(zA)[PGA_{1,j} - PG_{1,j} + P_{1,j}]$$

$$+ GG_{1,j} - Bx_{1,j} D_j PA_{1,j+1} - BBx_{1,j} DD_j PA_{1,j-1}.$$

Eq. [33] can be reduced to the form

$$PA_{1,j} = \frac{Ax_{1,j} C_1 PA_{2,j} - HHH_{1,j}}{DELT}, \qquad [34]$$

where,

$$DELT = Ax_{1,j} C_1 + Bx_{1,j} D_j + BBx_{1,j} DD_j - (EE)(F)(zA).$$

Since $PA_{1,j} = uu_1 PA_{2,j} + VV_2$,

$$uu_1 = \frac{Ax_{1,j} C_1}{DELT}, \qquad [35]$$

$$VV_1 = -\frac{HHH_{1,j}}{DELT}. \qquad [36]$$

uu_1 and VV_1 are initial coefficients in the matrix solution of the water equation.

APPENDIX B

STABILITY ANALYSIS

Stability of numerical techniques can be shown in a variety of ways. A method commonly employed is the Von Neuman or Fourier series method. This method consists of examining the propagation of a single error. The error is represented by a finite Fourier series, the number of terms equal to the number of mesh points.

For the stability analysis, the equations for two-phase flow can be written in a simplified form:

$$e^{-2u} \frac{\partial}{\partial u} \left(k_{rw} \frac{\partial P}{\partial u}\right) = \frac{\partial S}{\partial t} \tag{1b}$$

$$e^{-2u(m+1)} \frac{\partial}{\partial u} \left(PG^m k_{rn} \frac{\partial PG}{\partial u}\right) = \frac{\partial}{\partial t}[PG^m(1-S)] \tag{2b}$$

Eq. (1b) and (2b) can be written in the form:

$$e^{-2u} \frac{\partial}{\partial u} \left(k_{rw} \frac{\partial P}{\partial u}\right) = \frac{dS}{dP_C} \left[\frac{\partial PG}{\partial t} - \frac{\partial P_w}{\partial t} \right] \tag{3b}$$

$$e^{-2u(m+1)} \frac{\partial}{\partial u} \left(k_{rn} PG^m \frac{\partial PG}{\partial u}\right) = \left[m(1-S)\frac{PG^{m-1}}{\partial t} - PG^m \frac{dS}{dP_C}\right]\frac{\partial PG}{\partial t} + PG^m \frac{S}{dP_C} \frac{\partial P}{\partial t}$$

where the various terms are defined in Appendix A. (4b)

Writing Eqs. (3b) and (4b) in finite difference form,

$$\frac{e^{-2u}}{\Delta u^2} \left[(k_{rw})^{n+1/2}_{j+1/2}\left(p^{n+1/2}_{i,j+1} - p^{n+1/2}_{i,j}\right) - (k_{rw})^{n+1/2}_{j-1/2}\left(p^{n+1/2}_{i,j} - p^{n+1/2}_{i,j-1}\right)\right]$$

$$= -\beta^{n+1}_x \frac{p^{n+1}_{i,j} - p^n}{\Delta\tau} + \beta^{n+1}_x \frac{PG^{n+1} - PG^n}{\Delta t} \tag{5b}$$

$$\frac{e^{-2u}}{\Delta u^2}(m+1)\left[\left(P^m k_{rn}\right)^{n+1/2}_{j+1/2}\left(PG^{n+1/2}_{i,j+1}-PG^{n+1/2}_{i,j}\right)-\left(P^m k_{rn}\right)^{n+1/2}_{j-1/2}\left(PG^{n+1/2}_{i,j}-PG^{n+1/2}_{i,j-1}\right)\right]$$

$$= \beta_n^{n+1/2}\,\frac{PG^{n+1}_{i,j}-PG^{n}_{i,j}}{\Delta t} + \beta_w\,\frac{P^{n+1}_{i,j}-P^{n}_{i,j}}{\Delta t} \qquad (6b)$$

where:

$$\beta_x = \frac{dS}{dP_C}$$

$$\beta_n = \left[m(1-S)\,\frac{\partial PG^{m-1}}{\partial t} - PG^m\frac{dS}{dP_C}\right]$$

$$\beta_w = PG^m\,\frac{dS}{dP_C}$$

Now let $PG^n_{i,j} = Ar^n e^{i\beta j\Delta u}$

$$P^n_{i,j} = Wr^n e^{i\beta j\Delta u}$$

Eqs. (5b) and (6b) are expressed:

$$\frac{e^{-2u}}{\Delta u^2}\left[\left(k_{rw}\right)^{n+1/2}_{i,j+1/2}\left(Wr^{n+1/2}e^{i\beta\Delta u}-Wr^{n+1/2}e^{-\beta\Delta u}\right)-\left(k_{rw}\right)\left(Wr^{n+1/2}e^{i\beta\Delta u}-Wr^{n+1/2}e^{i\beta\Delta u}\right)\right.$$

$$= -\beta_x^{n+1/2}\,\frac{Wr^{n+1}e^{i\beta j\Delta u}-Wr^{n}e^{i\beta j\Delta u}}{\Delta t} + \beta_x^{n+1/2}\,\frac{Ar^{n+1}e^{i\beta j\Delta u}-Ar^{n}e^{i\beta j\Delta u}}{\Delta t} \qquad (7b)$$

$$\frac{e^{-2u(m+1)}}{\Delta u^2}\left[\left(P^m k_{rn}\right)^{n+1/2}_{i,j+1/2}\left(Ar^{n+1/2}e^{i\beta\Delta u}-Ar^{n+1/2}e^{i\beta\Delta u}\right)\right.$$

$$\left.-\left(P^m k_{rn}\right)^{n+1/2}_{i,j-1/2}\left(Ar^{n+1/2}e^{i\beta\Delta u}-Ar^{n+1/2}e^{i\beta\Delta u}\right)\right]$$

$$= \beta_n^{n+1/2}\,\frac{Ar^{n+1}e^{i\beta\Delta u}-Ar^{n}e^{i\beta\Delta u}}{\Delta t} + \beta_w^{n+1/2}\,\frac{Wr^{n+1}e^{i\beta\Delta u}-Wr^{n}e^{i\beta\Delta u}}{\Delta t} \qquad (8b)$$

Eq. (7b) reduces to:

$$- \beta_x^{n+1/2} W(r-1) + B_x^{n+1/2} A(r-1)$$

$$= \frac{We^{-2u} r^{1/2} \Delta t}{\Delta u^2} \{ [(k_{rw})_{i,j+1/2}^{n+1/2} (e^{i\beta\Delta u} - 1)] - [(k_{rw})_{i,j-1/2}^{n+1/2} (1 - e^{i\beta\Delta u})] \} \quad (9b)$$

Eq. (8b) reduces to:

$$\beta_n^{n+1/2} A(r-1) + B_w^{n+1/2} W(r-1) = \frac{Ae^{-2u(m+1)} r^{1/2} \Delta t}{\Delta u^2}$$

$$\{ [(P^m k_{rn})_{i,j+1/2}^{n+1/2} (e^{i\beta\Delta u} - 1)] - [(P^m k_{rn})_{i,j-1/2}^{n+1/2} (1 - e^{i\beta\Delta u})] \} \quad (10b)$$

Now let $r^{1/2} = 1/2(r+1)$. Eqs. (9b) and (10b) reduce to the form:

$$- \beta_x (r-1) W + A B_x (r-1) = (r+1) C W \quad (11b)$$

$$B_n (r-1) A + B_w (r-1) W = (r+1) D A \quad (12b)$$

where

$$C = \frac{e^{-2u} \Delta t}{2\Delta u^2} \{ [(k_{rw})_{i,j+1/2}^{n+1/2} (e^{i\beta\Delta u} - 1)] - [(k_{rw})_{i,j-1/2}^{n+1/2} (1 - e^{i\beta\Delta u})] \}$$

$$D = \frac{e^{-2u(1+m)} \Delta t}{2\Delta u^2} \{ [(P^m k_{rn})_{i,j+1/2}^{n+1/2} (e^{i\beta\Delta u} - 1)] - [(P^m k_{rn})_{i,j-1/2}^{n+1/2} (1 - e^{i\beta\Delta u})] \}$$

Solving for A in Eq. (11b) and substituting it into (12b),

$$\beta_n \left[\frac{(r+1)C + \beta_x (r-1)}{\beta_w} \right] + \beta_w (r-1) = (r+1) D \left[\frac{(r-1)C + \beta_x (r-1)}{\beta_w (r-1)} \right] \quad (13b)$$

Multiplying by $_{W}(r-1)$, Eq. (13b) reduces to,

$$[\beta_n(r+1)C + \beta_x(r-1)B_n](r-1) + \beta_x\beta_w(r-1)^2 = (r+1)^2 DC + (r+1)D\beta_x(r-1) \tag{14b}$$

Factoring Eq. (14b),

$$r^2[\beta_n-\beta_xD+\beta_n\beta_x+\beta_x\beta_w-DC] + 2r[-\beta_n\beta_x-\beta_x\beta_w-DC] - [\beta_n-\beta_xD-\beta_n\beta_x-\beta_x\beta_w+DC] \tag{15b}$$

r can then be solved by the quadratic equation:

$$r = -b \pm \frac{\sqrt{b^2-4ac}}{2a}$$

where:

a = coefficient of r^2

b = coefficient of r

c = coefficient of r^0

We can then say that, for stability:

$$|r| \leq -b * \sqrt{b^2-4ac} \leq 2a \tag{16b}$$

Since r is the error term, it cannot grow under the conditions imposed in Eq. (16b).

Hirt (1968) presented a simple but powerful technique for determining the stability of non-linear differential equations. It consists essentially of expanding the difference equation about a point, n+θ and j. An expansion of this type after discarding higher order terms results in an additional diffusion term. When the additional diffusion term is positive the difference form is stable. A negative term indicates solutions with errors that grow exponentially in time.

$$\frac{e^{-2u}}{\Delta u^2}\left[(k_{rw})^{n+1/2}_{j+1/2}\left(P^{n+1/2}_{i,j+1}-P^{n+1/2}_{i,j}\right)-(k_{rw})^{n+1/2}_{j-1/2}\left(P^{n+1/2}_{i,j}-P^{n+1/2}_{i,j-1}\right)\right]$$

$$= -\beta_x^{n+1}\frac{P^{n+1}_{i,j}-P^{n}}{\Delta t}+\beta_x^{n+1}\frac{PG^{n+1}-PG^{n}}{\Delta t} \qquad (5b)$$

$$\frac{e^{-2u}}{\Delta u^2}(m+1)\left[\left(P^m k_{rn}\right)^{n+1/2}_{j+1/2}\left(PG^{n+1/2}_{i,j+1}-PG^{n+1/2}_{i,j}\right)-\left(P^m k_{rn}\right)^{n+1/2}_{j-1/2}\left(PG^{n+1/2}_{i,j}-PG^{n+1/2}_{i,j-1}\right)\right]$$

$$= \beta_n^{n+1/2}\frac{PG^{n+1}_{i,j}-PG^{n}_{i,j}}{\Delta t}+\beta_w\frac{P^{n+1}_{i,j}-P^{n}_{i,j}}{\Delta t} \qquad (6b)$$

Expanding about the point n+θ and j, and taking the first two terms of the expansion, Eqs. (5b) and (6b) take the form:

$$\frac{e^{-2u}}{\Delta u^2}\left[\left(k+\frac{\Delta u}{2}\frac{\partial k}{\partial u}\right)\left(\Delta u\frac{\partial P}{\partial u}+\frac{\Delta u}{2}\frac{\partial^2 P}{\partial u^2}\right)-\left(k-\frac{\Delta u}{2}\frac{\partial k}{\partial u}\right)\left(\Delta u\frac{\partial P}{\partial u}-\frac{\Delta u^2}{2}\frac{\partial^2 P}{\partial u^2}\right)\right]$$

$$= \beta_x\left[\Delta t\frac{\partial P}{\partial t}+(1-2\theta)\frac{\Delta t^2}{2}\frac{\partial^2 P}{\partial t^2}\right]+\beta_x\left[\frac{\partial PG}{\partial t}+(1-2\theta)\frac{\Delta t}{2}\frac{\partial^2 PG}{\partial t^2}\right] \qquad (17b)$$

$$\frac{e^{-2u}}{\Delta u^2}\left[\left(k+\frac{\Delta u}{2}\frac{\partial k}{\partial u}\right)\left(\Delta u\frac{\partial PG}{\partial u}+\frac{\Delta u^2}{2}\frac{\partial^2 PG}{\partial u^2}\right)-\left(k-\frac{\Delta u}{2}\frac{\partial k}{\partial u}\right)\left(\Delta u\frac{\partial PG}{\partial u}-\frac{\Delta u^2}{2}\frac{\partial^2 PG}{\partial u^2}\right)\right]$$

$$= \beta_n\left[\frac{\partial PG}{\partial t}+(1-2\theta)\frac{\Delta t}{2}\frac{\partial^2 PG}{\partial t^2}\right]+\beta_w\left[\frac{\partial P}{\partial t}+(1-2\theta)\frac{\Delta t}{2}\frac{\partial^2 P}{\partial t^2}\right] \qquad (18b)$$

Eqs. (17b) and (18b) can be reduced to the forms:

$$e^{-2u}\left[\frac{\partial k}{\partial u}\frac{\partial P}{\partial u}+k\frac{\partial^2 P}{\partial u^2}\right]$$

$$= \beta_x\left[\Delta t\frac{\partial P}{\partial t}+(1-2\theta)\frac{\Delta t^2}{2}\frac{\partial^2 P}{\partial t^2}\right]+\beta_x\left[\frac{\partial PG}{\partial t}+(1-2\theta)\frac{\Delta t}{2}\frac{\partial^2 PG}{\partial t^2}\right]+0(\Delta u^2) \qquad (19b)$$

$$e^{-2u}\left[\frac{\partial k}{\partial u} PG^m \frac{\partial PG}{\partial u} + kP^m \frac{\partial^2 PG}{\partial u^2}\right]$$

$$= \beta_n\left[\frac{\partial PG}{\partial t} + (1-2\theta)\frac{\Delta t}{2}\frac{\partial^2 PG}{\partial t^2}\right] + \beta_w\left[\frac{\partial P}{\partial t} + (1-2\theta)\frac{\Delta t}{2}\frac{\partial^2 P}{\partial t^2}\right] + O(\Delta u^2) \qquad (20b)$$

Solving for:

$$\frac{\partial PG}{\partial t} \text{ and } \frac{\partial P}{\partial t},$$

The following equations are obtained,

$$\frac{\partial P}{\partial t} = \frac{1}{\beta_x\beta_n+\beta_w\beta_x}\{\beta_x[-\beta_n(1-2\theta)\frac{\Delta t}{2}\frac{\partial^2 PG}{\partial t^2}$$

$$- \beta_w(1-2\theta)\frac{\Delta t}{2}\frac{\partial^2 P}{\partial t^2} + e^{-2u}\left(\frac{\partial kPG^m}{\partial u}\frac{\partial PG}{\partial u} + KPG^m\frac{\partial^2 PG}{\partial u^2}\right)]$$

$$- \beta_n[\beta_x(1-2\theta)\frac{\Delta t}{2}\frac{\partial^2 P}{\partial t^2} - \beta_x(1-2\theta)\frac{\Delta t}{2}\frac{\partial^2 PG}{\partial t^2} + e^{-2u}[\frac{\partial k}{\partial u}\frac{\partial P}{\partial u} + K\frac{\partial^2 P}{\partial u^2}]]\} \qquad (21b)$$

$$\frac{\partial PG}{\partial t} = \frac{1}{\beta_x\beta_n+\beta_w\beta_x}\{-\beta_x[\beta_n(1-2\theta)\frac{\Delta t}{2}\frac{\partial^2 P}{\partial t} - \beta_x(1-2\theta)\frac{\Delta t}{2}\frac{\partial^2 PG}{\partial^2} + e^{-2u}[\frac{\partial k}{\partial u}\frac{\partial P}{\partial u} + K\frac{\partial^2 P}{\partial u^2}]]$$

$$- \beta_w[\beta_n(1-2\theta)\frac{\Delta t}{2}\frac{\partial^2 PG}{\partial t^2} - \beta_w(1-2\theta)\frac{\Delta t}{2}\frac{\partial^2 P}{\partial t^2} + e^{-2u}[\frac{\partial kPG^m}{\partial u}\frac{\partial PG}{\partial u} + KPG^m\frac{\partial^2 PG}{\partial u^2}]]\} \qquad (22b)$$

Neglecting terms with coefficients of second order in Δt and retaining terms of interest containing additional diffusion terms:

$$\frac{\partial P}{\partial t} = \frac{-1}{\beta_x\beta_n+\beta_w\beta_x}[\beta_n e^{-2u}\{\frac{\partial k}{\partial u}\frac{\partial P}{\partial u} + K\frac{\partial^2 P}{\partial u^2}\}] \qquad (23b)$$

$$\frac{\partial PG}{\partial t} = \frac{-1}{\beta_x\beta_n+\beta_w\beta_x}\left[\beta_w e^{-2u}\left\{\frac{\partial kPG^m}{\partial u}\frac{\partial PG}{\partial u} + KPG^m\frac{\partial^2 PG}{\partial u^2}\right\}\right] \tag{24b}$$

Examination of the additional components in Eqs. (23b) and (24b) shows the Eqs. to be stable since both the head and permeability terms are always positive.

The preceding general examinations of the differential equations for stability, while not absolutely rigorous, substantiate the author's findings. Also of interest is a bound on the error involved in approximating derivatives by numerical forms. If we write the general expressions for the differential equations:

$$\frac{1}{\Delta x}\left[k_{i+1/2,j}\left(\frac{P_{i+1,j}-P_{i,j}}{\Delta x}\right) - k_{i-1/2,j}\left(\frac{P_{i,j}-P_{i-1,j}}{\Delta x}\right)\right]$$

$$+\frac{1}{\Delta y}\left[k_{i,j+1/2}\left(\frac{P_{i,j+1}-P_{i,j}}{\Delta y}\right) - k_{i,j-1/2}\left(\frac{P_{i,j}-P_{i,j-1}}{\Delta y}\right)\right] = \frac{\partial S}{\partial t} \tag{25b}$$

$$\frac{1}{\Delta x}\left[k_{i+1/2,j}\left(\frac{P_{i+1,j}-P_{i,j}}{\Delta x}\right) - k_{i-1/2,j}\left(\frac{P_{i,j}-P_{i-1,j}}{\Delta x}\right)\right]^n$$

$$+\frac{1}{\Delta y}\left[k_{i,j+1/2}\left(\frac{P_{i,j+1}-P_{i,j}}{\Delta y}\right) - k_{i,j-1/2}\left(\frac{P_{i,j}-P_{i,j-1}}{\Delta y}\right)\right]^n = \left(\frac{\partial S}{\partial t}\right)^n$$

We see that all boundaries except the interior boundary can be properly handled to conserve mass by setting the appropriate values of $k_{i,j}$ equal to zero. In the interior boundary the entire numerical part is replaced by a flux condition (see Appendix A). The numerical procedure therefore conserves mass and the error involved in the calculations becomes a function of the convergence criterion and machine roundoff.

The convergence called for in this study was 1.0×10^{-3} and machine roundoff is of the order of 1.0×10^{-5}. Since the extrapolation routine alternated high and then low, 1.0×10^{-3} is considered a maximum value of error (see section on mathematical formulation).

APPENDIX C

APPENDIX C

Computer Flow Diagram

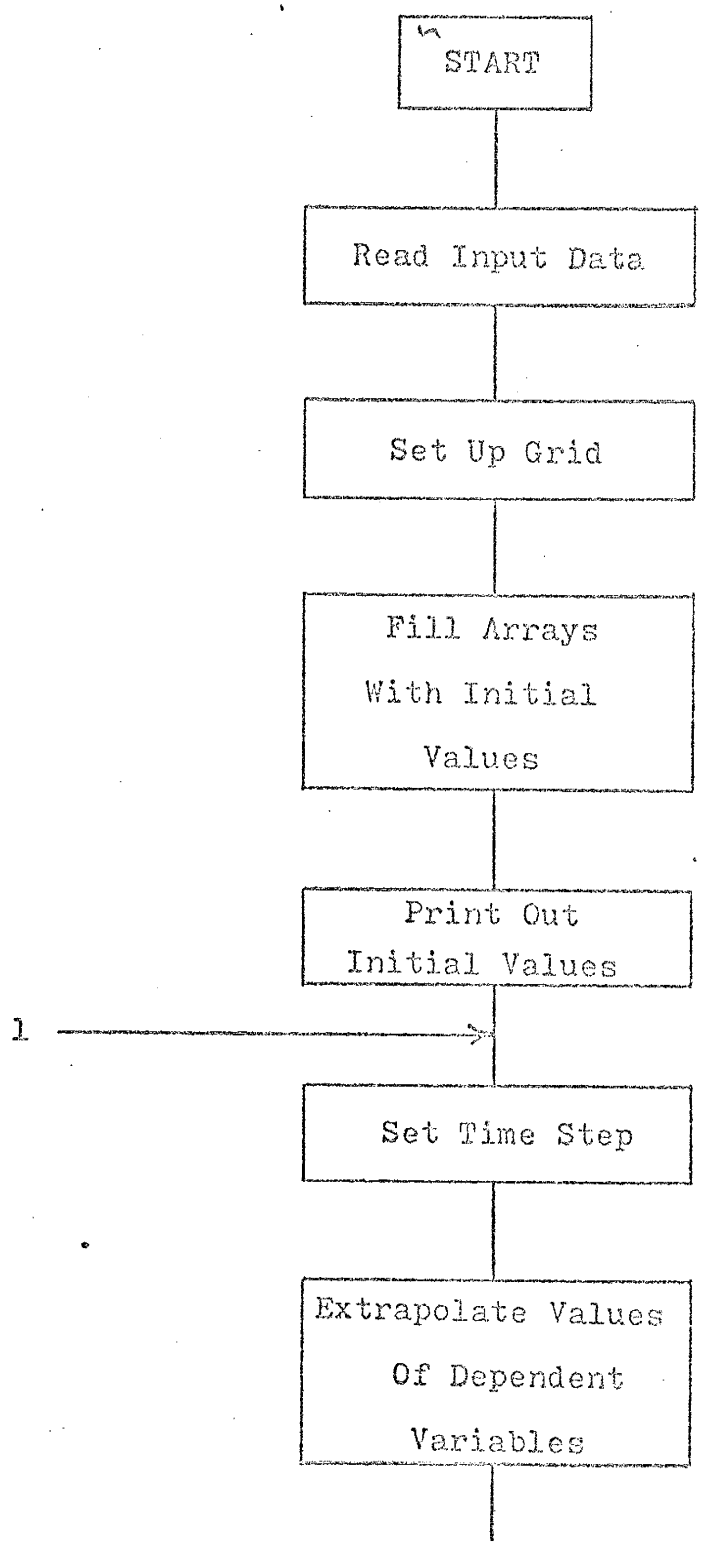

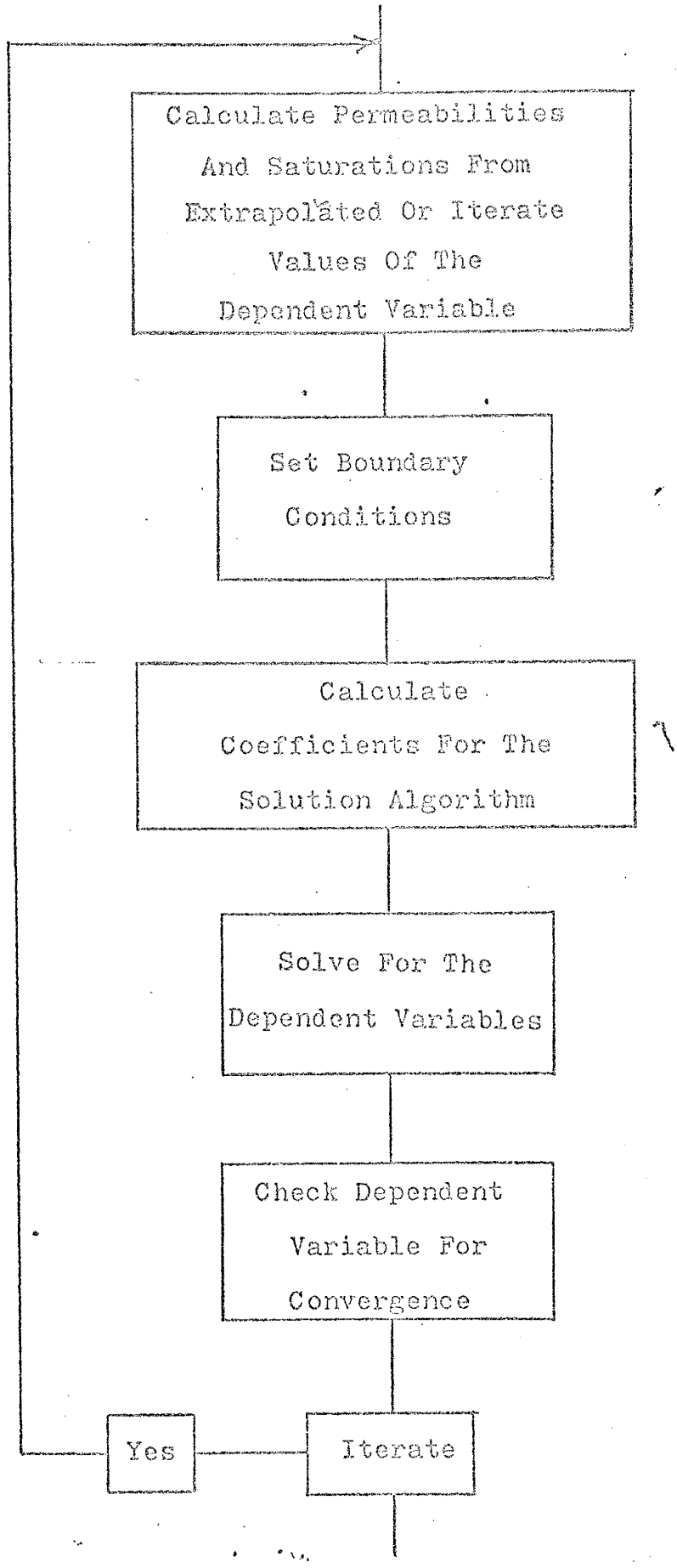
Calculate Permeabilities And Saturations From Extrapolated Or Iterate Values Of The Dependent Variable
Set Boundary Conditions
Calculate Coefficients For The Solution Algorithm
Solve For The Dependent Variables
Check Dependent Variable For Convergence
Yes
Iterate

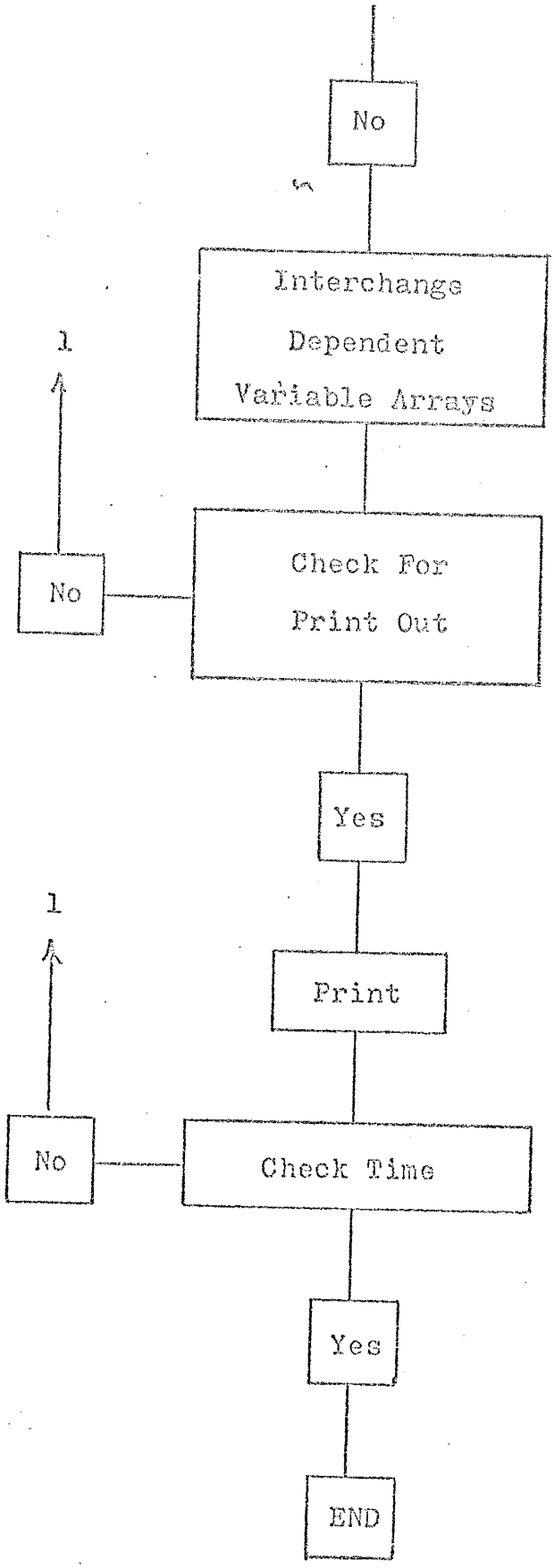
No
Interchange
Dependent
Variable Arrays
1
Check For
Print Out
No
Yes
1
Print
Check Time
No
Yes
END

REFERENCES QUOTED IN THE TEXT

Ames, W. F., Nonlinear Partial Differential Equations in Engineering, Academic Press, New York, 1965.

Ames, W. F., Numerical Methods for Partial Differential Equations, Oxford University Press, New York, 1969.

Buckley, S. E., and M. C. Leverett, Mechanism of Fluid Displacements in Sands, Trans. AIME 146, pp 107-116, 1942.

Coats, K. H., and J. G. Richardson, Calculation of Water Displacement by Gas in Development of Aquifer Storage, Soc. Pet. Eng. Jour., June, pp 105-112, 1967.

Douglas, Jim, Jr., D. W. Peaceman, and H. H. Rachford, Jr., A Method for Calculating Multi-Dimensional Immiscible Displacement, Pet. Trans. AIME 216, pp 297-308, 1959

Higgins, R. V., and A. J. Leighton, A Computer Method to Calculate Two-Phase Flow in Any Irregularly Bounded Porous Medium, Jour. Pet. Tech., June, pp 679-683, 1962.

Hirt, C. W., Heuristic Stability Theory for Finite-Difference Equations, Jour. Comp. Phys. 2, pp 339-355, 1968.

Knapp, Roy M., James H. Henderson, John R. Dempsey, and Keith H. Coats, Calculation of Gas Recovery Upon Ultimate Depletion of Aquifer Storage, AIME Preprint, Paper SPE 1815, 1967.

McFarlane, Robert C., T. D. Mueller, and F. G. Miller, Unsteady-State Distributions of Fluid Compositions in Two-Phase Oil Reservoirs Undergoing Gas Injection, Soc. Pet. Eng. Jour., March, pp 61-74, 1967.

Muskat, Morris, Flow of Homogeneous Fluids, J. W. Edwards, Ann Arbor, Mich., 1946.

Muskat, Morris, and Milan W. Meres, The Flow of Heterogeneous Fluids Through Porous Media, Physics 7, 1936.

Peaceman, D. W., Numerical Solution of the Nonlinear Equations for Two-Phase Flow through Porous Media, in "Nonlinear Partial Differential Equations: A Symposium on Methods of Solution" (W. F. Ames, ed.), Academic Press, New York, 1967.

Richtmyer, Robert D., and K. W. Morton, Difference Methods for Initial-Value Problems, Second Edition, John Wiley & Sons, Inc., New York, 1967.

Scheidegger, Adrian E., The Physics of Flow Through Porous Media, Revised Edition, The MacMillan Co., New York, 1960.

Smith, G. D., Numerical Solution of Partial Differential Equations, Oxford University Press, London, 1965.

Von Rosenberg, Dale U., Methods for the Numerical Solution of Partial Differential Equations, American Elsevier Publishing Co., Inc., New York, 1969.

Westlake, Joan R., A Handbook of Numerical Matrix Inversion and Solution of Linear Equations, John Wiley & Sons, Inc., New York, 1968.

Witherspoon, P. A., T. D. Mueller, and R. W. Donovan, Evaluation of Underground Gas-Storage Conditions in Aquifers Through Investigations of Groundwater Hydrology, Jour. Pet. Tech., May, pp 555-561, 1962.

Woods, E. G., and A. G. Comer, Saturation Distribution and Injection Pressure for a Radial Gas-Storage Reservoir, Jour. Pet. Tech., Dec., pp 1389-1393, 1962.

Wyckoff, R. D., and H. G. Botset, The Flow of Gas-Liquid Mixtures Through Unconsolidated Sands, Physics 7, pp 325-345, 1936.

BACKGROUND REFERENCES

Agarwal, R. G., R. Al-Hussainy, and H. J. Ramey, Jr., The Importance of Water Influx in Gas Reservoirs, Jour. Pet. Tech., Nov., pp 1336-1342, 1965.

Ames, William F., Nonlinear Partial Differential Equations: A Symposium on Methods of Solution, Academic Press, New York, 1967.

Bjordammen, J., and K. H. Coats, Comparison of Alternating-Direction and Successive Overrelaxation Techniques in Simulation of Two- and Three-Dimensional, Two-Phase Flow in Reservoirs, AIME Preprint, Paper SPE 1880, 1967.

Blair, P. M., and D. W. Peaceman, An Experimental Verification of a Two-Dimensional Technique for Computing Performance of Gas-Drive Reservoirs, Soc. Pet. Eng. Jour., 3, pp 19-27, 1963.

Breitenbach, E. A., D. H. Thurnau, and H. K. van Poolen, Solution of the Immiscible Fluid Flow Simulation Equations, AIME Preprint, Paper SPE 2021, 1968.

Briggs, James E., and Thomas N. Dixon, Some Practical Considerations in the Numerical Solution of Two-Dimensional Reservoir Problems, AIME Preprint, Paper SPE 1879, 1967.

Burnett, Peter, Robert Ryan, and C. L. Elliott, Estimating Gas-Water Contacts in Aquifer Storage Fields Using Shut-In Wellhead Pressures, Jour. Pet. Tech., July, pp 877-883, 1967.

Chierici, Gian Luigi, Guiseppe M. Ciucci, and Guiseppe Pizzi, A Systematic Study of Gas and Water Coning by Potentiometric Models, Jour. Pet. Tech., Aug., pp 923-929, 1964.

Coats, K. H., An Analysis for Simulating Reservoir Performance Under Pressure Maintenance by Gas and/or Water Injection, Soc. Pet. Eng. Jour., Dec., pp 331-340, 1968.

Coats, K. H., R. L. Nielse, Mary H. Terhune, and A. G. Weber, Simulation of Three-Dimensional, Two-Phase Flow in Oil and Gas Reservoirs, Soc. Pet. Eng. Jour., Dec., pp 377-388, 1967.

Coats, K. H., L. A. Rapoport, J. R. McCord, and W. P. Drews, Determination of Aquifer Influence Functions from Field Data, Jour. Pet. Tech., Dec., pp 1417-1424, 1964.

Conte, S. D., Elementary Numerical Analysis, McGraw-Hill Book Co., New York, 1965.

Culham, W. E., and R. S. Varga, Numerical Methods for Time Dependent Nonlinear Boundary Value Problems, AIME Preprint, Paper SPE 2806, 1970.

Douglas, J., Jr., Alternating Direction Methods for Three Space Variables, Numer. Math. 4, pp 41-63, 1962.

Douglas, J., Jr., A Numerical Method for the Solution of a Parabolic System, Numer. Math. 2, pp 91-98, 1960.

Douglas, J., Jr., and B. F. Jones, Jr., On Predictor-Corrector Methods for Nonlinear Parabolic Differential Equations, J. Soc. Indust. Appl. Math. 11, pp 195-204, 1963.

Eilerts, C. Kenneth, Integration of Partial Differential Equation for Transient Linear Flow of Gas-Condensate Fluids in Porous Structures, Soc. Pet. Eng. Jour., Dec., pp 291-306, 1964.

Eilerts, C. K., E. F. Sumner, and N. L. Potts, Integration of Partial Differential Equation for Transient Radial Flow of Gas-Condensate Fluids in Porous Structures, Soc. Pet. Eng. Jour., June, pp 141-152, 1965.

Hall, H. N., Analysis of Gravity Drainage, Jour. Pet. Tech., Sept., pp 927-936, 1961.

Havlena, D., and A. S. Odeh, The Material Balance as an Equation of a Straight Line, Jour. Pet. Tech., Aug., pp 896-900, 1963.

Hirasaki, G. J., and P. M. O'Dell, Mathematical Modeling of Reservoir Geometry, AIME Preprint, Paper SPE 2807, 1970.

Holst, P. H., and K. Aziz, Numerical Simulation of Three-Dimensional Natural Convection in Porous Media, AIME Preprint, Paper SPE 2805, 1970.

Jacobson, R. H., Numerical Solution of the Radial Flow Equation Through Porous Media in One Dimension, Unpublished Paper, New Mexico Tech, 1969.

Lantz, R. B., Quantitative Evaluation of Numerical Diffusion (Truncation Error), AIME Preprint, Paper SPE 2811, 1970.

MacDonald, R. C., and K. H. Coats, Methods for Numerical Simulation of Water and Gas Coning, AIME Preprint, Paper 2796, 1970.

Mueller, Thomas D., and Paul A. Witherspoon, Pressure Interference Effects Within Reservoirs and Aquifers, Jour. Pet. Tech., April, pp 471-474, 1965.

Nabor, G. W., and R. H. Barham, Linear Aquifer Behavior, Jour. Pet. Tech., May, pp 561-563, 1964.

Peaceman, D. W., and H. H. Rachford, Jr., The Numerical Solution of Parabolic and Elliptic Differential Equations, J. Soc. Indust. Appl. Math. 3, pp 28-41, 1955.

Sheffield, M., A Non Iterative Technique for Solving Parabolic Partial Differential Equation Problems, AIME Preprint, Paper SPE 2803, 1970.

Snyder, R. W., and H. J. Ramey, Jr., Application of Buckley-Leverett Displacement Theory to Noncommunicating Layered Systems, Jour. Pet. Tech., Nov., pp 1500-1506, 1967.

Spivak, A., and K. H. Coats, Simulation Techniques for Two- and Three-Phase Coning Studies, AIME Preprint, Paper SPE 2595, 1969.

Thomas, G. B., Analysis of Pressure Build-Up Data, Pet. Trans. AIME 198, pp 125-128, 1953.

Watts, J. W., An Iterative Matrix Inversion Method Suitable for Anisotropic Problems, AIME Preprint, Paper SPE 2802, 1970.

Wilson, J. F., Water Flooding--Down-Structure Displacement in the Presence of a Gas Cap, Jour. Pet. Tech., Dec., pp 1383-1388, 1962.

This thesis is accepted on behalf of the faculty of the Institute by the following committee:

Date 17 Sept '70